

# ADVANCED STEEL CONSTRUCTION

*An International Journal*

Volume 4 Number 4

December 2008

## CONTENTS

### Technical Papers

Behavior and Design of Laterally Braced Inelastic Compression Members

*Eric M. Lui and Ajit C. Khanse*

Performance on Split Tee Type W.F. Beam-to-R.H.S. Column Connection  
Using Plug Weld

*T. Murai and I. Kohzu*

In-Plane Strength of Steel Arches

*Yong-Lin Pi, Mark Andrew Bradford and Francis Tin-Loi*

Structural Design of a Practical Suspendome

*Zhi-Hong Zhang, Qing-Shuai Cao, Shi-Lin Dong and Xue-Yi Fu*

A Nonlinear Analysis Method of Steel Frames Using Element with  
Internal Plastic Hinge

*Yu-Shu Liu and Guo-Qiang Li*

### Conference Announcements

Copyright © 2008 by :

The Hong Kong Institute of Steel Construction

Website: <http://www.hkisc.org>

ISSN 1816-112X

Science Citation Index Expanded, Materials Science Citation Index and ISI Alerting

ADVANCED STEEL CONSTRUCTION

# ADVANCED STEEL CONSTRUCTION

*an International Journal*

ISSN 1816-112X

Volume 4 Number 4

December 2008



### Editors-in-Chief

**S.L. Chan**, *The Hong Kong Polytechnic University, Hong Kong*

**W.F. Chen**, *University of Hawaii at Manoa, USA*

**R. Zandonini**, *Trento University, Italy*

VOL. 4, NO. 4 (2008)



ISSN 1816-112X

Science Citation Index Expanded,  
Materials Science Citation Index  
and ISI Alerting

## EDITORS-IN-CHIEF

### Asian Pacific, African and organizing Editor

S.L. Chan

*The Hong Kong Polyt. Univ.,  
Hong Kong*

### American Editor

W.F. Chen

*Univ. of Hawaii at Manoa, USA*

### European Editor

R. Zandonini

*Trento Univ., Italy*

## INTERNATIONAL EDITORIAL BOARD

F.G. Albermani

The Univ. of Queensland, Australia

F.S.K. Bijlaard

Delft Univ. of Technology, The Netherlands

R. Bjorhovde

The Bjorhovde Group, USA

M.A. Bradford

The Univ. of New South Wales, Australia

D. Camotim

Technical Univ. of Lisbon, Portugal

C.M. Chan

Hong Kong Univ. of Science & Technology,  
Hong Kong

S.P. Chiew

Nanyang Technological Univ., Singapore

K.F. Chung

The Hong Kong Polyt. Univ., Hong Kong

G.G. Deierlein

Stanford Univ., California, USA

L. Dezi

Univ. of Ancona, Italy

D. Dubina

The Politehnica Univ. of Timisoara, Romania

R. Greiner

Technical Univ. of Graz, Austria

G.W.M. Ho

Ove Arup & Partners Hong Kong Ltd.,  
Hong Kong

B.A. Izzuddin

Imperial College of Science, Technology  
and Medicine, UK

J.P. Jaspart

Univ. of Liege, Belgium

S. A. Jayachandran

SERC, CSIR, Chennai, India

S. Kitipornchai

City Univ. of Hong Kong, Hong Kong

D. Lam

Univ. of Leeds, UK

G.Q. Li

Tongji Univ., China

J.Y.R. Liew

National Univ. of Singapore, Singapore

X. Liu

Tsinghua Univ., China

E.M. Lui

Syracuse Univ., USA

Y.L. Mo

Univ. of Houston, USA

J.P. Muzeau

CUST, Clermont Ferrand, France

D.A. Nethercot

Imperial College of Science, Technology  
and Medicine, UK

D.J. Oehlers

The Univ. of Adelaide, Australia

K. Rasmussen

The Univ. of Sydney, Australia

T.M. Roberts

Cardiff Univ., UK

J.M. Rotter

The Univ. of Edinburgh, UK

C. Scawthorn

Scawthorn Porter Associates, USA

P. Schaumann

Univ. of Hannover, Germany

G.P. Shu

Southeast Univ. China

J.G. Teng

The Hong Kong Polyt. Univ., Hong Kong

G.S. Tong

Zhejiang Univ., China

K.C. Tsai

National Taiwan Univ., Taiwan

C.M. Uang

Univ. of California, USA

B. Uy

University of Western Sydney

M. Veljkovic

Univ. of Lulea, Sweden

F. Wald

Czech Technical Univ. in Prague, Czech

Y.C. Wang

The Univ. of Manchester, UK

D. White

Georgia Institute of Technology, USA

E. Yamaguchi

Kyushu Institute of Technology, Japan

Y.B. Yang

National Taiwan Univ., Taiwan

B. Young

The Univ. of Hong Kong, Hong Kong

X.L. Zhao

Monash Univ., Australia

## General Information

### *Advanced Steel Construction, an international journal*

#### **Aims and scope**

The International Journal of Advanced Steel Construction provides a platform for the publication and rapid dissemination of original and up-to-date research and technological developments in steel construction, design and analysis. Scope of research papers published in this journal includes but is not limited to theoretical and experimental research on elements, assemblages, systems, material, design philosophy and codification, standards, fabrication, projects of innovative nature and computer techniques. The journal is specifically tailored to channel the exchange of technological know-how between researchers and practitioners. Contributions from all aspects related to the recent developments of advanced steel construction are welcome.

#### **Instructions to authors**

**Submission of the manuscript.** Authors may submit double-spaced manuscripts preferably in MS Word by emailing to one of the chief editors as follows for arrangement of review. Alternatively papers can be submitted on a diskette to one of the chief editors.

Asian Pacific, African and organizing editor : Professor S.L. Chan, Email: ceslchan@polyu.edu.hk  
American editor : Professor W.F. Chen, Email: waifah@hawaii.edu  
European editor : Professor R. Zandonini, Email: riccardo\_zandonini@ing.unitn.it

All manuscripts submitted to the journal are recommended to accompany with a list of four potential reviewers suggested by the author(s). This list should include the complete name, address, telephone and fax numbers, email address, and at least five keywords that identify the expertise of each reviewer. This scheme will improve the process of review.

#### **Style of manuscript**

**General.** Author(s) should provide full postal and email addresses and fax number for correspondence. The manuscript including abstract, keywords, references, figures and tables should be in English with pages numbered and typed with double line spacing on single side of A4 or letter-sized paper. The front page of the article should contain:

- a) a short title (reflecting the content of the paper);
- b) all the name(s) and postal and email addresses of author(s) specifying the author to whom correspondence and proofs should be sent;
- c) an abstract of 100-200 words; and
- d) 5 to 8 keywords.

The paper must contain an introduction and a conclusion. The length of paper should not exceed 25 journal pages (approximately 15,000 words equivalents).

**Tables and figures.** Tables and figures including photographs should be typed, numbered consecutively in Arabic numerals and with short titles. They should be referred in the text as Figure 1, Table 2, etc. Originally drawn figures and photographs should be provided in a form suitable for photographic reproduction and reduction in the journal.

**Mathematical expressions and units.** The Systeme Internationale (SI) should be followed whenever possible. The numbers identifying the displayed mathematical expression should be referred to in the text as Eq. (1), Eq. (2).

**References.** References to published literature should be referred in the text, in the order of citation with Arabic numerals, by the last name(s) of the author(s) (e.g. Zandonini and Zanon [3]) or if more than three authors (e.g. Zandonini et al. [4]). References should be in English with occasional allowance of 1-2 exceptional references in local languages and reflect the current state-of-technology. Journal titles should be abbreviated in the style of the Word List of Scientific Periodicals. References should be cited in the following style [1, 2, 3].

Journal: [1] Chen, W.F. and Kishi, N., "Semi-rigid Steel Beam-to-column Connections, Data Base and Modelling", Journal of Structural Engineering, ASCE, 1989, Vol. 115, No. 1, pp. 105-119.

Book: [2] Chan, S.L. and Chui, P.P.T., "Non-linear Static and Cyclic Analysis of Semi-rigid Steel Frames", Elsevier Science, 2000.

Proceedings: [3] Zandonini, R. and Zanon, P., "Experimental Analysis of Steel Beams with Semi-rigid Joints", Proceedings of International Conference on Advances in Steel Structures, Hong Kong, 1996, Vol. 1, pp. 356-364.

**Proofs.** Proof will be sent to the corresponding author to correct any typesetting errors. Alternations to the original manuscript at this stage will not be accepted. Proofs should be returned within 48 hours of receipt by Express Mail, Fax or Email.

**Copyright.** Submission of an article to "Advanced Steel Construction" implies that it presents the original and unpublished work, and not under consideration for publication nor published elsewhere. On acceptance of a manuscript submitted, the copyright thereof is transferred to the publisher by the Transfer of Copyright Agreement and upon the acceptance of publication for the papers, the corresponding author must sign the form for Transfer of Copyright.

**Permission.** Quoting from this journal is granted provided that the customary acknowledgement is given to the source.

**Page charge and Reprints.** There will be no page charges if the length of paper is within the limit of 25 journal pages. A total of 30 free offprints will be supplied free of charge to the corresponding author. Purchasing orders for additional offprints can be made on order forms which will be sent to the authors. These instructions can be obtained at the Hong Kong Institute of Steel Construction, Journal website: <http://www.hkisc.org>

The International Journal of Advanced Steel Construction is published quarterly by non-profit making learnt society, The Hong Kong Institute of Steel Construction, c/o Department of Civil & Structural Engineering, The Hong Kong Polytechnic University, Hung Hom, Kowloon, Hong Kong.

**Disclaimer.** No responsibility is assumed for any injury and / or damage to persons or property as a matter of products liability, negligence or otherwise, or from any use or operation of any methods, products, instructions or ideas contained in the material herein.

**Subscription inquiries and change of address.** Address all subscription inquiries and correspondence to Member Records, IJASC. Notify an address change as soon as possible. All communications should include both old and new addresses with zip codes and be accompanied by a mailing label from a recent issue. Allow six weeks for all changes to become effective.

#### **The Hong Kong Institute of Steel Construction**

HKISC

c/o Department of Civil and Structural Engineering,

The Hong Kong Polytechnic University,

Hunghom, Kowloon, Hong Kong, China.

Tel: 852- 2766 6047 Fax: 852- 2334 6389

Email: [ceslchan@polyu.edu.hk](mailto:ceslchan@polyu.edu.hk) Website: <http://www.hkisc.org/>

ISSN 1816-112X

Science Citation Index Expanded, Materials Science Citation Index and ISI Alerting

Copyright © 2008 by:

The Hong Kong Institute of Steel Construction.



ISSN 1816-112X

Science Citation Index Expanded,  
Materials Science Citation Index and  
ISI Alerting

**EDITORS-IN-CHIEF**

**Asian Pacific, African  
and organizing Editor**

S.L. Chan

*The Hong Kong Polyt. Univ.,  
Hong Kong*

*Email: ceslchan@polyu.edu.hk*

**American Editor**

W.F. Chen

*Univ. of Hawaii at Manoa, USA*

*Email: waifah@hawaii.edu*

**European Editor**

R. Zandonini

*Trento Univ., Italy*

*Email: riccardo.zandonini@ing.unitn.it*

# Advanced Steel Construction

*an international journal*

---

VOLUME 4 NUMBER 4

DECEMBER 2008

---

**Technical Papers**

Behavior and Design of Laterally Braced Inelastic Compression Members 260  
*Eric M. Lui and Ajit C. Khanse*

Performance on Split Tee Type W.F. Beam-to-R.H.S. Column Connection Using Plug Weld 284  
*T. Murai and I. Kohzu*

In-Plane Strength of Steel Arches 306  
*Yong-Lin Pi, Mark Andrew Bradford and Francis Tin-Loi*

Structural Design of a Practical Suspendome 323  
*Zhi-Hong Zhang, Qing-Shuai Cao, Shi-Lin Dong and Xue-Yi Fu*

A Nonlinear Analysis Method of Steel Frames Using Element with Internal Plastic Hinge 341  
*Yu-Shu Liu and Guo-Qiang Li*

Conference Announcements

# BEHAVIOR AND DESIGN OF Laterally Braced Inelastic Compression Members

Eric M. Lui<sup>1,\*</sup> and Ajit C. Khanse<sup>2</sup>

<sup>1</sup> Meredith Professor and Chair, Department of Civil and Environmental Engineering, Syracuse University, Syracuse, NY 13244-1240

\*(Corresponding author. E-mail: emlui@syr.edu)

<sup>2</sup> Graduate student, Department of Civil and Environmental Engineering, Syracuse University, Syracuse, NY 13244-1240

Received: 23 July 2007; Revised: 5 October 2007; Accepted: 10 October 2007

**ABSTRACT:** This paper presents a numerical study of the inelastic response of laterally braced geometrically imperfect columns under uniform compression. The study employs the pseudo load method of inelastic analysis in which the load deflection behavior of the member is traced from the beginning of loading to ultimate failure. The compression member to be analyzed is pinned at both ends and is supported at some intermediate point by a brace. The brace is modeled as a spring and its location can vary within the length of the compression member. Although this spring brace is assumed to behave in an elastic fashion, the compression member being braced can experience inelasticity. The inelastic behavior of this braced compression member as well as the lateral bracing requirements and the effect of brace location on the ultimate strength of the braced member are investigated. Contrary to the usual design practice in which the braced point is assumed to be rigid and undergo no lateral movement, studies have shown that such a so-called fully-braced condition is rarely realized. As a result, the actual strength of the compression member will fall below its code-specified value. To ensure a safe design, due considerations must be given to the proper design of the brace. Design equations for the stiffness and strength of a brace required to develop at least 90% of this code-specified design compressive strength for the braced member are proposed.

**Keywords:** Compression members; bracing; inelastic behavior; geometrical imperfection; instability

## 1. INTRODUCTION

The nominal design strength  $P_n$  of a compression member is a function of its unbraced length, support conditions, cross-section and material properties, and any geometrical and material imperfections that are present in the member. Although the behavior of centrally loaded geometrically imperfect inelastic compression members has been extensively studied and documented (see for example, Bleich [1], Bjorhovde [2], Galambos [3]), the study of such members with lateral braces is mostly restricted to elastic behavior (Winter [4], Timoshenko and Gere [5], Urdal [6], Mutton and Trahair [7], Brush and Almroth [8], Trahair and Nethercot [9], Lutz and Fisher [10], Nair [11], Plaut [12], Plaut and Yang [13], Zhang, et al. [14], Wang and Nazmul [15]). In the event that inelasticity is considered, the investigation is limited to cases with equally spaced braced points (Pincus [16], Kitipornchai and Finch [17], Ales and Yura [18], Clarke and Bridge [19], Gil and Yura [20]).

For a pinned-pinned geometrically perfect elastic column braced at midpoint by an elastic spring, the theoretical relationship between the column critical load  $P_{cr}$  and the brace stiffness  $k_s$  is given by Timoshenko and Gere (1961) as

$$\frac{k_s L}{P_e} = \frac{2\pi \left( \sqrt{\frac{P_{cr}}{P_e}} \right)^3}{\frac{\pi}{2} \sqrt{\frac{P_{cr}}{P_e}} - \tan \left( \frac{\pi}{2} \sqrt{\frac{P_{cr}}{P_e}} \right)} \quad (1)$$

where  $P_e = \pi^2 EI/L^2$  is the Euler buckling load of the column. This relationship is shown

graphically in Figure 1. It can be seen that  $P_{cr}$  increases almost linearly with  $k_s$  until the brace stiffness reaches a limiting value of  $16P_e/L$  or  $2P_{e_s}/l$ , where  $P_{e_s} = \pi^2 EI/l^2$  is the segment Euler load, and  $l=L/2$  is the unbraced length (i.e., distance between braced points) of the column. At this limiting value, referred to as the ideal brace stiffness, the buckling load reaches a cut off value of  $4\pi^2 EI/L^2$ . This value represents the buckling load that corresponds to the second buckling mode of the pinned-pinned column. When the stiffness of the brace is less than the ideal brace stiffness, the column will buckle in a symmetric mode with lateral displacement occurring at the braced point. However, once the ideal brace stiffness is reached, the column will buckle in an antisymmetric mode with no lateral displacement occurring at the braced point. The condition under which this occurs is called full bracing. At full bracing, the column will behave as if a rigid support were placed at the braced point.

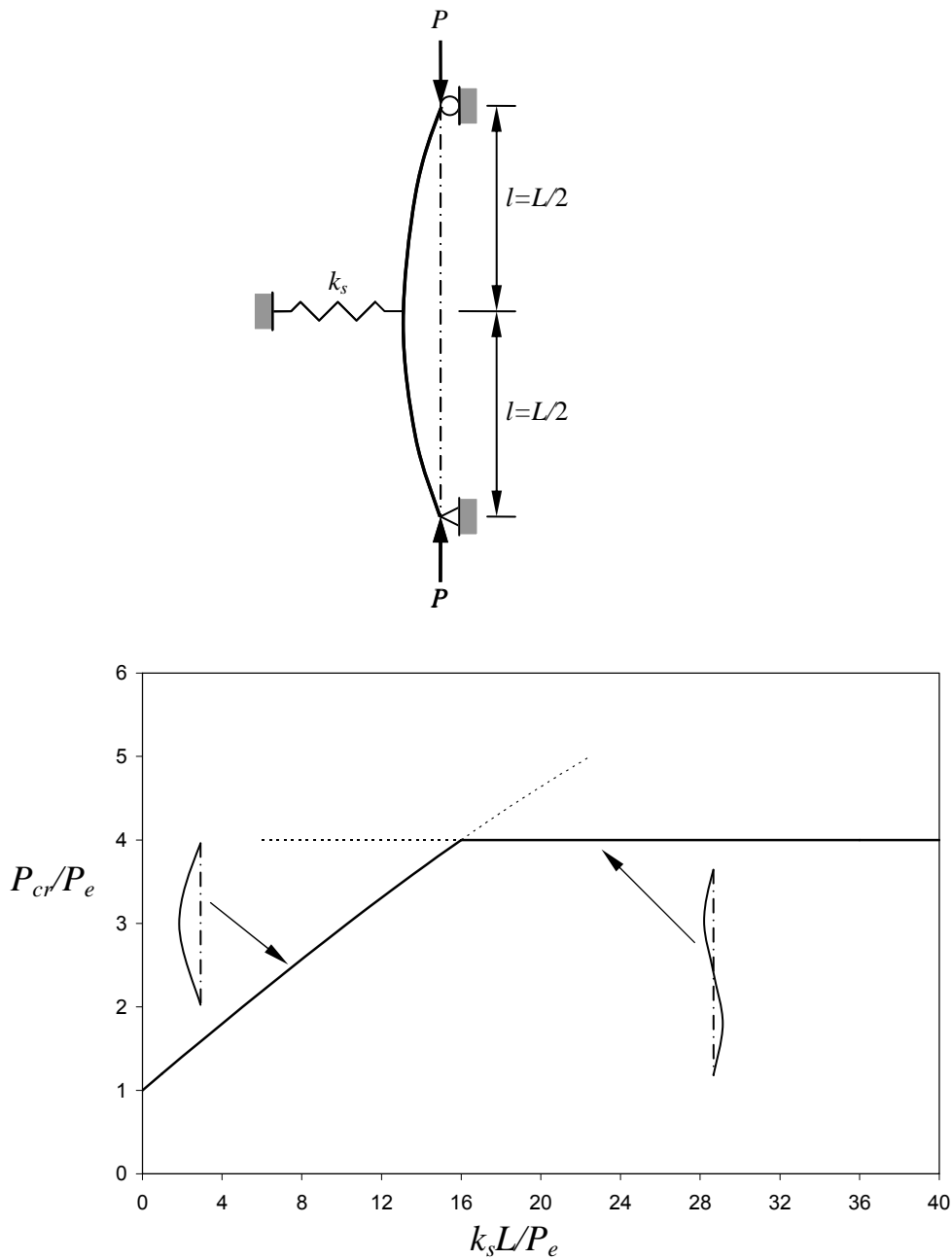


Figure 1. Behavior of a Centrally Braced Elastic Column

## 1.1 Winter's Model

For purpose of design, the ideal stiffness for a geometrically perfect elastic column can be calculated using a simple mechanistic model shown in Figure 2a (Winter [4]). The model consists of two rigid links hinged together at the braced point and supported by a translational spring. By drawing a free body diagram of one of the rigid links in its deflected configuration and summing moment about the braced point, it can be shown that  $k_s=2P/l$ . The ideal braced stiffness is obtained by replacing  $P$  by  $P_{es}$  in the preceding equation. The Winter model can be extended to columns with equally spaced multiple braced points as well as for columns with unequally spaced braced points (Yura [21]). The model works as long as the locations of the hinges joining the rigid links coincide with the natural buckling node points of the real column. In other words, the Winter approach is valid only if the critical load of the column ( $P_{cr}$ ) is equal to the Euler load of the longest segment of the column ( $P_{es}$ ). This condition is often violated for columns with unequally spaced braced points.  $P_{cr}$  for these columns are not equal to the Euler load of the longest segment because the shorter segments tend to restrain the longer segments at buckling. More importantly, it has been shown by Plaut [12] that a fully-braced condition (i.e., no lateral movement at the braced point) can not be attained for these columns using the ideal braced stiffness calculated using the Winter's model. To reach the fully-braced condition, the brace stiffness has to be unrealistically high.

## 1.2 Geometrically Imperfect Columns

Even for columns with equally spaced braced points, Winter noted that the required brace stiffness was appreciably higher than the ideal brace stiffness because of the presence of geometrical imperfections in the columns. The initial out-of-straightness present in real columns means lateral deflection will occur at the braced point as soon as the load is applied to the column. This deflection and hence the brace force increase as the column load increases. The deflection and brace force will be exceedingly high at incipient instability of the column unless a brace stiffness much higher than the ideal brace stiffness is used. To account for the effect of geometrical imperfections, the model in Figure 2a was modified to include an initial deflection  $d_0$  in the system as shown in Figure 2b. Again, by drawing a free body diagram of one of the rigid links in its deflected configuration and summing moment about the braced point, an equation for the required brace stiffness can be written as

$$k_{s,req'd} = \frac{2P}{l} \left(1 + \frac{d_0}{d}\right) \quad (2)$$

At incipient instability  $P=P_{es}$ . Substituting  $P_{es}$  for  $P$  in the above equation, and realizing that  $2P_{es}/l$  is the ideal brace stiffness for a pinned-pinned column with a central brace, Eq. (2) can be written as

$$k_{s,req'd} = k_{s,ideal} \left(1 + \frac{d_0}{d}\right) \quad (3)$$

If the brace behaves elastically, the force in the brace can be calculated from the equation

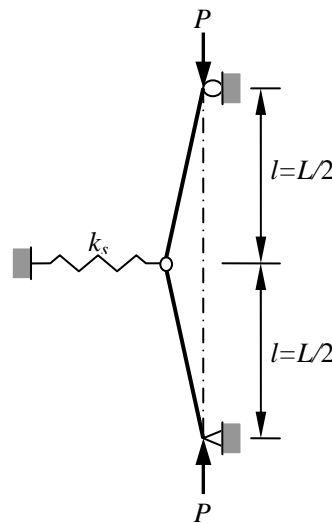
$$F_s = k_{s,req'd} \cdot d = k_{s,ideal} (d + d_0) \quad (4)$$

Eqs. 3 and 4 form the basis for the design requirements for the stiffness and strength of discrete braces that are equally spaced along the length of the column (Galambos [3], McGuire [22], Salmon and Johnson [23], CSA [24]).

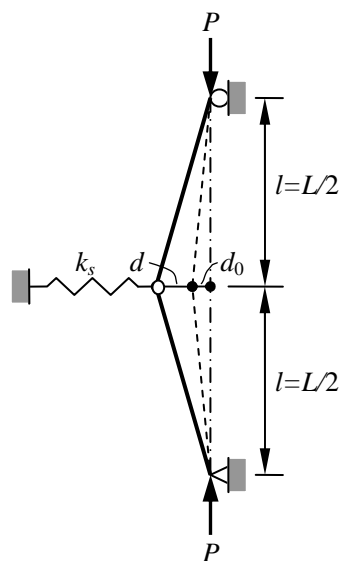
Using an elastic pinned-pinned column with different initial imperfection shapes braced at midpoint by a spring brace, Plaut [12] showed that Eq. (3) would be inadequate and proposed the following equation for the required brace stiffness

$$k_{s,req'd} = k_{s,ideal} \left(1 + 1.5 \frac{d_0}{d}\right) \tag{5}$$

The inadequacy of Eq. 3 is due to the assumption of zero moment at the braced point when in reality a moment is present as a result of column out-of-straightness. If the design stipulates that the additional deflection  $d$  is not to exceed the initial deflection  $d_0$ , Eq. 5 gives a required brace stiffness that is 25% higher than that computed using Eq. 3.



(a) Without Initial Geometrical Imperfections



(b) With Initial Geometrical Imperfections

Figure 2. Winter's Braced Column Models



### 1.3 Unequally Spaced Braces

If the brace is not located at the midpoint of the pinned-pinned column, the fully braced condition can be attained only if the brace stiffness is unrealistically high. That is,  $k_{s,ideal}$  has to approach that of a rigid support to prevent lateral movement from occurring at the brace point. For this situation, it is more logical to express the required brace stiffness as a function of the expected load-carrying capacity of the column, rather than as a function of the ideal brace stiffness. To this end, Plaut [12] proposed the following equation

$$k_{s,req'd} = \frac{PL}{(L - a_1)a_1} \left(1 + 1.5 \frac{d_0}{d}\right) \quad (6)$$

where  $P$  is the column load (which is less than  $P_{rigid}$ , where  $P_{rigid}$  is the load-carrying capacity of the column if a rigid support is placed at the location of the brace),  $a_1$  is the distance from one end of the column to the location of the brace, and  $L$  is the length of the column. Eq. 6 was developed based on an analysis of a pinned-pinned elastic column supported by a spring brace. Other equations for  $k_{s,req'd}$  for this condition are given by Urdal [6] and Stanway et al. [25].

### 1.4 Column Inelasticity

Most columns in real structures exhibit inelastic behavior at their design strengths. By introducing a rotational spring to the Winter's model at the braced point to simulate the flexural rigidity effect of the column and by using the tangent modulus concept, Pincus [16] showed that the required brace stiffness was higher for an inelastic than an elastic column. This argument was supported by Trahair and Nethercot [9], but disputed by Ales and Yura [18] and Gil and Yura [20]. In this paper it will be shown that as long as the applied load is less than 70% of the maximum load-carrying capacity of the column, the required brace stiffness to attain a certain load level is virtually the same regardless of whether the column is elastic or inelastic. However, it should be noted that the maximum load-carrying capacity of an inelastic column is often lower than that of an elastic column. The required braced stiffness to attain the maximum load-carrying capacity for the two columns will therefore be different.

## 2. METHOD OF ANALYSIS

The model used for the numerical analysis is shown in Figure 3. The compression member of length  $L$ , pinned at both ends, is braced at an intermediate point by a spring brace located at a distance  $a_1$  from one of the supports. The stiffness of the brace is denoted as  $k_s$ . In this study,  $k_s$  is assumed to be a constant although under certain circumstances the brace stiffness can exhibit nonlinear behavior (Kitipornchai and Finch [17]). The use of a constant brace stiffness is justified here because the amount of deformation experienced by the brace is relatively small. To simulate geometrical imperfections that are unquestionably present in a real member, an initial crookedness in the form of a half sine curve is introduced to the model. The maximum out-of-straightness of the member is taken as  $0.001L$  at midspan. The initial deflection from the member chord due to member crookedness is denoted as  $d_0$ , and any additional deflection due to member buckling is denoted as  $d$ .

A load-deflection analysis using the pseudo load method of inelastic analysis (Lui and Zhang [26]) was employed to obtain maximum compressive strengths  $P_{max}$  of the member for different values of

brace stiffness  $k_s$ , slenderness parameter  $\lambda$  (where  $\lambda = \frac{KL}{r\pi} \sqrt{\frac{F_y}{E}}$ , in which  $K$  is the effective length factor - set equal to 1 for a pinned-pinned column,  $L$  is the column length, and  $r$ ,  $F_y$  and  $E$  are the radius of gyration, yield strength and modulus of elasticity, respectively), and non-dimensional brace location  $a_1/L$ . An incremental iterative method was used to trace the nonlinear load-deflection curve and  $P_{max}$  was obtained as the peak point of this curve. The nonlinear behavior of the system is attributed to both geometrical and material effects. In the pseudo load method of inelastic analysis, geometrical nonlinearity is accounted for by the application of pseudo in-span and member end shears to the structure and material nonlinearity is accounted for by the use of a predetermined cross-section moment-curvature-thrust relationship in forming the member stiffness matrix and in calculating the pseudo loads. Details of the method are given in Lui and Zhang [26] and will not be repeated here. However, it is important to note that because the pseudo-load method is a load control method, it is not capable of tracing the descending branch of the load-deflection curve. As a result, the post-buckling behavior of the system can not be evaluated in this study. Furthermore, it should be pointed out that depending on the stiffness and location of the brace, the braced column may fail in a symmetric or an asymmetric mode as shown in Figure 4. For instance, a pinned-pinned unbraced column will fail in a symmetric mode (in the form of a half sine wave) while a fully-braced column will fail in an asymmetric mode when a sufficiently stiff brace is provided at the midpoint of the column. From these two extreme conditions it can be inferred that there is a transitional brace stiffness at which the failure mode will switch from one of symmetrical to one of asymmetrical. In a numerical analysis, a symmetrical model will always produce symmetrical solution even though the solution may not be the controlling one. In order to generate results for the asymmetrical mode, small disturbing forces were applied in the transverse direction to guide the column to fail in this mode. Based on a series of numerical analyses, it was found that a disturbing force of magnitude  $0.001P$  (where  $P$  is the column axial force) applied in an asymmetrical pattern at six evenly spaced points along the length of the column would provide the desired results. Thus, to obtain the correct  $P_{max}$  when the brace was at or near the midpoint of the column, two analyses were performed. One would give a symmetrical solution and the other would give an asymmetrical solution. The lower of the two  $P_{max}$  was then taken as the ultimate capacity of the braced member. If the location of the brace is away from the midpoint of the column, the correct failure mode will automatically be obtained and no transverse disturbing forces are needed in the numerical analyses to arrive at the correct solution.

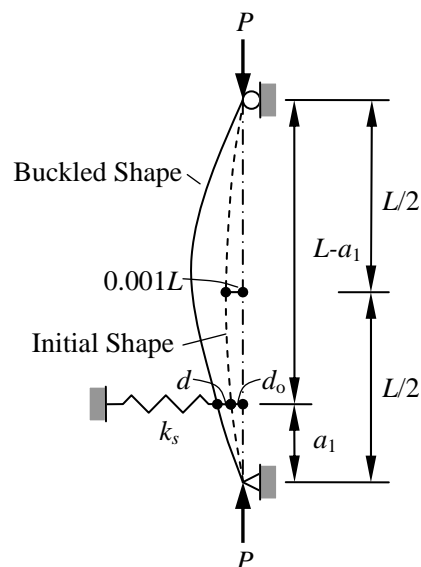


Figure 3. Geometrically Imperfect Braced Column Model

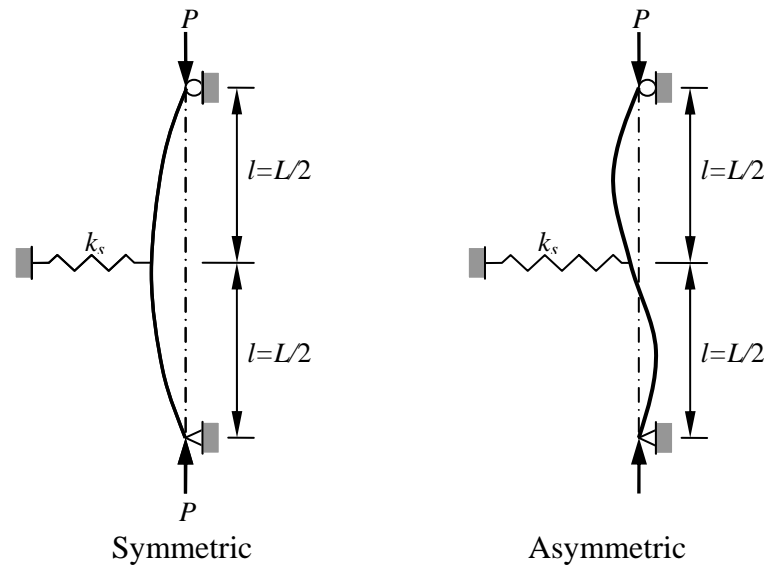


Figure 4. Symmetric and Asymmetric Buckling Modes

### 3. VERIFICATION STUDIES

To validate the method of analysis discussed in the preceding section, numerical results obtained using the pseudo load method are compared with results reported in the literature. Two comparisons will be made: The first is a comparison of critical loads for an elastic column braced by an elastic spring to show the effect of the brace location on the column critical load. The second is a comparison of ultimate strengths of a centrally-braced inelastic column to show the effect of brace stiffness on the column compressive strength.

#### 3.1 Geometrically Perfect Elastic Column Braced by an Elastic Spring

The theoretical solution for a geometrically perfect elastic column braced by an elastic spring located at an arbitrary location within the length of the column was given by Timoshenko and Gere [5]. The results, obtained using an eigenvalue analysis, were reported by Plaut and Yang [13]. Numerical values for the nondimensional critical load  $P_{cr}/P_e$  ( $=P_{cr}L^2/\pi^2EI$ ) plotted as a function of the nondimensional brace stiffness  $k_sL/P_e$  ( $=k_sL^3/\pi^2EI$ ) at various brace locations  $a_1/L$  are shown in Figure 5. The solid lines in the figure represent theoretical results and the diamond markers in the figure represent numerical results generated using the pseudo load method. As can be seen, excellent correlation is observed between the theoretical and numerical results.

#### 3.2 Geometrically Imperfect Column Braced by an Elastic Spring

A pinned-pinned geometrically imperfect column with various values of segment slenderness

parameter  $\lambda_l = \frac{Kl}{r\pi} \sqrt{\frac{F_y}{E}}$  (where  $Kl$  is the effective length of the column segment between braced

points,  $r$  is the radius of gyration,  $F_y$  is the yield stress, and  $E$  is the modulus of elasticity of the material) braced by a centrally placed spring brace was analyzed by Clark and Bridge [19] using a plastic zone method of inelastic analysis. Both the symmetric and asymmetric modes of failure were investigated. The results for the nondimensional ultimate strength  $P_{max}/P_e$  of the column reported by Clark and Bridge [19] are compared in Table 1 with those generated using the pseudo load method. It can be seen that the results compared quite well with each other.

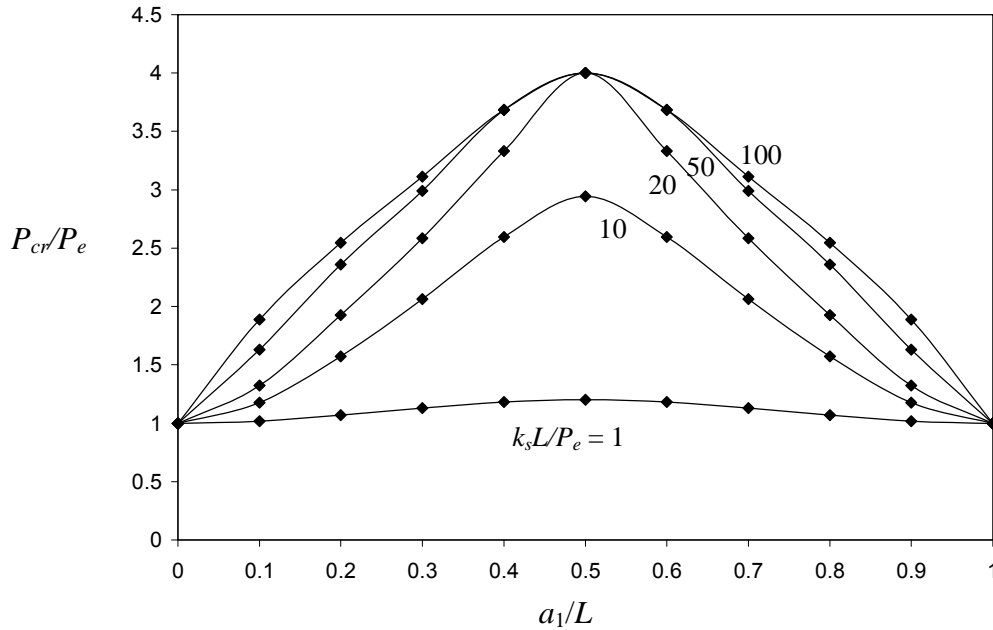


Figure 5. Comparison of Numerical Results with Theoretical Results

Table 1. Comparison of  $P_{max}/P_e$  for a Braced Geometrically Imperfect Inelastic Column

	$\lambda_f=0.5$		$\lambda_f=0.75$		$\lambda_f=1.0$		$\lambda_f=2.0$	
	Sym.	Asym.	Sym.	Asym.	Sym.	Asym.	Sym.	Asym.
Clarke and Bridge [19]	0.92	0.89	2.0	1.8	3.1	2.6	6.5	3.7
Present	0.948	0.886	1.98	1.72	3.12	2.52	6.56	3.65
Error	3%	-0.45%	-1%	-4.4%	0.65%	-3.1%	0.92%	-1.4%

#### 4. NUMERICAL STUDIES

All analyses reported herein were carried out using the following material properties:  $E=29,000$  ksi ( $200 \times 10^3$  MPa), and  $F_y=36$  ksi (248 MPa) or 50 ksi (345 MPa). Slenderness parameter  $\lambda$  that varies from 0.5 to 4, brace location  $a_1/L$  that varies from 0.125 to 0.5, and nondimensional brace stiffness  $k_s L/P_e$  that varies from 6 to 100, were used in the parametric study. The pseudo load method was used to generate load deflection curves for various combinations of column slenderness, brace stiffness and brace location. The results are presented in the following sections.

##### 4.1 Effects of Brace Location and Brace Stiffness

Figures 6a-d depict graphically how brace location and stiffness affect the maximum load-carrying capacity of the braced column. Four observations can be made from these figures:

1. For a given brace stiffness, the maximum column strength is obtained when the brace is located at the midpoint of the column. There is a reduction in column strength when the brace is moved away from the midpoint. This observation is consistent with the general knowledge that bracing is the most effective when administered at a point where the lateral deflection of the braced member is a maximum at incipient instability.

2. The reduction in column strength is a function of the slenderness parameter. The reduction in  $P_{max}/P_e$  is less pronounced when  $\lambda$  is low. This can be seen readily in Figure 7a and b in which the variation of  $P_{max}/P_e$  is plotted against brace location for four values of  $\lambda$ . Regardless of the brace stiffness,  $P_{max}/P_e$  does not appear to vary significantly for  $\lambda=1$ , but noticeable change in  $P_{max}/P_e$  is observed for  $\lambda=4$ . This observation suggests that  $P_{max}/P_e$  is less sensitive to the location of the brace for shorter columns or columns that are more likely to experience inelasticity.
3. Returning to Figure 6, when  $a_1/L=0.5$  (i.e., when the brace is located at the midpoint of the column), the data points for  $P_{max}/P_e$  tend to collapse toward a stationary value when  $k_s L/P_e$  reaches or exceeds a certain value. This value of brace stiffness is what was referred to earlier at the ideal brace stiffness. The ideal brace stiffness occurs only for the case of a centrally braced column. Because no stationary value for  $P_{max}/P_e$  exists when the brace is not placed at the midpoint of the column, the concept of ideal brace stiffness does not apply to these cases.
4. Although no stationary value exists for  $P_{max}/P_e$  when  $a_1/L \neq 0.5$ , the variation of  $P_{max}/P_e$  with brace stiffness for a given brace location is less pronounced for small  $\lambda$  than for large  $\lambda$ . This observation suggests that  $P_{max}/P_e$  is less sensitive to brace stiffness for shorter columns or columns that are more likely to experience inelasticity.

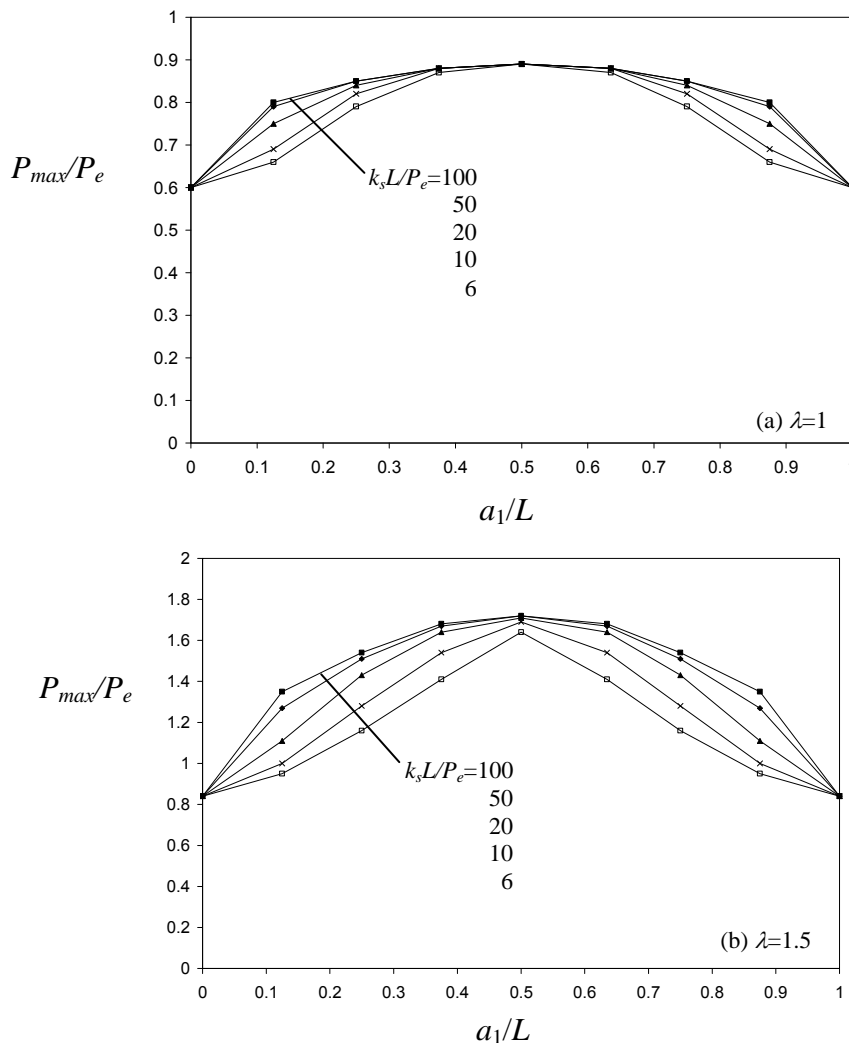


Figure 6. Effects of Brace Location and Stiffness on  $P_{max}$

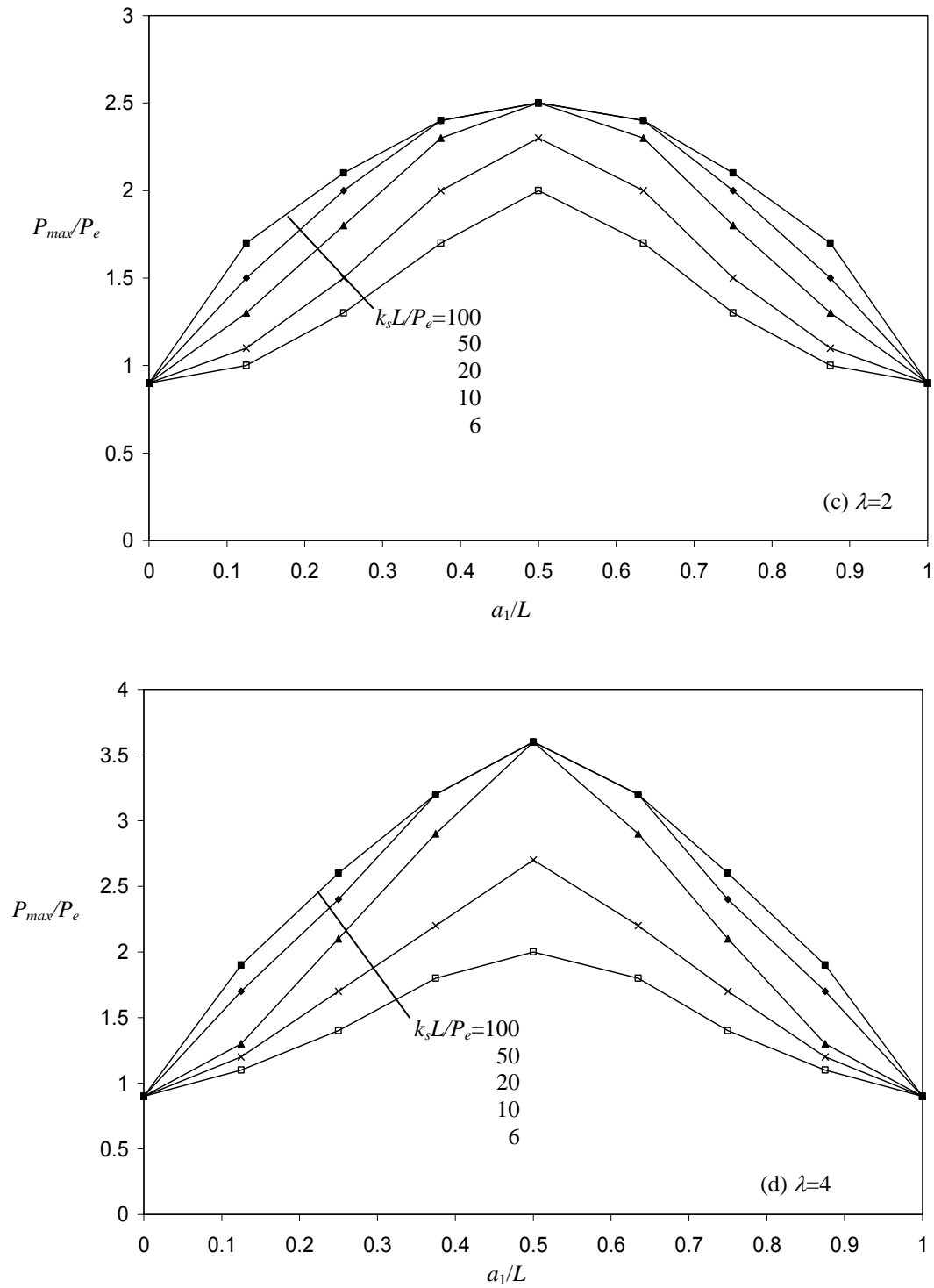


Figure 6 (Cont'd). Effects of Brace Location and Stiffness on  $P_{max}$

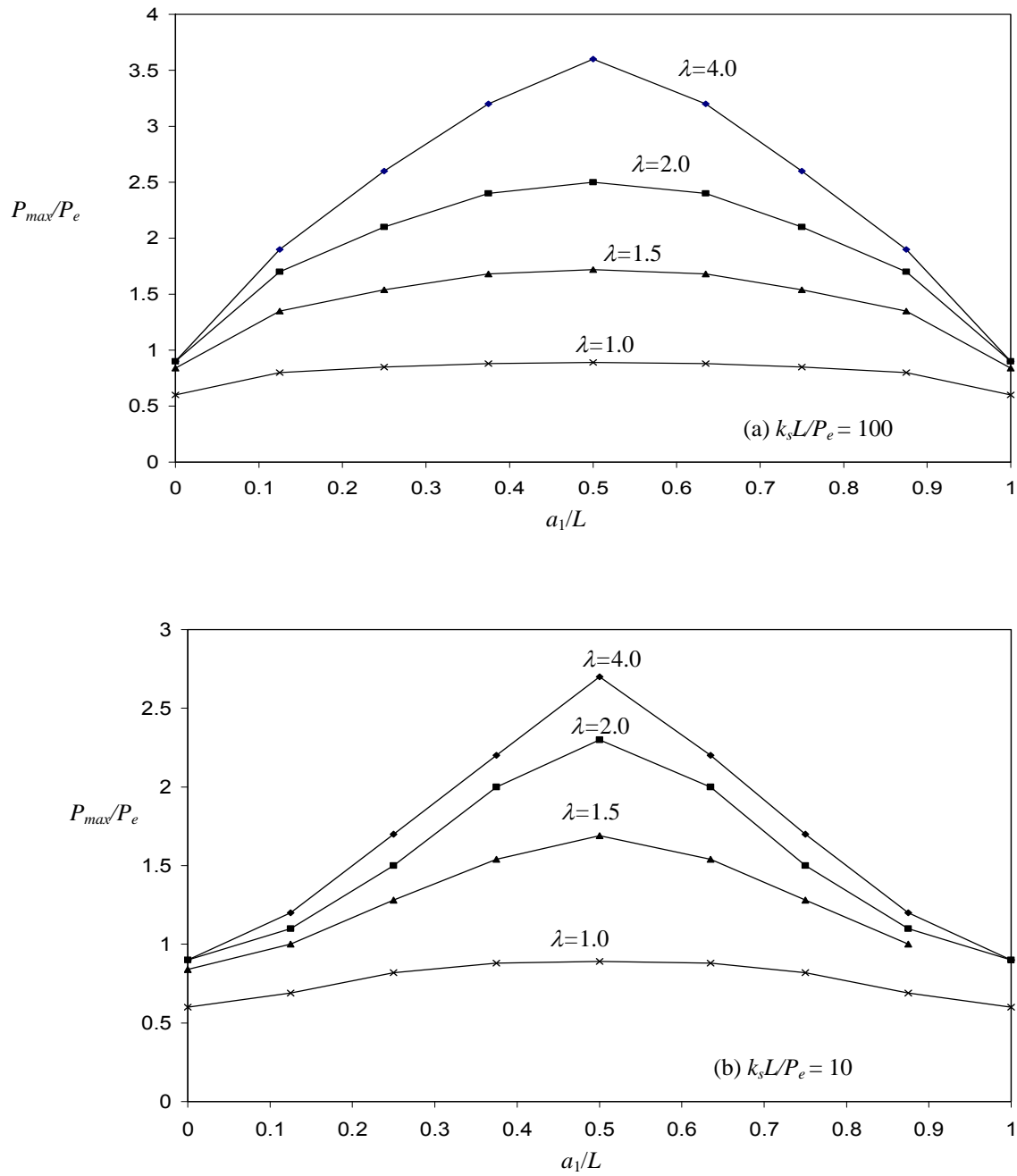


Figure 7. Effect of  $\lambda$  on  $P_{max}$

## 4.2 Effect of Column Inelasticity

It has been shown in the preceding section that the effects of brace location and brace stiffness on  $P_{max}/P_e$  are less pronounced when  $\lambda$  is small (i.e., when inelasticity is involved). A somewhat different but related question is: In order to reach a certain column load  $P$  where  $P < P_{max}$ , is a higher brace stiffness required for an inelastic column when compared to an elastic column? Based on the study by Pincus [16], the answer to the above question is yes. However, studies by Ales and Yura [18], and Gil and Yura [20] have disputed Pincus's assertion. Intuitively, one might be inclined to think that once inelasticity sets in, the flexural rigidity of the column will decrease and so a higher brace stiffness is required for the column to reach a given  $P$ . Nevertheless, from the load deflection curves that were generated in this study, it can be concluded that no additional brace stiffness is required for an inelastic column to attain a given value of  $P$  as long as  $P$  is less than about  $0.70P_{max}$ , where  $P_{max}$  is the maximum inelastic load capacity of the braced column.

Representative samples of load deflection curves are shown in Figures 8a and b. It can be seen that regardless of the brace location and brace stiffness, the load deflection curves of the elastic and the inelastic columns are quite comparable except when  $P$  reaches about 70% of  $P_{max}$ . From there on, the inelastic load deflection curves start to deviate from their elastic counterparts. This deviation occurs when yielding commences on the extreme compression fiber of the cross-section, and the load level of  $0.70P_{max}$  at which this deviation occurs roughly corresponds to a maximum compressive residual stress of  $0.3F_y$  present in most hot-rolled sections. Since the deviation of the inelastic load deflection curve from its elastic counterpart does not occur until  $P/P_{max} \geq 0.70$ , it can be concluded that as long as  $P < 0.70P_{max}$ , the required brace stiffness is independent of the state of the material. However, when  $P \geq 0.70P_{max}$ , additional deflection will be experienced by the inelastic column and a higher brace force will result.

## 4.3 Effect of the Form of Initial Out-of-Straightness

Based on an elastic analysis, Plaut [12] has demonstrated that the form of initial out-of-straightness of the braced member has an effect on the magnitude of displacement, and hence the brace deflection and brace force of the system. According to Plaut [12], for the same maximum initial deflection  $d_{0,max}$  (taken as  $0.001L$ ) at midspan of the column, an initial out-of-straightness in the form of a parabola given by the equation

$$d_0 = d_{0,max} \frac{4x}{L} \left(1 - \frac{x}{L}\right) \quad (7)$$

yields slightly larger central deflection and larger brace deflection and brace force than that of a half-sine wave given by the equation

$$d_0 = d_{0,max} \sin \frac{\pi x}{L} \quad (8)$$

However, the present study, which is based on an inelastic analysis, has shown that this effect is rather negligible. A comparison of the load deflection curves for two initial out-of-straightness shapes: sinusoidal and parabolic are shown in Figures 9a and b. Regardless of the brace location and brace stiffness, the two load deflection curves differ very little. In fact, they almost overlap each other regardless of the brace location and column slenderness. For design purpose, these slight discrepancies can practically be ignored.



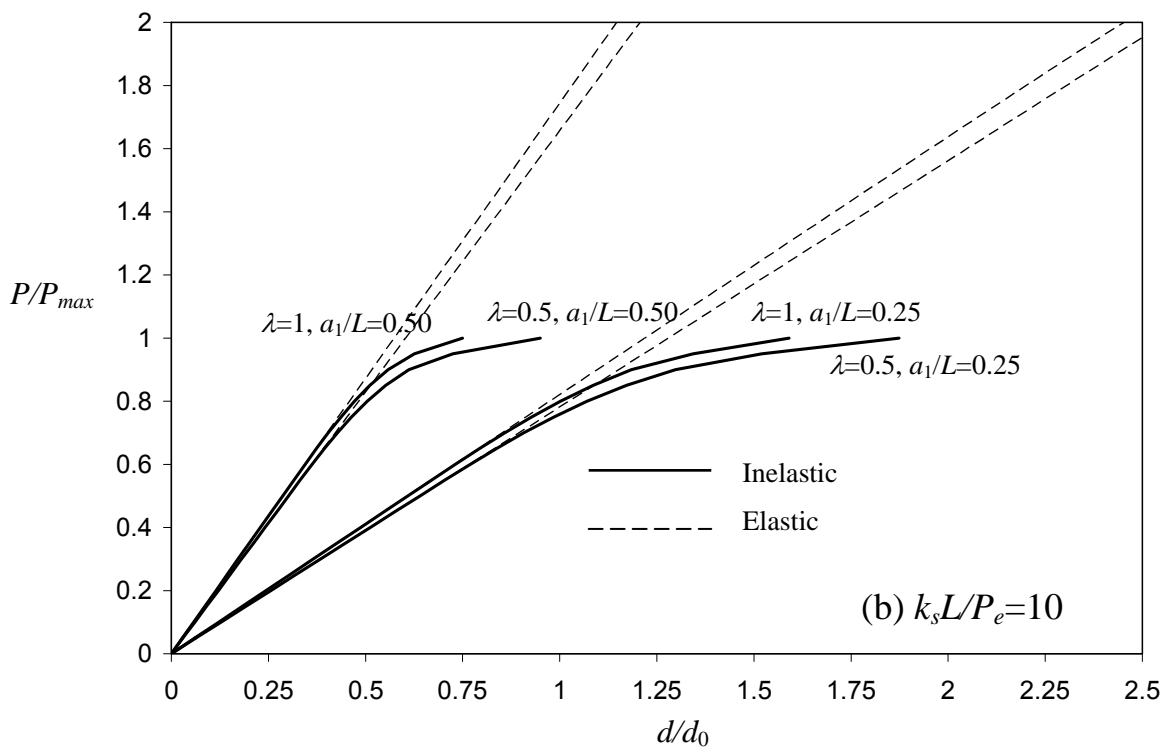
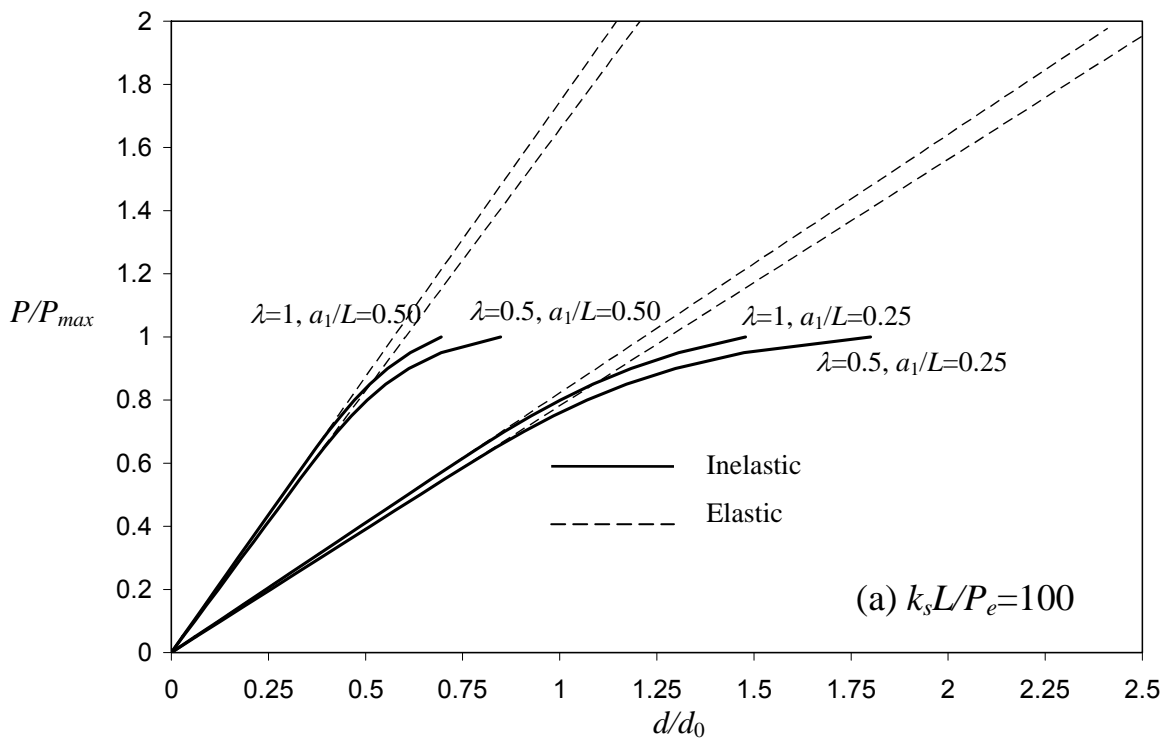


Figure 8. Comparison of Elastic and Inelastic Behavior

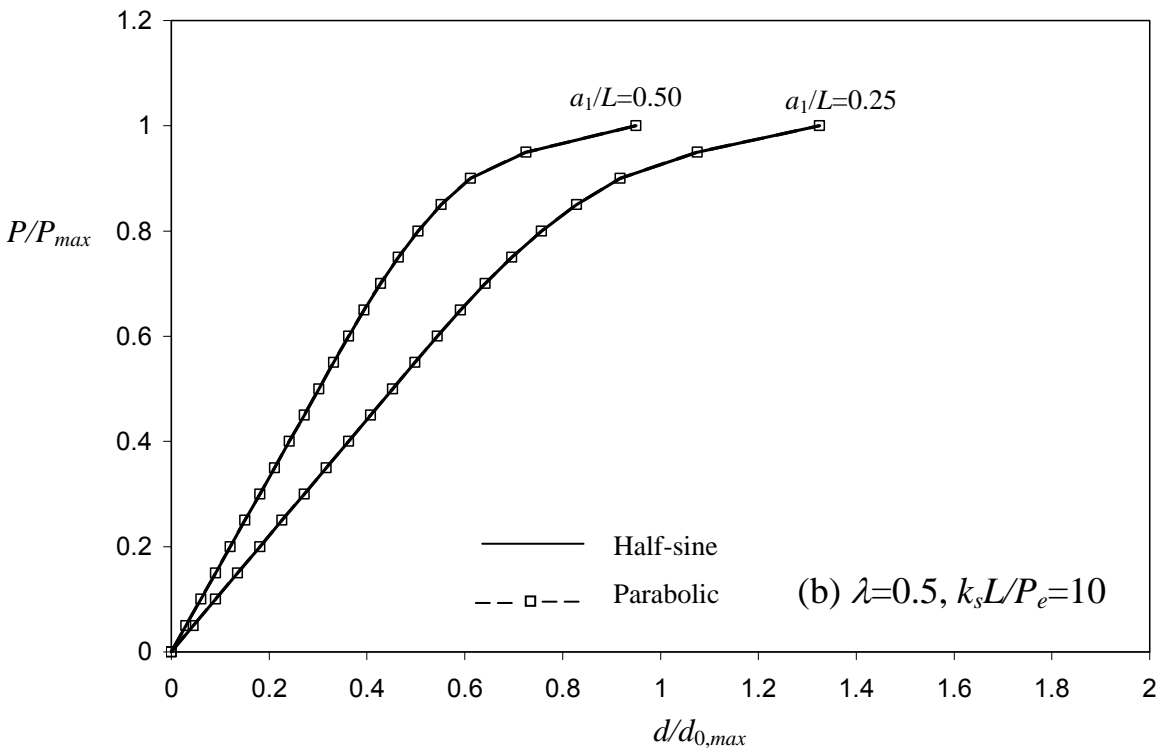
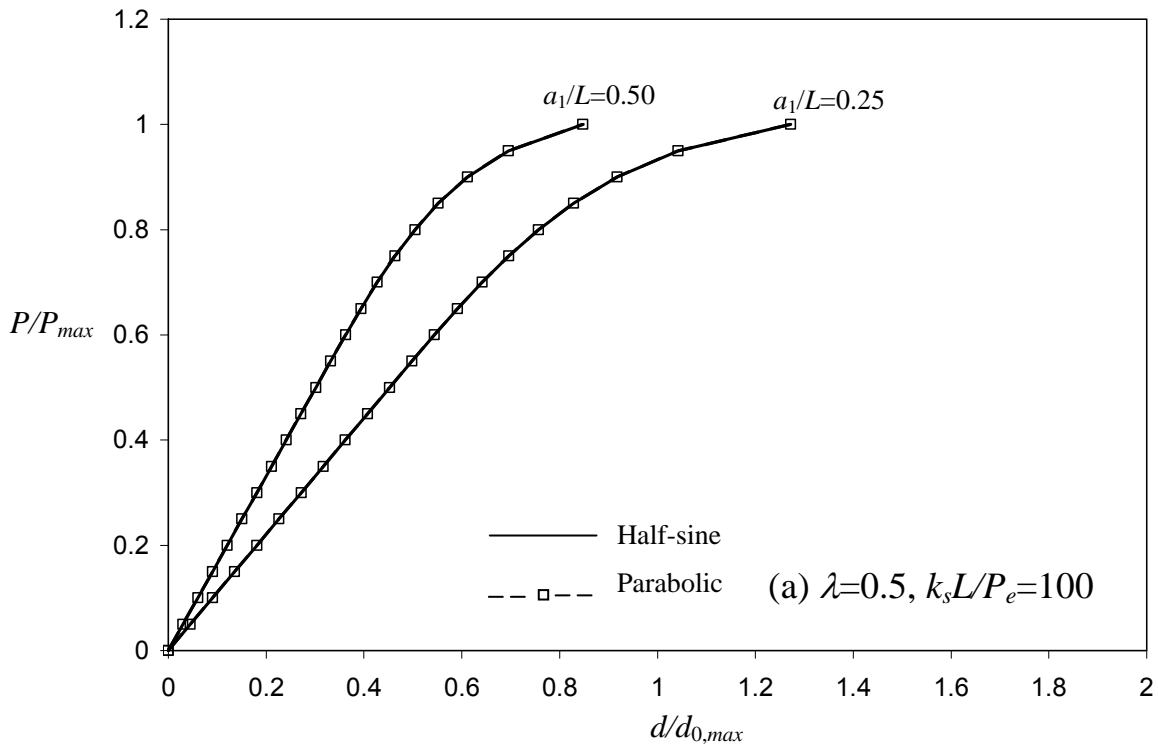


Figure 9. Effect of Different Initial Out-of-straightness Shapes

#### 4.4 Effect of Brace Stiffness on Column Deflection

When a geometrically imperfect braced column with an initial deflection of  $d_0$  measured at the braced point is loaded by a compressive axial force  $P$ , it experiences an additional deflection of  $d$ . This deflection is a function of the column slenderness, brace stiffness, brace location and  $P$ . Figures 10a-f show some representative plots of the deflection ratio  $d_0/d$  as a function of the non-dimensional brace stiffness  $k_s L/P_e$  for various values of  $P/P_{rigid}$ , three slenderness parameters ( $\lambda=1, 1.5, 2$ ), and two brace locations ( $a_1/L=0.25, 0.50$ ).  $P_{rigid}$  is the compressive strength of the column when the brace stiffness is infinite. From these figures it can be seen that the relationship between  $d_0/d$  and  $k_s L/P_e$  is linear. These graphs can be used as a design aid to determine the required brace stiffness to attain a certain compressive strength for a given column length, brace location and desired deflection.

For instance, if one wishes to attain 90% of  $P_{rigid}$  for a compression member with  $\lambda=1$  and limit the additional deflection  $d$  to  $d_0$ , one can draw a horizontal line from  $d_0/d=1$  to intersect the line where  $P/P_{rigid}=0.9$ , and read the required  $k_s L/P_e$  from the abscissa. Thus, if the brace is placed at the quarter point (i.e.,  $a_1/L=0.25$ ), the required  $k_s L/P_e$  from Figure 10a is about 11; and if the brace is placed at the midpoint (i.e.,  $a_1/L=0.5$ ), the required  $k_s L/P_e$  from Figure 10b reduces to about 6. Once the brace stiffness is known, the brace force can be determined from Eq. 4. The brace can then be designed to provide the necessary stiffness and strength.

#### 4.5 Relationship between Brace Force $F_s$ and Maximum Column Strength $P_{max}$

According to Eq. (4), the force in the brace  $F_s$  is a function of the brace stiffness  $k_s$  and the lateral deformation  $d$  of the column. Because a stiff brace tends to reduce the lateral deformation of the column and vice versa, the brace force may increase or decrease with brace stiffness. The mathematical relationship between the brace force and the maximum column strength is rather complex and highly nonlinear. In Figure 11, the envelope curves for the ratio of brace force to maximum column strength  $F_s/P_{max}$  is plotted against the nondimensional brace stiffness  $k_s L/P_e$  for the range of data used in the study (i.e.,  $0.5 \leq \lambda \leq 4$ ,  $0.125 \leq a_1/L \leq 0.5$ , and  $6 \leq k_s L/P_e \leq 100$ ). From the figure, it can be seen that an upper bound value for  $F_s/P_{max}$  can be taken as 4%. Thus, for design purpose a  $F_s/P_{max}$  value of 4% can be used. This value is higher than 2% normally assumed for  $F_s/P_{max}$ . However, it should be pointed out this 2% rule was based on elastic response of the column under service load. As was demonstrated in Figures 8a and b, additional deflection will result at or near  $P_{max}$  for an inelastic column, hence a higher brace force is justified in the context of a limit state design.

### 5. DESIGN RECOMMENDATION

In a conventional design of a braced compression member, the member is assumed to be fully braced (i.e., the braced point is assumed to undergo no lateral displacement). The design strength of the member is calculated based on the compressive strength of the longest segment of the member assuming an inflection point occurs at the brace point. However, as pointed out earlier, if the brace stiffness is finite the fully braced condition can be realized only for a centrally braced geometrically perfect pinned-pinned column. For other cases, lateral deflection will occur at the brace point, and the compressive strength of the member will be lower than its assumed fully-braced condition. The exact relationship between column capacity, brace stiffness, brace location, and brace deflection is rather complex. For design purpose, the use of simplified equations is desirable. If the design objective is for the column to develop at least 90% of its theoretical fully-braced strength (i.e., if  $P/P_{rigid}$  is  $\geq 90\%$ ), a design equation can be proposed as:

$$k_{s,req'd} = \frac{P_e}{(0.08 + 0.436\lambda^{-2.15}) \cdot a_1} \left(0.7 + \frac{d_0}{d}\right) \quad (9)$$

In the above equation,  $P_e = \pi^2 EI / (KL)^2$  is the elastic buckling strength of the column *without* using the fully-braced assumption,  $KL$  is the effective length,  $\lambda = KL / \pi r(\sqrt{F_y/E})$  is the slenderness parameter,  $a_1$  is the location of the brace measured from the *nearest* external pinned support or internal inflection point of the column,  $d_0$  and  $d$  are the initial out-of-straightness and additional lateral deflection of the column, respectively.

For comparison purposes, Eq. 9 is plotted in Figure 10 as a dashed line in each case. It is also plotted in Figure 12 for a slender (elastic) column braced at midpoint for which the theoretical solution is given by Timoshenko and Gere [15]. As can be seen, the equation gives value for the required brace stiffness that allows at least 90% of the theoretical fully-braced strength of the column to be developed.

## 5.1 Design Procedure

The following procedure is recommended for the design of a braced column:

1. Assuming a fully-braced condition (i.e., assuming that no lateral movement occurs at the braced point), select a section so that  $\phi_c P_n > P_u$ , where  $\phi_c P_n$  is the design strength of the segment of the compression member with the largest  $KL$  value, in which  $\phi_c = 0.90$  is the resistance factor as per ANSI/AISC 360-05 [27], and  $P_u$  is the required strength of the column.
2. Since the fully-braced condition is not attainable for a brace with finite brace stiffness, the actual design strength is less than its calculated value. However, a brace can be designed to assure that at least 90% of this design strength can be attained to resist the applied load. This can be done by specifying a  $d_0/d$  ratio, and compute the required brace stiffness  $k_s$  from Eq. 9.
3. Calculate the brace force using the equation  $F_{s,req'd} = k_{s,req'd} \cdot d$ , and check that it does not exceed 4% of the design compressive strength of the column.
4. Design the brace so that its stiffness  $k_s$  and strength  $F_s$  exceed their respectively required values.
5. Check that the actual design strength, which is equal to at least 90% of its code specified value, does not exceed the required strength, i.e., make sure  $0.90\phi_c P_n \geq P_u$ .

## 5.2 Design Examples

*Example 1: Determine the required stiffness and force of a brace required to brace the column shown in Figure 13 so that it can withstand an axial force of 1400 kips (6230 kN). The column is a W14×132 section made of A992 steel ( $F_y = 50$  ksi or 345 MPa). It is 16-ft (4.9-m) long, pinned at both ends, and braced against weak axis instability at a location shown in the figure. The column is assumed to have an initial out-of-straightness in the form of Eq. 8 with  $d_{0,max} = 0.001L$ . The additional deflection of the column  $d$  at the brace point is not to exceed  $d_0$ .*

**Solution:** According to ANSI/AISC [27], the design compressive strength for flexural buckling of members without slender elements is

$$\phi_c P_n = \phi_c F_{cr} A_g \quad (10)$$

where  $\phi_c=0.90$  is the resistance factor for compression,  $A_g$  is the gross cross-section area, and  $F_{cr}$  is the critical buckling stress given by

$$F_{cr} = \begin{cases} (0.658^{F_e/F_y}) F_y, & \frac{KL}{r} \leq 4.71 \sqrt{\frac{E}{F_y}} \\ 0.877 F_e, & \frac{KL}{r} > 4.71 \sqrt{\frac{E}{F_y}} \end{cases} \quad (11)$$

in which  $F_e = \pi^2 E / (KL/r)^2$  is the elastic buckling stress,  $F_y$  is the yield stress,  $E$  is the modulus of elasticity,  $KL$  is the effective length, and  $r$  is the radius of gyration.

For the W14×132 section,  $A_g=38.8 \text{ in}^2$  (250 cm<sup>2</sup>),  $r_x=6.28 \text{ in.}$  (16 cm),  $r_y=3.76 \text{ in.}$  (9.55 cm), and if we assume fully-braced condition,  $(KL)_x$  and  $(KL)_y$  are equal to 192 in. (488 cm) and 144 in. (366 cm), respectively. By using Eqs. 10 and 11, we have  $(\phi_c P_n)_x=1630 \text{ kips}$  (7250 kN) and  $(\phi_c P_n)_y=1570 \text{ kips}$  (6980 kN).

By comparing  $(\phi_c P_n)_x$  with  $(\phi_c P_n)_y$ , it can be seen that  $(\phi_c P_n)_y$  controls. However, it should be noted that the computed  $(\phi_c P_n)_y$  value assumes a fully-braced condition, which is not attainable in real life. As a result, we need to use Eq. 9 to calculate the required brace stiffness  $k_{s,req'd}$  to ensure that at least 90% of this computed  $(\phi_c P_n)_y$  value can be achieved, and that this value is still larger than the required compressive strength  $P_u=1400 \text{ kips}$  (6230 kN).

For a non fully-braced condition,  $(KL)_y=192 \text{ in.}$  (488 cm). Substituting  $P_e = P_{ey} = \pi^2 EI_y / (KL)_y^2 = 4255 \text{ kips}$  (18930 kN),  $\lambda = (KL/\pi r)_y (\sqrt{F_y/E}) = 0.675$ ,  $a_1 = 48 \text{ in.}$  (122 cm) and  $d_0/d = 1$  into Eq. 9, we obtain  $k_{s,req'd} = 138 \text{ k/in.}$  (241 kN/cm). By substituting  $d = d_0 = 0.001L \sin(\pi/4) = 0.136 \text{ in.}$  (3.45 mm) into Eq. 4, we obtain  $F_{s,req'd} = 18.8 \text{ kips}$  (83.6 kN).

If the brace is designed to have a stiffness of 138 k/in. (241 kN/cm) and can withstand a force of 18.8 kips (83.6 kN), the designed compressive strength about the weak axis will be at least 90% of its calculated code-specified strength, i.e.,  $0.90(\phi_c P_n)_y = 0.90(1570 \text{ kips}) = 1413 \text{ kips}$  (6285 kN). Since this value exceeds the required strength  $P_u$  of 1400 kips (6230 kN), and because  $F_s/P_{max} = F_s/0.90(\phi_c P_n)_y = 1.3\%$ , which is less than 4%, the design is considered acceptable.

*Example 2: Repeat Example 1 if the top end of the column is now fixed against rotation, and the axial force that needs to be carried is 1450 kips (6452 kN).*

**Solution:** The pinned-fixed column can be transformed into an equivalent pinned-pinned column through the use of the effective length factor  $K$ . In theory, the  $K$  factor for this case is 0.7. However, ANSI/AISC [27] recommends a value of 0.8 since a full fixity rarely occurs in real life. Assuming a fully-braced condition, we have  $(KL)_x = 154 \text{ in.}$  (390 cm), and  $(KL)_y = 115 \text{ in.}$  (293 cm). From Eqs. 10 and 11, we have  $(\phi_c P_n)_x=1670 \text{ kips}$  (7430 kN) and  $(\phi_c P_n)_y=1630 \text{ kips}$  (7250 kN). Again, we can see that the design is controlled by weak axis buckling.

Now, to correct for the non fully-braced condition, we use Eq. 9 with  $P_e$  and  $\lambda$  computed using  $(KL)_y=(0.8)(192'')= 154$  in. (391 cm). The result is  $k_{s,req'd} = 138.7$  k/in. (243 kN/cm). From Eq. 4,  $F_s=17.7$  k (78.7 kN), which is less than 4% of  $0.90(\phi_c P_n)_y = 0.04 \times (0.90)(1630) = 58.7$  kips ( 261 kN). Since  $0.90(\phi_c P_n)_y = 1467$  k (6525 kN) still exceeds  $P_u=1450$  k (6450 kN), the W14×132 section is acceptable.

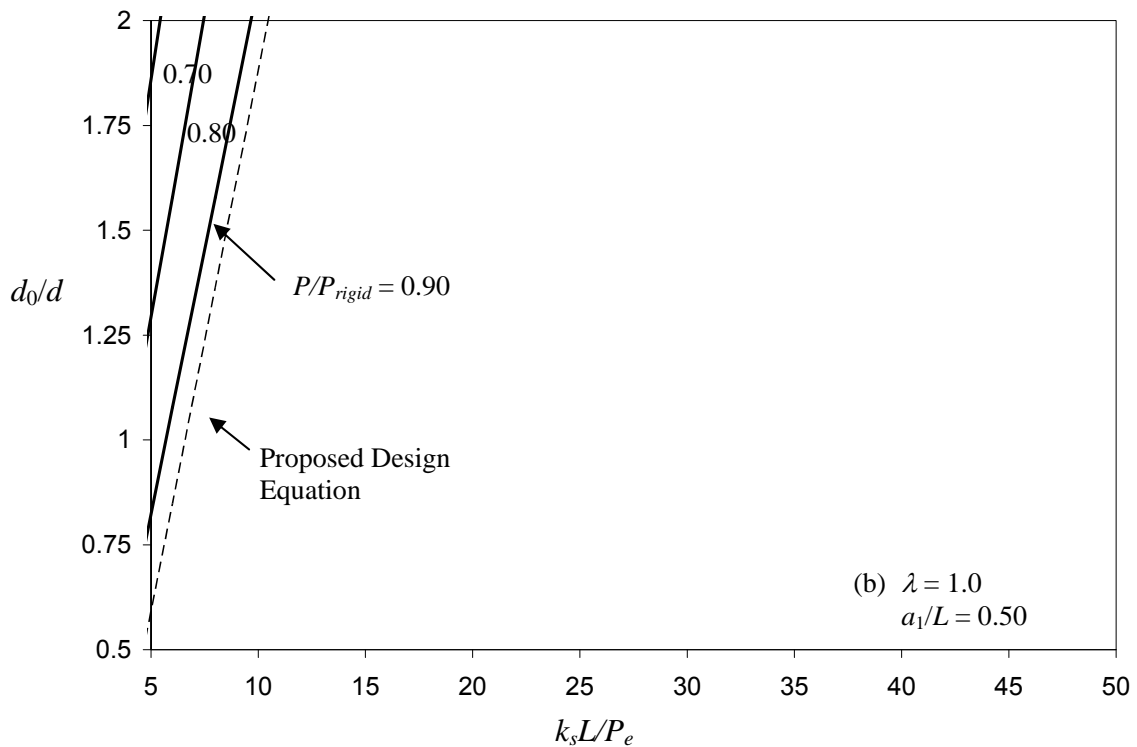
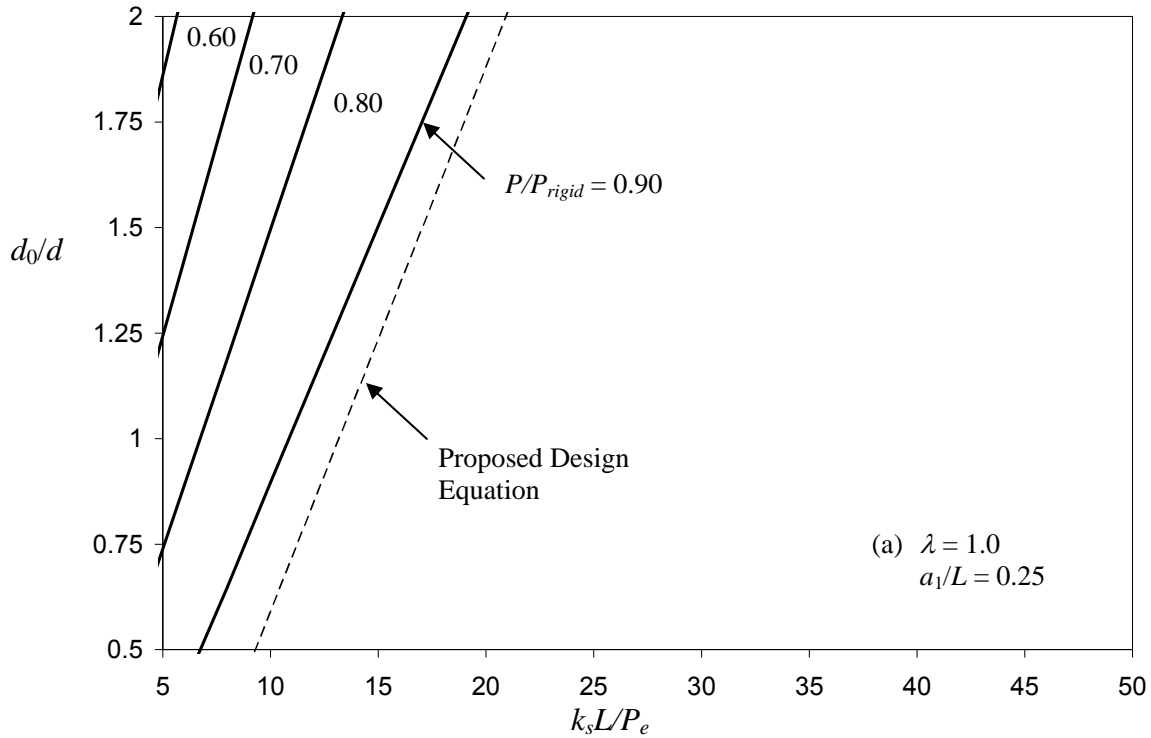


Figure 10. Relationship between Brace Stiffness and Deflection Ratio for a Given  $P/P_{rigid}$

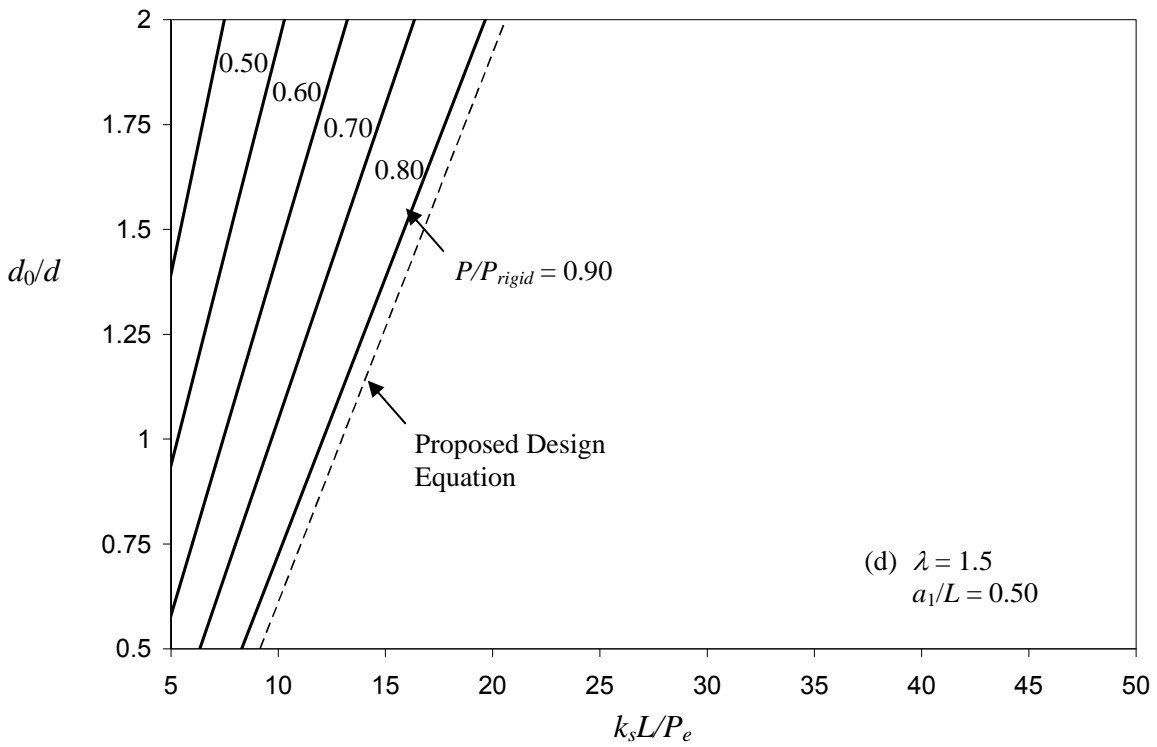
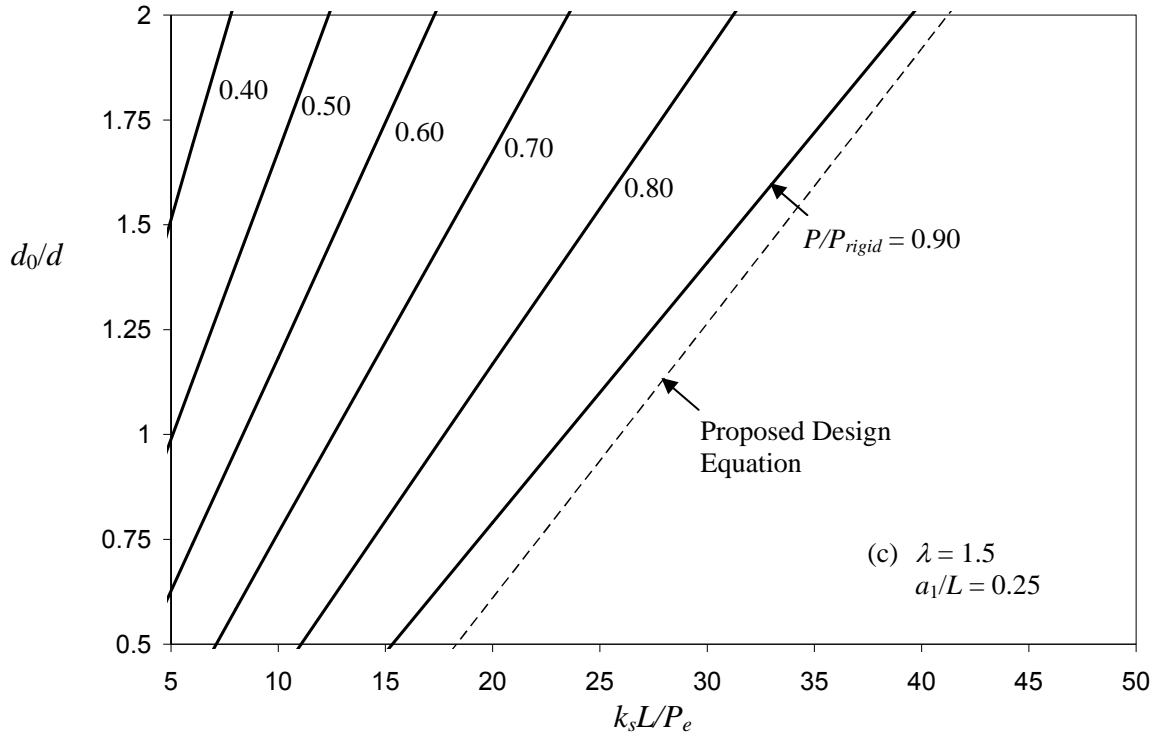


Figure 10 (Cont'd). Relationship between Brace Stiffness and Deflection Ratio for a Given  $P/P_{rigid}$

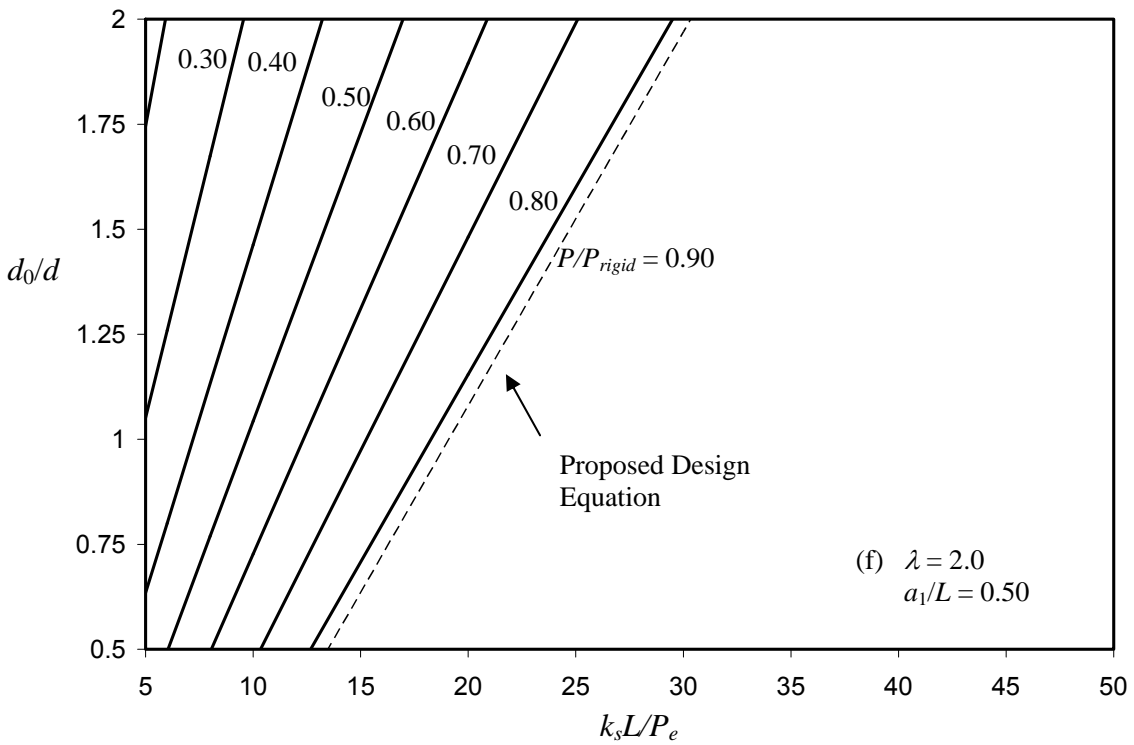
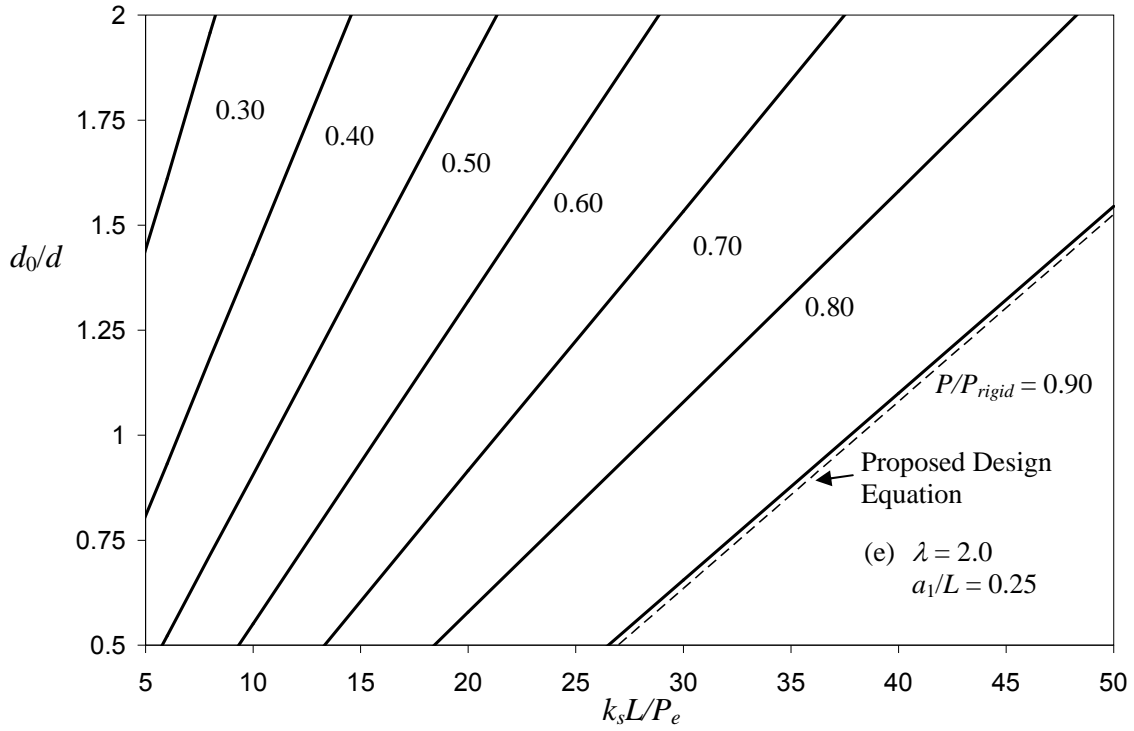


Figure 10 (Cont'd). Relationship between Brace Stiffness and Deflection Ratio for a Given  $P / P_{rigid}$



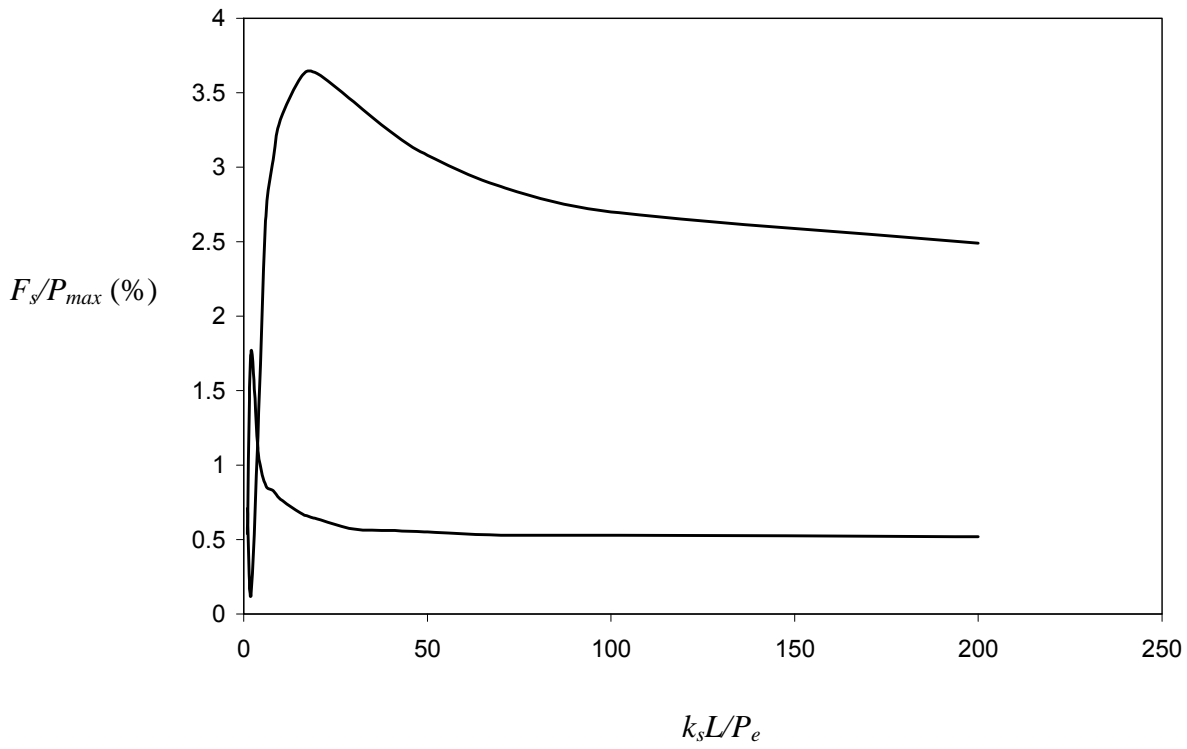


Figure 11. Envelope Curves for Brace Force

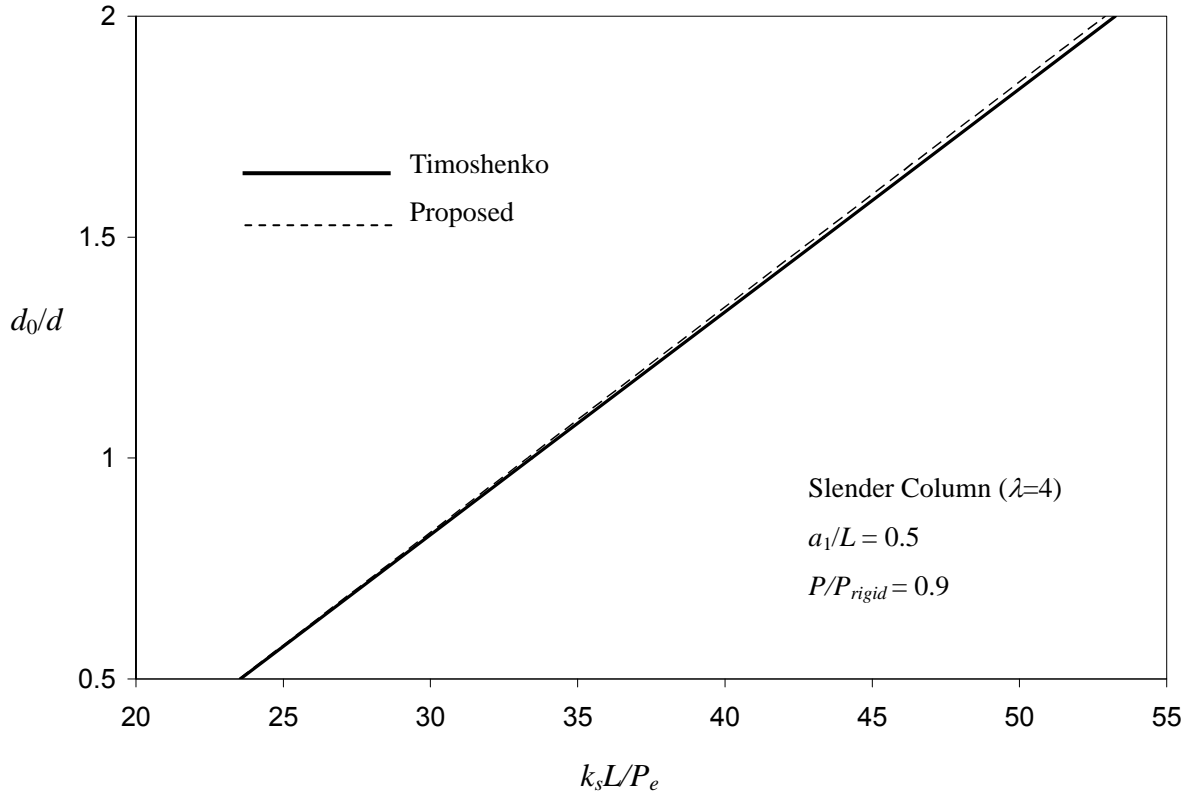


Figure 12. Comparison of Proposed Equation with Timoshenko's Solution

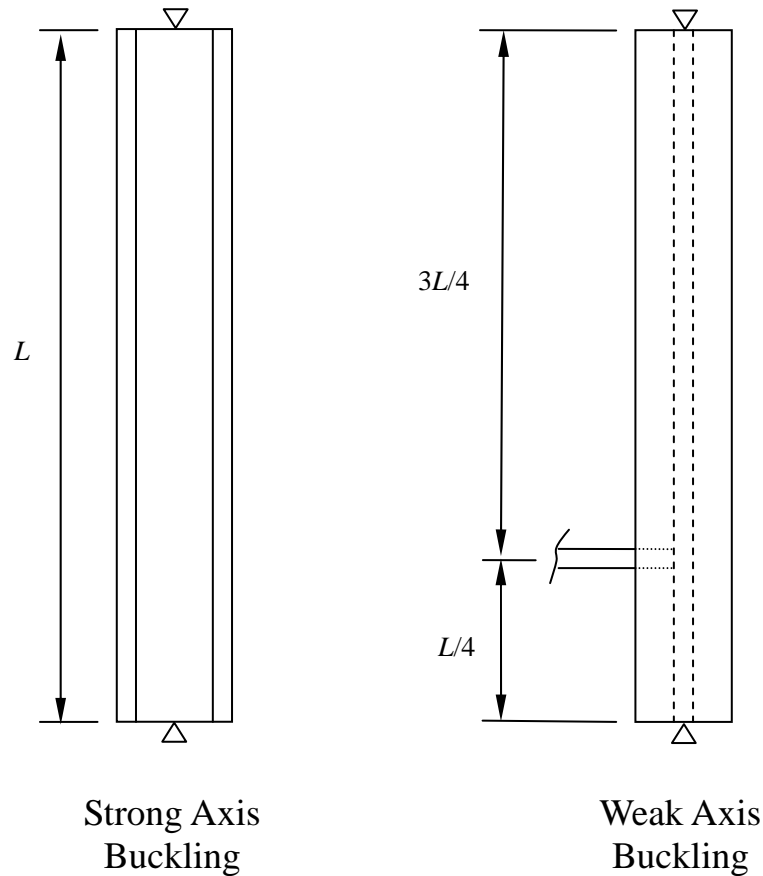


Figure 13. Example Problems

## 6. SUMMARY

In the conventional design of compression members braced against instability at some intermediate point, the practice is to assume that the brace is rigid and it does not undergo any deformation. As a result, the member being braced is assumed not to experience any lateral displacement at the location of the brace and can attain its fully-braced strength. In reality, this so-called fully-braced condition can only be realized if the brace is infinitely stiff. If the brace has a finite stiffness or if the compression member being braced is geometrically imperfect, the actual design compressive strength of the column will be less than its code-specified value. In this paper, the behavior of compression members with finite brace stiffness taking into considerations geometrical imperfection and inelastic effects was investigated. Based on the results of this study, the following conclusions can be drawn:

1. The brace is the most effective when it is placed at a point along the length of the column where maximum lateral deflection occurs at incipient instability.
2. The effect of the brace on the design compressive strength is less pronounced for short columns.
3. The concept of ideal brace stiffness applies only to a centrally braced pinned-pinned column.

4. When compared to the fully-elastic condition, the required force and stiffness of the brace increases once inelasticity sets in. For design purpose, the maximum brace force can be taken as 4% of the braced column strength.
5. The mathematical form of the initial out-of-straightness of the column is not an important design parameter as it has very little effect on the behavior of the braced column.
6. For a given  $P/P_{rigid}$ , a linear relationship exists between  $d_0/d$  and  $k_s L/P_e$ . Using this information, a design equation for  $k_s$  that allows a braced member to reach at least 90% of its fully-braced (i.e., code-specified) strength is proposed.

## ACKNOWLEDGMENT

The authors would like to thank the reviewers of this paper for their insightful comments and helpful suggestions. Their valuable inputs have helped us further address or clarify some of the concepts presented in this paper.

## REFERENCES

- [1] Bleich, F., "Buckling Strength of Metal Structures", McGraw-Hill, NY, 1952.
- [2] Bjorhovde, R., "Deterministic and Probabilistic Approaches to the Strength of Steel Columns," Ph.D. Dissertation, Lehigh University, Bethlehem, PA, 1972.
- [3] Galambos, T.V. ed., "Guide to Stability Design Criteria for Metal Structures", 5<sup>th</sup> edition, John Wiley and Sons, NY, 1998.
- [4] Winter, G., "Lateral Bracing of Columns and Beams," J. of Struct. Div., Proc. ASCE, 1958, Vol. 84, No. 2, pp. 1561-1-1561-22.
- [5] Timoshenko, S. and Gere, J.M., "Theory of Elastic Stability", McGraw-Hill, NY, 1961.
- [6] Urdal, T.B., "Bracing of Continuous Columns," Engrg. J., AISC, 1969, Vol. 6, No. 3, pp. 80-83.
- [7] Mutton, B.R. and Trahair, N.S., "Stiffness Requirements for Lateral Bracing," J. Struct. Engrg., ASCE, 1973, Vol. 99, No. 10, pp. 2167-2182.
- [8] Brush, D.O. and Almroth, B.O., "Buckling of Bars, Plates and Shells", McGraw-Hill, NY, 1975.
- [9] Trahair, N.S. and Nethercot, D.A., "Bracing Requirements in Thin-Walled Structures," in Developments in Thin-Walled Structures, Vol. 2, (J. Rhodes and A.C. Walker, editors), Elsevier, London, 1984, pp. 93-130.
- [10] Lutz, L.A. and Fisher, J.M., "A Unified Approach for Stability Bracing Requirements," Engrg. J., AISC, 1985, Vol. 22, No. 4, pp. 163-167.
- [11] Nair, R.S., "Forces on Bracing Systems," Engrg. J., AISC, 1992, Vol. 29, No. 1, pp. 45-47.
- [12] Plaut, R.H., "Requirements for Lateral Bracing of Columns with Two Spans," J. Struct. Engrg., ASCE, 1993, Vol. 119, No. 10, pp. 2913-2931.
- [13] Plaut, R.H. and Yang, J.-G., "Lateral Bracing Forces in Columns with Two Unequal Spans," J. Struct. Engrg., ASCE, 1993, Vol. 9, No. 10, pp. 2896-2911.
- [14] Zhang, H.-Y., Beliveau, J.-G., and Huston, D.R., "Minimum Lateral Stiffness for Equally Spaced Braces in Columns," J. Engrg. Mech., ASCE, 1993, Vol. 119, No. 9, pp. 1888-1897.
- [15] Wang, C.M. and Nazmul, I.M., "Buckling of Columns with Intermediate Elastic Restraint," J. Engrg. Mech., ASCE, 2003, Vol. 129, Issue 2, pp. 241-244.
- [16] Pincus, G., "On the Lateral Support of Inelastic Columns," Engrg. J., AISC, 1964, Vol. 1, No. 4, pp. 113-115.

- [17] Kitipornchai, S. and Finch, D.L., "Stiffness Requirements for Cross-Bracing," *J. Struct. Engrg.*, ASCE, 1986, Vol. 112, No. 12, pp. 2702-2707.
- [18] Ales, J.M, Jr. and Yura, J.A., "Bracing Design for Inelastic Structures," *Is Your Structure Suitably Braced*, SSRC, 1993, pp. 29-37.
- [19] Clarke, M.J. and Bridge, R.Q., "Bracing Force and Stiffness Requirements to Develop the Design Strength of Columns," *Is Your Structure Suitably Braced*, SSRC, 1993, pp. 175-86.
- [20] Gil, H. and Yura, J.A., "Bracing Requirements of Inelastic Columns," *J. of Constructional Steel Research*, 1999. Vol. 51, pp. 1-19.
- [21] Yura, J.A., "Winter's Bracing Approach Revisited," *Engineering Structures*, 1996, Vol. 18, No. 10, pp. 821-825.
- [22] McGuire, W., "Steel Structures", Prentice-Hall, Englewood Cliff, NJ, 1968.
- [23] Salmon, C.G. and Johnson, J.E., "Steel Structures - Design and Behavior", 4<sup>th</sup> edition, HarperCollins, NY, 1996.
- [24] CSA, Limit States Design of Steel Structures, CSA Standard CAN/CSA S16-01, Canadian Standards Association, Mississauga, Ontario, 2001.
- [25] Stanway, G.S., Chapman, J.C., and Dowling, P.J., "A Simply-Supported Column with a Transverse Elastic Restraint at any Position. Part 1: Behavior; Part 2: Design Models," *Proc. Instn. Civ. Engrs, Strucs. and Bldgs*, 1992, Vol. 94, No. 2, pp. 205-228
- [26] Lui, E.M. and Zhang, C.-Y., "Nonlinear Frame Analysis by the Pseudo Load Method," *Comp. and Struct.*, 1990, Vol. 37, No. 5, pp. 707-716.
- [27] ANSI/AISC 360-05, "Specification for Structural Steel Buildings, American Institute of Steel Construction", Chicago, IL, 2005.

# PERFORMANCE ON SPLIT TEE TYPE W.F. BEAM-TO-R.H.S. COLUMN CONNECTION USING PLUG WELD

T. Murai<sup>1</sup> and I. Kohzu<sup>2,\*</sup>

<sup>1</sup>Former Graduate Student, Division of Global Architecture,  
Graduate School of Eng., Osaka Univ., Suita, Japan

<sup>2</sup>Professor, Division of Global Architecture, Graduate School of Eng., Osaka Univ., Suita, Japan

\*(Corresponding author: E-mail: kohzu@arch.eng.osaka-u.ac.jp)

Received: 22 August 2007; Revised: 11 October 2007; Accepted: 15 October 2007

**ABSTRACT:** This paper presents an experimental investigation, dealing with mechanical property on a newly developed split tee type WF beam-to-RHS column connection using both plug and fillet welds in steel moment resisting frame. Initially, strength of plug weld subjected to tensile load has been evaluated from the test result of simple T-T joint experiment. Next, experiment of subassembly being welded split tee bracket to RHS column by means of plug weld and/or fillet weld has been conducted. And it has been shown that the proposed design formulae can predict fairly well the yield and ultimate strengths of the connection, after comparing with the experimental result.

**Keywords:** Steel moment resisting frame; beam-to-column connection; plug weld; fillet weld; bearing strength; loading experiment

## 1. INTRODUCTION

As an effective solution in order to avoid premature and brittle failure at the beam end due to weld defect and/or excessive strain concentration of welded beam-to-column connection in weak beam type steel moment resisting frame, it may be desired to adopt design method to share damage due to seismic inelastic behavior among the components of the connection, instead of applying conventional method to limit plastic zone only to beam end. For this reason, a newly developed beam-column connecting method is proposed here. In the connection, only tee shaped brackets are incorporated between WF beam and RHS column, as shown in Figure 1. The flange of the bracket is connected to the column face by means of plug welding as well as fillet welding at the corners. The bracket web is bolted together with the beam flange in order to transfer the beam bending moment and shear force to the column. The beam web, if necessary, can be connected to the column through a gusset plate, by using high strength bolts, to transfer beam shear, when the shear is dominant among beam stresses. The present work is intended to verify performance of the proposed connection using both plug and fillet welds, as shown in the figure.

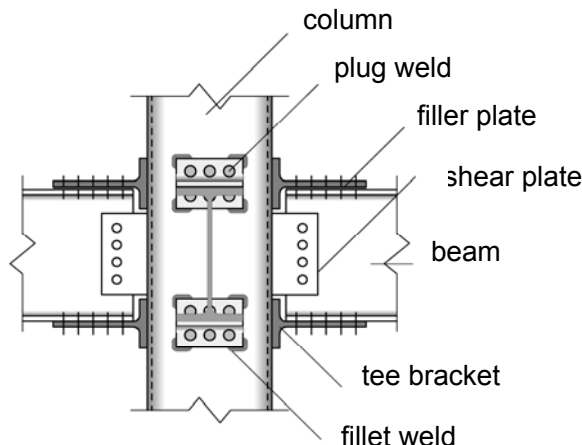


Figure 1. WF Beam-to-RHS Column Connection using Tee Bracket

## 2. TEST ON PLUG WELDED T-T JOINT SUBJECTED TO TENSION

### 2.1 Experimental Procedure

Plug weld is not commonly used as practical method to join members together in steel building structures, since such welding method is only applicable to shear joints in which the members are subjected to in-plane shear force, in many design standards as A.I.J. 1979[1] and 2005 [2], A.W.S. 2000[3] and A.I.S.C. 2005[4]. However, it seems to be useful to adopt the method to the connections of main members like as columns and beams, because of ease of fabrication and economy in comparison with ordinary beam-to-column connection with through diaphragm in seismic moment resisting frame, if the welding procedure would be adequately performed. For this reason, simple T-stub test was carried out in order to evaluate strength and deformation capacities as well as welding performance of plug welded connection.

Grade SM490B steel plates of JIS G3106 rolled steels specified for welded structure were used for the test. The plates were fabricated and assembled. And then, the flange plates were connected by plug welding, so as to shape T-T joint as illustrated in Figure 2. Mechanical properties of the plates obtained by coupon test are tabulated in Table 1. The lower T-stub was shaped so as to behave as rigid throughout the monotonic tensile experiment, by adding a pair of stiff rib plates between the flange and the web. The upper flange plates of 22 and 32 mm thick were used and connected to the lower flange plates of 32 mm thick, by means of plug welding of 28 mm diameter. CO<sub>2</sub> shielded arc welding, using JIS Z3312 YGW11 as MAG welding solid wire for mild and high strength steel up to the tensile strength of 490 N/mm<sup>2</sup>, was performed for jointing both the upper and the lower flange plates. Welders belonging to two different fabricators performed plug welding, in order to examine the effect of difference of welding performance on the mechanical properties of the joint. The welding condition by every welder, named as T or W, is tabulated in Table 2. Specimen types, named as T22 to W32, are identified in Tables 1 and 2.

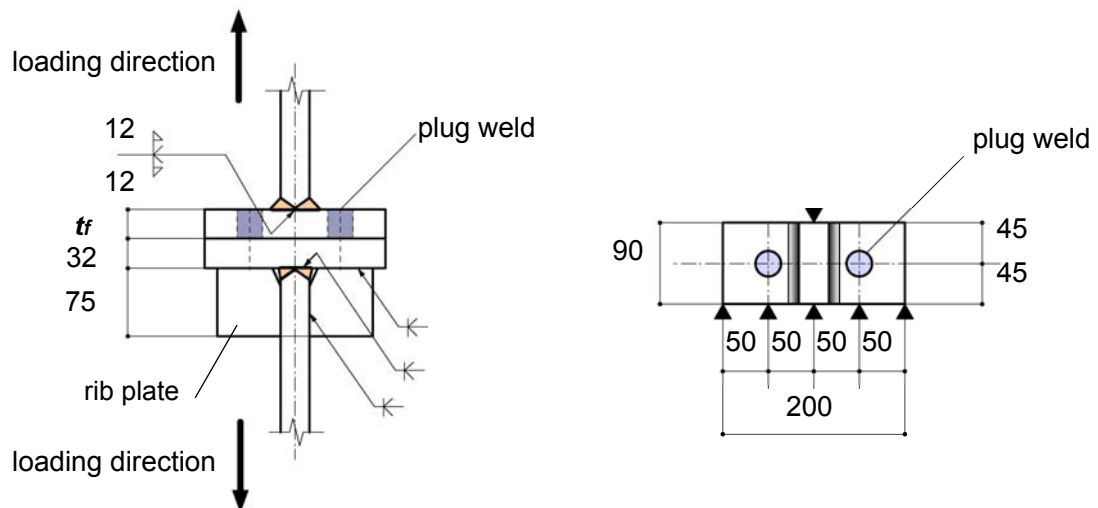


Figure 2. Geometrical Property of T-T Joint Specimen (unit : mm)

Universal testing machine (capacity 2000 kN) was used so that the specimen was statically loaded under monotonic loading condition by pulling the tip of the web until failure. Clip gauge type extensometers were set on the points shown as triangular symbols in Figure 2, in order to detect local distortion of the specimen during the experiment. The test set-up is shown in Figure 3.

Table 1. Mechanical Properties of Steel Plates used for T-T Joint

specimen type	plate thickness (mm)	yield strength (N/mm <sup>2</sup> )	tensile strength (N/mm <sup>2</sup> )	yield ratio (%)	elongation (%)
T22	22	397	554	72	21.2
T32	32	339	523	65	22.8
W22	22	390	537	73	22.5
W32	32	350	534	65	22.7

Table 2. Types of T-T Joint Specimens and Welding Conditions

specimen type	fabricator	$t_f$ (mm)	plug welding condition		
			current (A)	voltage (V)	arc time (sec)
T22	T	22	280	32	77
T32		32	280	32	107
W22	W	22	240	34	76
W32		32	240	34	104



Figure 3. Specimen mounted on the Testing Machine

## 2.2 Experimental Result

The typical load-local distortion relations are schematically shown in Figure 4. In accordance with that the abscissa of the figure gives positive in tension, it is recognized that the edge of flange (tip of flange) is subjected to compressive force. In addition, it can be observed that the load carrying capacity depends on the thickness of upper tee flange.

At the final stage of experiment, the plug welds fractured for every specimen after the upper tee flange deflected due to out of plane bending. Fracture surface in Figure 5, shows that the weld metal is pulled out throughout the cross section of plug weld without any defect like as incomplete penetration. In order to inspect weldability in the above proposed method, macro-structure test was performed, prior to T-T joint test. The example of test result is shown in Figure 6. From the figure, it can be observed that penetration is well achieved both in the upper and the lower flanges.

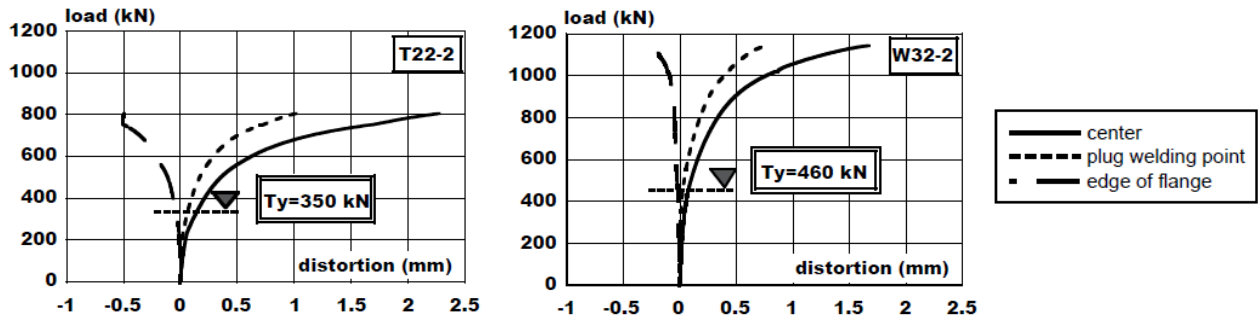
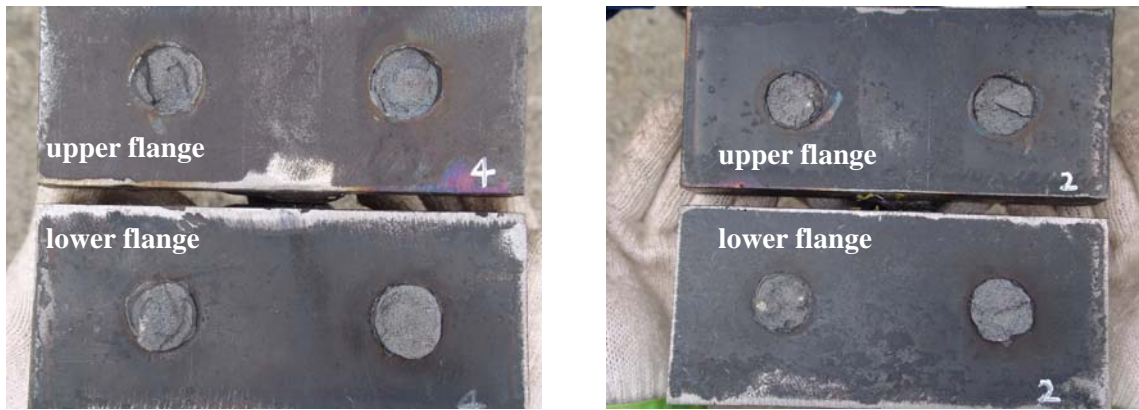
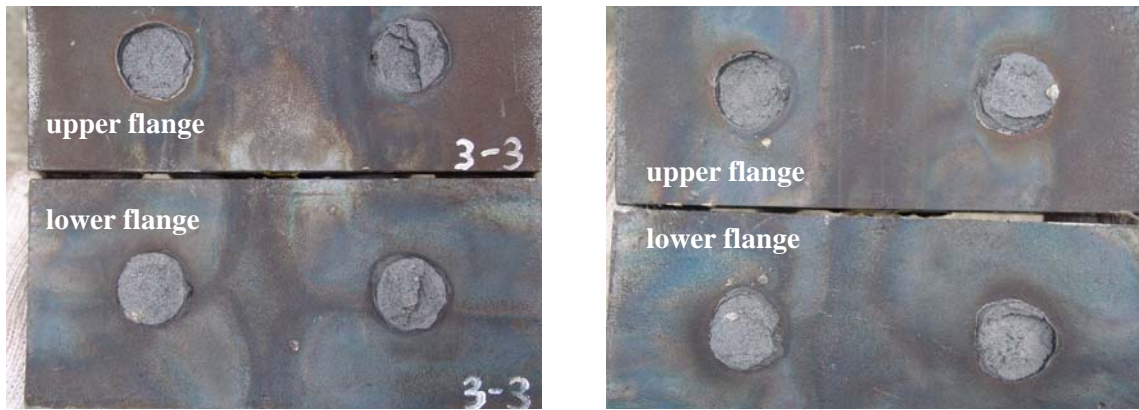


Figure 4. Load-Local Distortion Relation of T-T Joint Specimen



(a) T22-1

(b) T32-2



(a) W22-3

(b) W32-3

Figure 5. Fracture Surface of Plug Weld

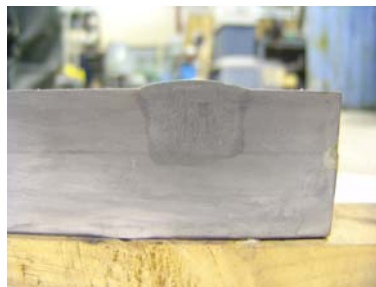


Figure 6. Macro-Structure Test Result of Plug Weld



## 2.3 Discussion

In this section, the strength of plug weld is evaluated based on the test result. From Figure 4, it can be recognized that force due to prying at the tip of tee flange is generated for every specimen. For this reason, the experimental resisting force of plug weld has to be evaluated in taking into consideration the effect of so called prying action.

Procedure to evaluate the experimental yield strength is as follows.

- I. Prepare experimental data set of load  $T$  and the corresponding local distortions.
- II. Formulate a model in which the upper flange plate is composed of a pair of uniform cantilever beams fixed at the point  $size / 2$  apart from the face of tee web. Where  $size$  is the size of fillet weld for reinforcement. Assume the loading condition where each beam is subjected to the loads  $P_p$  and  $P_r$  at the plug welded point and the tip of the beam, respectively, and that the reaction  $T / 2$  is generated at the fixed point. The above assumption is schematically shown in Figure 7. In the figure,  $\delta_c$ ,  $\delta_p$  and  $\delta_r$  are the distortions at the center, the point of plug weld and the edge of the flange, respectively. Derive elastic load-deflection relation of the beam under bending and shear, to formulate  $P_p$  as a function of  $T$  and the local distortion.
- III. Estimate load  $P_p$  by substituting the experimental data of load  $T / 2$  and local distortions in step I for the analytical relation in step II.
- IV. Plot the points with co-ordinates,  $(P_p, T)$ , on a graph.
- V. Draw the linear regression line of  $P_p - T$  plots from the origin to the proportional limit. Draw again a line with a slope of 1/3 of the regression line, and tangent to the  $P_p - T$  curve.
- VI. Define the ordinate of intersection point of the linear regression line and the tangential line, to the experimental yield strength of plug weld,  $P_{py(ex)}$ . After evaluating  $P_{py(ex)}$ , it is necessary to confirm that beam yielding occur only after yielding of plug weld. The yield load  $T_y$  can be found as the abscissa of intersection point.

The procedure from step IV to VI is illustrated in Figure 8.  $T_y$  in Figure 4, shows the example of experimental yield load obtained from the above procedure.

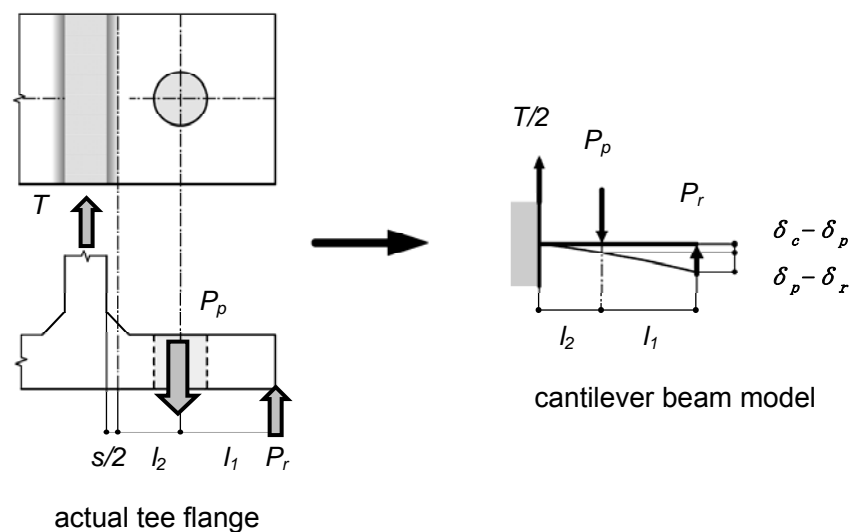


Figure 7. Cantilever beam model of actual tee flange subjected to tension

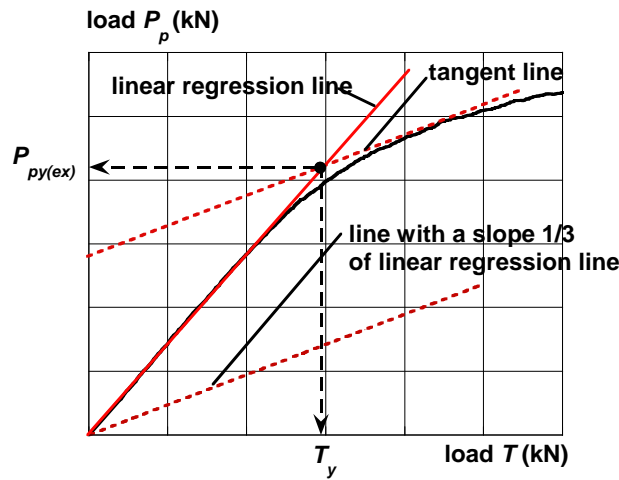


Figure 8. Evaluation of  $P_{py(ex)}$  and  $T_y$  from Experimental Result

The experimental ultimate strength of plug weld can be evaluated by the following procedure.

- VII. Perform step-by-step elasto-plastic analysis of the cantilever beam in the manner of numerical integration. Calculate the bending moment corresponding to the rotation angle at the fixed end, under the assumption where a bi-linear moment-curvature relation with the second flexural rigidity of 0.005 times the initial one is applicable to the material of beam.
- VIII. Perform bi-linear approximation of the fixed end moment-rotation relation of the beam, in order to derive the moment-rotation relation in the continuous form.
- IX. Calculate the rotation angle,  $\theta_{end}$ , from the experimental local distortion by using Eq. 1, and evaluate the fixed end moment by substituting the rotation angle for the bi-linear moment-rotation relation.

$$\theta_{end} = (\delta_c - \delta_p) / l_2 \tag{1}$$

where  $l_2$  is the distance between fixed end and the center line of plug weld.

- X. Estimate  $P_p$  so as to satisfy equilibrium condition.
- XI. Find the maximum value of  $P_p$ , and define the value as the experimental ultimate strength of plug weld,  $P_{pu(ex)}$ .

As pointed out in the fracture surface observation in Figure 5, it is rational to consider that plug weld can resist over the cross section until the fracture. Therefore, the estimated strength of plug weld,  $P_{ps(cal)}$ , can be derived in Eq. 2.

The experimental strength of plug weld,  $P_{ps(ex)}$ , derived from above described procedure, is compared with the estimated value,  $P_{ps(cal)}$ .

$$P_{ps(cal)} = \frac{\pi d_p^2}{4} \sigma_{ps} \tag{2}$$

where the letter,  $s$ , of subscript,  $ps$ , is rewritten to  $y$  in the case of yielding, or  $u$  at the ultimate state. Notations,  $\sigma_{ps}$  and  $d_p$ , indicate the yield or the ultimate strength of plug weld

metal, and the diameter of plug weld, respectively. However, in the present case, the material strength of upper flange plate,  $\sigma_{fs}$ , is used in place of the actual strength of weld metal because of difficulty of direct measurement.

The experimental strength of plug weld,  $P_{ps(ex)}$ , derived from above described procedure, is compared with the estimated value,  $P_{ps(cal)}$ , and the results are shown in Figure 9. From the figure, it can be recognized that  $P_{py(cal)}$  estimates the yield strength fairly well, though  $P_{pu(cal)}$  is comparatively lower than  $P_{pu(ex)}$  at the ultimate state, in spite of difference between two welding conditions.

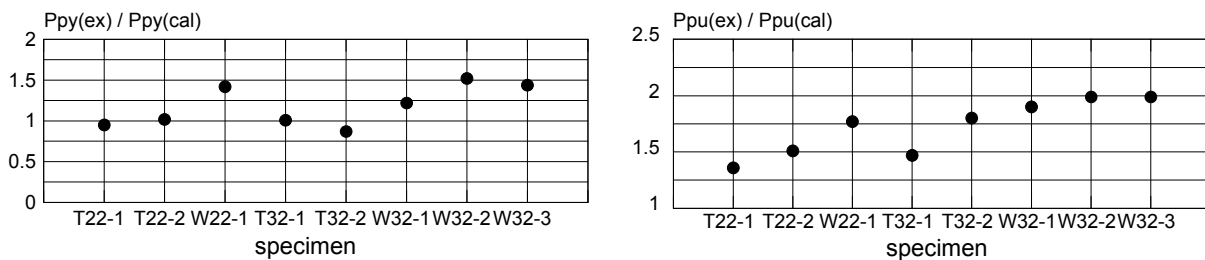


Figure 9. Comparison of Experimental and Estimated Strengths of Plug Weld

### 3. TEE BRACKET-RHS COLUMN SUBASSEMBLAGE TEST

#### 3.1 Objective of Experiment

In order to confirm the applicability utilizing the proposed connecting method, subassembly specimens composed of RHS column and split tee bracket were fabricated and used for monotonic tensile loading test.

#### 3.2 Specimen and Experimental Method

Figure 10 illustrates the general view of specimen. The columns were cold formed rectangular hollow sections for steel building structure, specified as BCR295, whose yield and tensile strengths in the specification were greater than 295 and 400 N/mm<sup>2</sup>, respectively. Tee brackets were made from JIS SS400 wide flange sections. As tabulated in Table 3, the specimens were classified into two groups such as A and C-types, and B and D-types, in accordance with whether the tee flanges were fillet welded to the columns additionally, or not. Their details of welding are shown in Figure 11 and Table 4. When fillet welding, the specimens were tilted to an angle of 45 degrees, so as to shape the bead into right isosceles triangle. Three identical specimens for each type were prepared and tested. Several extensometers were installed in order to measure both global and local deformations of the specimens, as shown in Figures 12 and 13. Specimens set on a universal testing machine (capacity of 1000 kN) in Figure 12, were loaded along the direction as shown in Figure 13, until they were torn out or deformed excessively so that interruption of the test was indispensable.

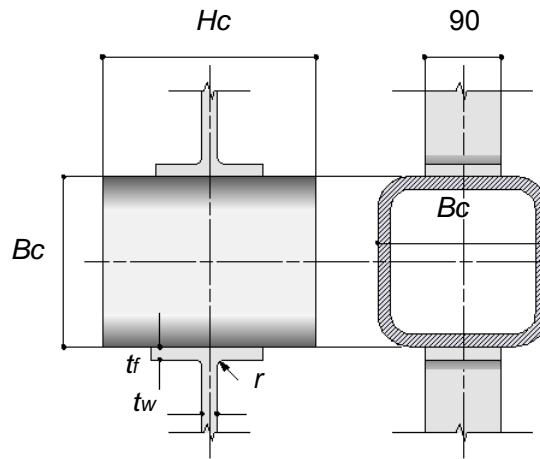


Figure 10. Overall View of Subassemblage Specimen

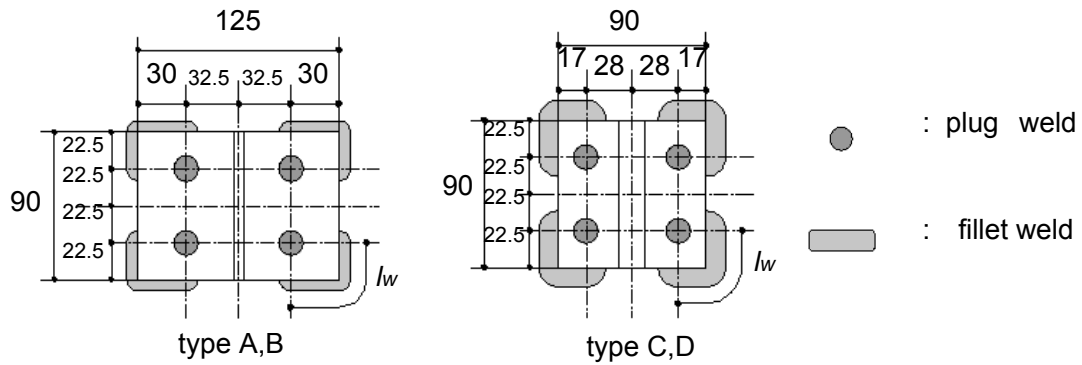


Figure 11. Plug and Fillet Welds of Subassemblage Specimen (unit : mm)

Table 3. Geometrical properties of component members

specimen type	component member		$t_f^*$	$t_w^*$	$r^*$	$B_c^*$	$H_c^*$	$l_w^*$
	tee bracket	column	(mm)					
A	T-220x125x6x9 (cut from H-250x125x6x9)	SHS-200x200x9	9	6	8	200	250	52.5
B								-
C	T-220x90x16x16 (cut from H-900x300x16x28)	SHS-300x300x16	16	16	18	300	350	39.5
D								-

\*: Notations in the table are identified in Figures 10 and 11.

Table 4. Welding Condition

specimen	welding condition	
	fillet weld	plug weld
A	size 7 mm, 1 pass	diameter 15 mm depth : 9 mm
B	-	
C	size 12 mm, 3 passes	diameter 15 mm depth : 16 mm
D	-	



### 3.4 Calculated Design Strength of Specimen

As seen in Figures 10 and 11, the specimen consists of three or four component members like as split tee, column, plug weld and/or fillet weld. For this reason, in order to estimate the strength of the subassembly specimen as one unit, the strength of each component member initially has to be evaluated. The strength of individual member can be found as the minimum value among the strengths, which have been computed for considerable failure modes, as will be described in following sections. Finally, the overall strength of the subassembly specimen can be estimated by adopting the lowest of the strengths of the component members.

#### 3.4.1 Strength of plug weld

In designing the specimen, three types of failure modes like as mode 1 to 3, that is, plug weld fracture (mode-1), shear failure of plug weld (mode-2) and punching shear failure of plate (mode-3), were assumed. These three modes are illustrated in Figure 14, and the corresponding design equations to three failure modes are formulated as follows.

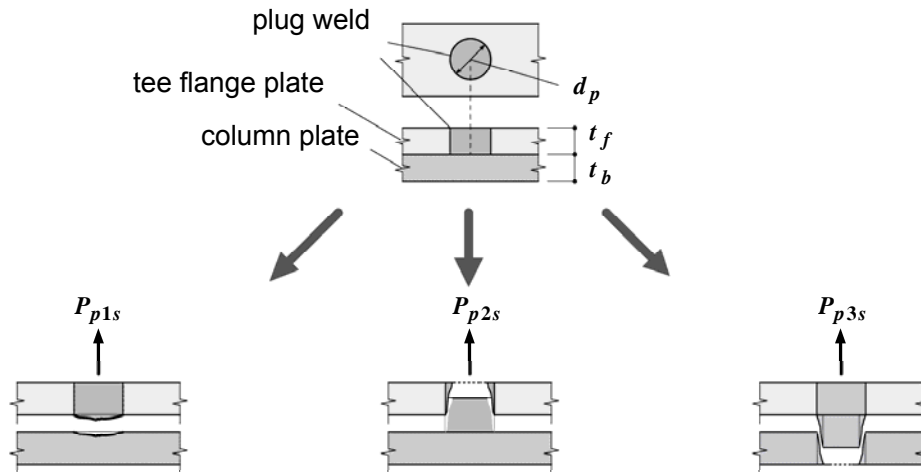


Figure 14. Failure Mechanisms of Plug Weld

For mode 1, Eq. 3, the identical equation with Eq. 2, can be formulated. When the thickness of tee flange plate is comparatively thin, shear yielding or failure of the plate will occur around the plug weld as shown in mode 2, and the strength per single plug weld can be formulated in Eq. 4. On the other hand, in the case of the connection with the column plate thinner than the tee flange plate, so called punching shear will occur as shown in mode 3, the corresponding strength can be formulated in Eq. 5.

$$P_{p1s} = \frac{\pi d_p^2}{4} \sigma_{ps} \quad (3)$$

$$P_{p2s} = \pi d_p t_f \frac{\sigma_{fs}}{\sqrt{3}} \quad (4)$$

$$P_{p3s} = \pi d_p t_b \frac{\sigma_{cs}}{\sqrt{3}} \quad (5)$$

where  $\sigma_{ps}$  and  $\sigma_{cs}$  are the yield or tensile strength of plug weld and the column plate, respectively. In Eq. 3, the strength of plug weld refers to the lower of the strengths of tee flange plate and column plate. Finally, the design strength of plug weld in tension can be decided as the minimum among Eqs. 3, 4 and 5, as formulated in Eq. 6.

$$P_{ps} = \min\{P_{p1s}, P_{p2s}, P_{p3s}\} \tag{6}$$

After substituting the material strengths shown in Table 5 for Eqs. 3 to 5, the design strengths of single plug weld for type-A to D specimens can be calculated as in Table 6.

Table 6. Calculated Strength of Single Plug Weld in Tension

specimen type	yield strength				ultimate strength			
	$P_{p1y}$	$P_{p2y}$	$P_{p3y}$	$P_{py}$	$P_{p1u}$	$P_{p2u}$	$P_{p3u}$	$P_{pu}$
	(kN)			(kN)	(kN)			(kN)
A, B	54	69	86	54	80	103	104	80
C, D	51	134	180	51	79	208	211	79

□ : show the lowest of the strengths which result in  $P_{ps}$ .

### 3.4.2 Strength of tee bracket

It is well known that three failure modes, like as shown in Figure 15, can be assumed in response of the strength of the component, when bolted T-stub is subjected to tensile force, as has already been reported by Faella et al. [5] and [6]. After substituting the bolt for plug weld, the conventional equations can be applied for strength prediction of the presented connection.

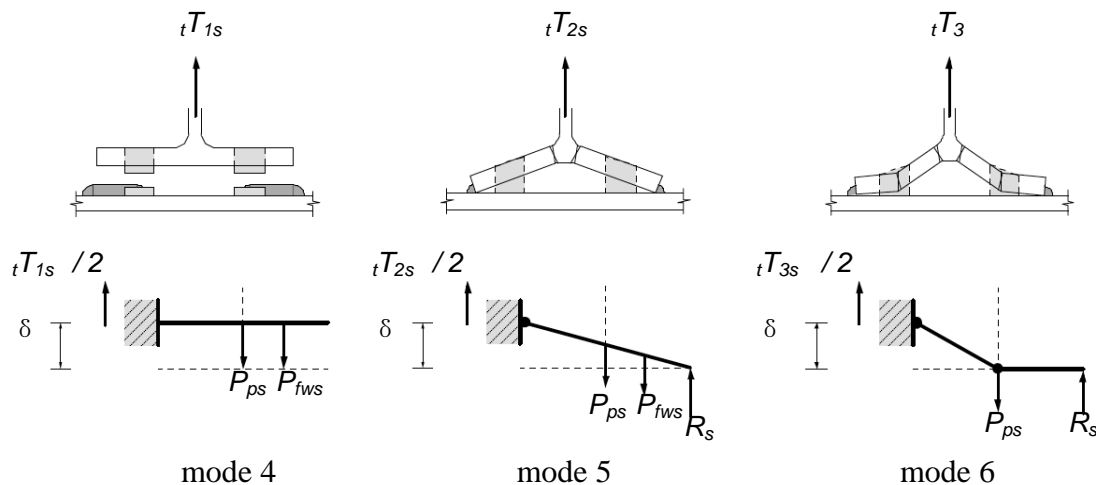


Figure 15. Failure Mechanisms of Tee Bracket

When the tee bracket is loaded in tension, it is assumed that the flange behaves like as a pair of cantilever beams as shown in Figure 16. In the figure,  $r$  denotes the radius of web fillet. Depending on the stiffness and the strength of tee flange, it can be drawn that there are three failure modes as in Figure 15.

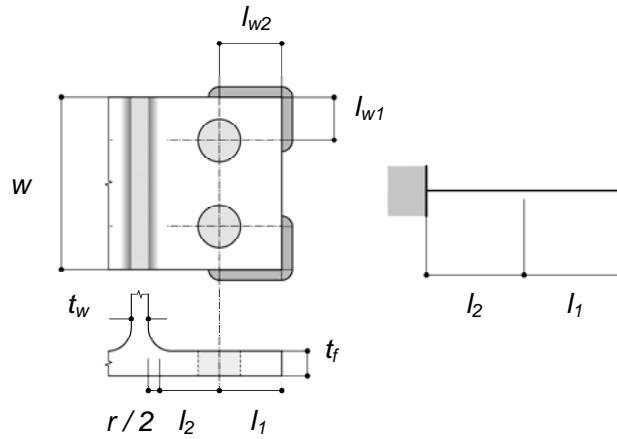


Figure 16. Cantilever Beam Model of Tee Bracket

Mode 4 corresponds to the case where the tee flange is very stiff and yielding or fracture will occur only at the plug weld and/or fillet weld. In this case, the strength of tee bracket,  $T_{s1}$ , can be evaluated in Eq. 7.

$$T_{s1} = 2nP_{ps} + 4(l_{w1} + l_{w2})p_{fws} \quad (7)$$

where  $n$  indicates the number of plug weld at each projection of the bracket flange, and  $P_{ps}$  is the strength of plug weld determined by Eq. 6. The second term of the right side in the equation indicates the strength of the fillet weld, and  $l_{w1}$ ,  $l_{w2}$  and  $p_{fws}$  are the lengths of fillet weld shown in Figure 16 and the strength of fillet weld per unit length, respectively.  $p_{fws}$  can be calculated using the yield or tensile strength of fillet weld per unit area,  $\sigma_{fws}$ , and the throat thickness,  $a$ , as in Eq. 8. The thickness,  $a$ , can be evaluated using the size of fillet weld,  $size$ , as in Eq. 9.

$$p_{fws} = 1.4a \frac{\sigma_{fws}}{\sqrt{3}} \quad (8)$$

$$a = 0.7size \quad (9)$$

In mode 5, failure mechanism can be established when plastic zones are generated at the fixed ends of the bracket flanges and the plug welds as well as the fillet welds. In this case, the strength of tee bracket,  $T_{s2}$ , can be evaluated as follows.

$$T_{s2} = \frac{2 \left( wM_{0s} + nP_{ps}l_1 + 2M_{fws}l_{w1} + p_{fws}l_{w2}^2 \right)}{l} \quad (10)$$

where  $w$  and  $l_1$  are the width and the partial length of tee bracket as shown in Figure 16, respectively.  $M_{0s}$  is the fully plastic or ultimate moment per unit width of bracket flange, and can be calculated using the thickness of flange,  $t_f$ , and using the yield or tensile strength of flange as equated in Eq. 11. If the fillet weld at the free end of bracket flange becomes yielding or collapse due to out of plane bending, the fully plastic or ultimate moment of fillet weld per unit



length,  $M_{fws}$ , as equated in Eq. 12, has to be accounted in Eq. 10. The total length of bracket flange as a cantilever beam,  $l$ , can be equated as in Eq. 13.

$$M_{0s} = \frac{t_f^2 \sigma_{fs}}{4} \quad (11)$$

$$M_{fws} = \frac{a^2 \sigma_{fws}}{4} \quad (12)$$

$$l = l_1 + l_2 \quad (13)$$

If yielding does occur only at the bracket flanges as shown in Figure 15, the strength of tee bracket in mode 6,  $tT_{s3}$ , can be equated as follows.

$$tT_{s3} = \frac{4wM_{0s}}{l_2} \quad (14)$$

After applying the above formulae and the material strengths to every type of subassembly specimen, the design strength of tee bracket,  $tT_s$ , can be estimated from Eq. 15, as the lowest of the strengths of three types of failure modes in Table 7.

$$tT_s = \min\{tT_{s1}, tT_{s2}, tT_{s3}\} \quad (15)$$

Table 7. Calculated Strength of Tee Bracket

specimen type	yield strength (kN)				ultimate strength (kN)				failure mode
	$tT_{y1}$	$T_{y2}$	$tT_{y3}$	$T_y$	$tT_{u1}$	$T_{u2}$	$tT_{u3}$	$T_u$	
A	466	185	120	120	666	270	179	179	mode 6
B	214	138	82	82	318	205	122	122	mode 6
C	511	404	1260	404	794	627	1970	627	mode 5
D	203	314	1260	203	315	488	1970	315	mode 4

□ : show the lowest of the strengths which result in  $tT_s$ .

### 3.4.3 Strength of column due to out-of-plane bending

Since the width-thickness ratio of column used in this experiment, is comparatively large, the plate of the column attached to the tee bracket tends to deform out of plane. It is well known that strength of RHS column due to out-of-plane bending can be well predicted by applying yield line theory, as has been reported by Morita et al. [7], Yamamoto et al. [8] and Harada et al. [9]. Taking into consideration existence of fillet weld at the corners of tee flange, two types of failure mechanism can be assumed, as shown in Figure 17.

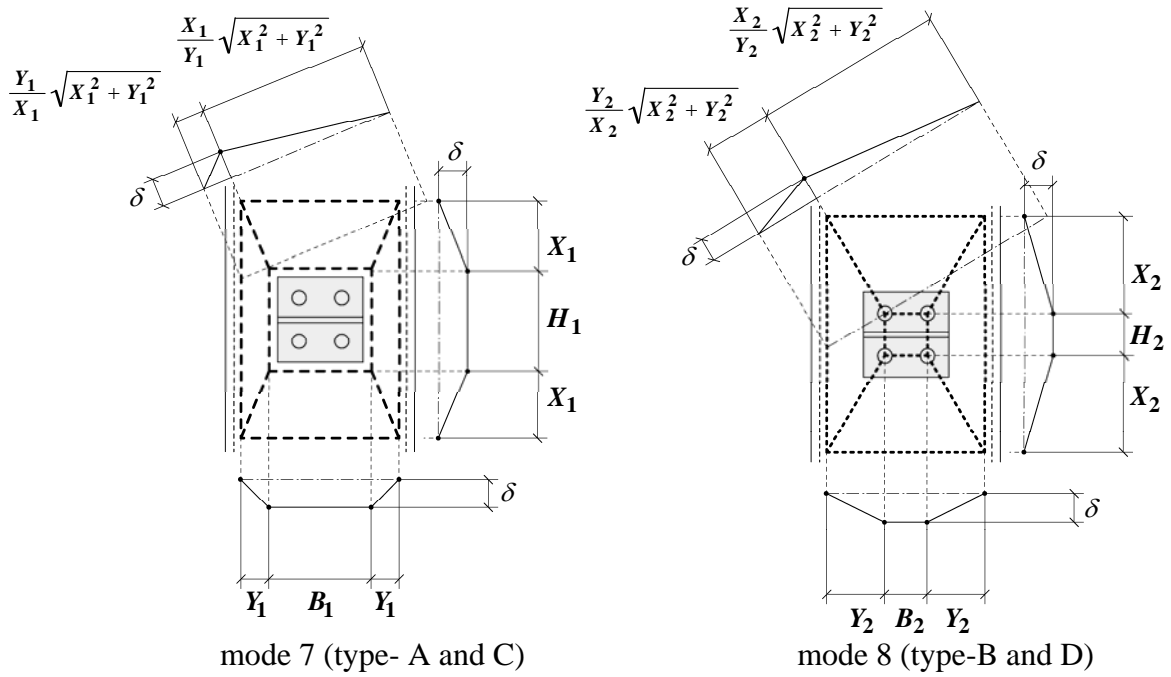


Figure 17. Failure Mechanisms of RHS Column

As a result, the tensile force transferred to the column through the tee bracket,  ${}_cT_{sm}$ , can be derived from Eq. 16. The subscript  $m$  is set to 1 or 2, for mode 7 or 8, respectively.

$${}_cT_{sm} = \frac{t_c^2 \sigma_{cs}}{2} \left( \frac{2Y_m + B_m}{X_m} + \frac{4X_m + 2H_m}{Y_m} \right) \tag{16}$$

$X_m$  and  $Y_m$  in Eq. 16 can be calculated by Eqs. 17 and 18.

$$X_m = \frac{1}{2} \sqrt{Y_m (B_m + 2Y_m)} \tag{17}$$

$$Y_m = \frac{1}{2} (B_c - B_m - 2r_c t_c) \tag{18}$$

where  $t_c$  and  $r_c$  denote the thickness and the corner radius of column, respectively. Notations,  $B_m$  and  $H_m$ , are the lengths shown in Figure 17.

After substituting the specific values for Eq. 16, the column strength due to out-of-plane bending,  ${}_cT_s$ , can be evaluated by applying the corresponding  $m$  to Eq. 19. The results are tabulated in Table 8.

$${}_cT_s = {}_cT_{sm} \tag{19}$$

Table 8. Calculated Out-of-Plane Bending Strength of Column

specimen type	$cT_y$	$cT_u$	$m$	failure mode
	(kN)	(kN)		
A	359	433	1	mode 7
B	171	206	2	mode 8
C	877	1026	1	mode 7
D	514	602	2	mode 8

Finally, the calculated strength of connection for every specimen,  $_{cal}T_s$ , can be evaluated as the lowest strength in Tables 7 and 8, by adopting Eq. 20, and the calculated result is summarized in Table 10.

$$_{cal}T_s = \min\{T_s, cT_s\} \quad (20)$$

### 3.4 Experimental Result

The test was terminated after fracture due to bending of tee flanges for A-type specimens, or after rupture due to tearing of plug welds for D-type specimens, whereas the test of B or C-type specimens was interrupted because of excessive deformation due to out of plane bending of column flanges. Typical load-displacement relations obtained from the test result are illustrated in Figure 18. The figure shows responses of the global as well as the local displacements such as the inside measurement of column, the distance between the upper or the lower tee flange and the column detected by displacement transducers shown in Figure 13. From the Figure 18, it can be observed that the load-inside measurement of column relation is very close to the load-global displacement relation in the cases of B and D-type specimens, whereas for A and C-type specimens, the inside measurement of column is comparatively smaller than the global displacement. Since each tee bracket flange of B and D-type specimens is connected to the column at only 4 points by means of plug weld, the global displacement of the specimen is governed by the deformation of column due to out-of-plane bending and it results in lower rigidity of the connection. On the other hand, the stiffness of the connection becomes comparatively higher for A and C-type specimens with fillet welds added to each tee bracket flange at the corner, because the tee bracket can efficiently resist against out-of-plane bending of column plate. Figure 19 shows the typical example of geometrical configuration of the connection after finishing of the test. As observed in (a) of the figure, tee bracket flange of specimen A3 is torn out near the plug weld and the fillet welds are ruptured, with excessive deformation of the tee flange at the center. On the contrary, specimen B2 in (b), whose component members are identical with those of specimen A3, deflects due to excessive out-of-plane deformation of the column, because of absence of fillet welds at the corners of tee bracket flange. Comparison of test results of specimen C1 in (c) and D3 in (d) suggests that fillet welds at the corners of tee flanges are effective in increase of both strength and rigidity of connection.

C and D-type specimens consist of thicker plates of members but lower contact areas between tee flange plates and column faces in comparison with those of A and B-type specimens. Findings obtained from experimental results of 4 types specimens will lead to essential guidelines required in designing the proposed connection illustrated in Figure 1, like as proportioning tee brackets and columns in respect to rigidity of the connection. However, in the present study, the attention is only focused on evaluating the strength of subassembly specimens. For this reason, further research concerning with rigidity of the subassembly with different proportions will be needed.

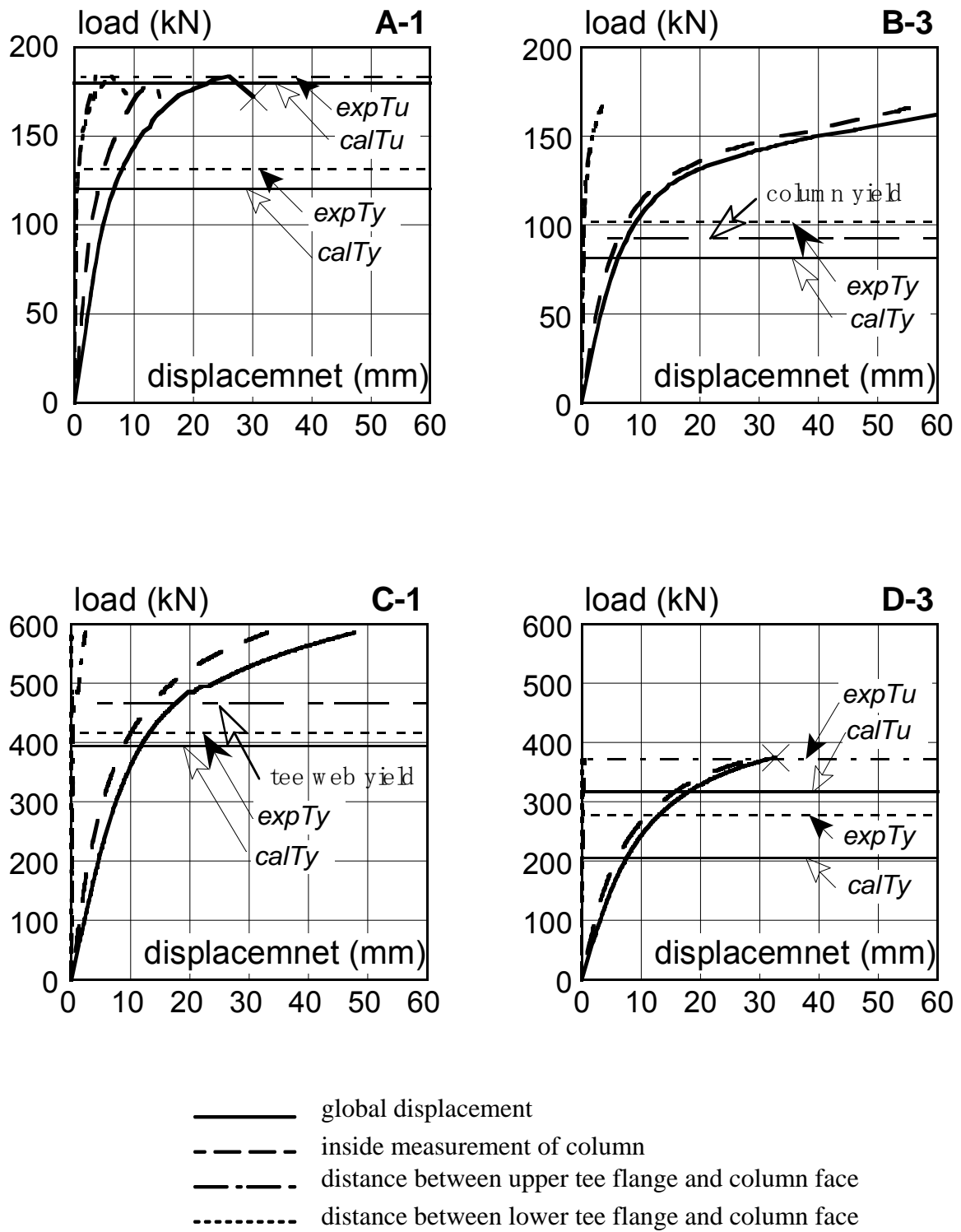
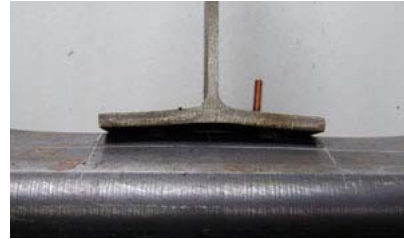


Figure 18. Result of Load-Displacement Relation of Subassemblage Specimen



(a) rupture of bracket flange and fillet weld (specimen A3)



(b) deformed column and flexure of tee bracket flange (specimen B2)



(c) deformed column and detail of fillet weld (specimen C1)



(d) deformed column and fracture surface of plug weld (specimen D3)

Figure 19. Test Result of Subassemblage Specimen

### 3.5 Discussion

The experimental yield strength for each specimen is defined as follows: In the load-global displacement relation, let draw a straight line having a slope of initial stiffness through the origin, furthermore, draw a tangential line having a slope of one thirds of initial stiffness on the load-global displacement curve and get the intersection point between the above two lines. Set the ordinate of the intersection point as the yield strength. Such procedure is schematically shown in Figure 20.

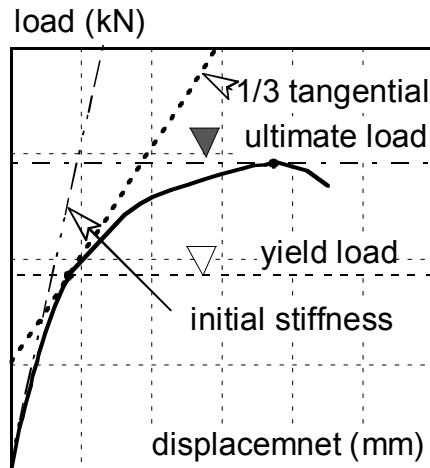


Figure 20. Definition of Experimental Yield Load of Specimen

It is evident from the test result of B -type specimen as shown in (b) of Figure 19 that the failure mode observed after the test termination is somewhat different from the initially predicted mode. That is, the column plate was folded at the center like as house roof along the longitudinal direction. For this reason, other failure modes consisted of three or four yield lines along the longitudinal direction of the column have been considered for four types of specimens, as illustrated in Figure 21. The locations of plastic hinge lines have been identified from the bending moment distribution of the columns which can be idealized as rigid frames. Since the tee bracket flanges are rigidly connected to the columns in the manner of both plug and fillet welds for A and C-type specimens, plastic hinge lines along the longitudinal directions of the columns will be formed just outside the fillet weld lines (mode 9). In the cases of B and D-type specimens, the plastic hinge lines will be formed at the centers of the column faces beneath the tee bracket flanges (mode 10), because the bracket flanges are connected to the columns only at the points of plug welds. For this reason, the number 3 or 4 is added to notation  $m$ , to identify mode 9 or 10, respectively. From the above consideration, the strength of the connection for two additional failure modes can be evaluated as tabulated in Table 9.

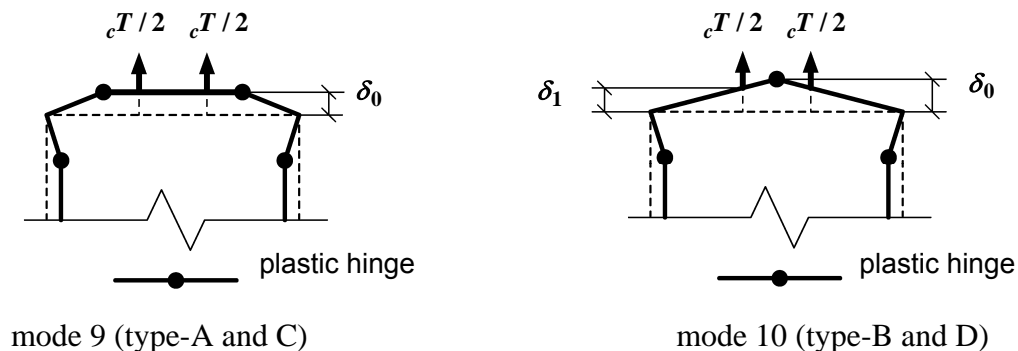


Figure 21. Additional Failure Mechanisms of Column

Table 9. Additional Out-of-Plane Bending Strength of Column

specimen type	yield strength (kN)	ultimate strength (kN)	$m$	failure mode
	$cT_y$	$cT_u$		
A	150	180	3	mode 9
B	93	112	4	mode 10
C	397	464	3	mode 9
D	290	338	4	mode 10

Table 10 summarizes the calculated and the experimental strengths, and the accuracy of prediction. These specific strengths are also shown in Figure 18, as  $_{exp}T_s$  and  $_{cal}T_s$ .

Table 10. Comparison with Calculated and Experimental Strengths of Subassemblage Specimen

specimen		$_{cal}T_y$	$_{exp}T_y$	$_{exp}T_y / _{cal}T_y$	$_{cal}T_u$	$_{exp}T_u$	$_{exp}T_u / _{cal}T_u$	failure mode	
		(kN)			(kN)			predicted	exp.
A	1	117	132	1.13	173	184	1.06	mode 6	mode 6
	2		133	1.14		196	1.13		
	3		117	1.00		178	1.03		
B	1	82 (93)	93	1.14	(112)	146<	(1.30)<	mode 6 (mode 10)	-
	2		102	1.25		165<	(1.47)<		
	3		102	1.25		167<	(1.49)<		
C	1	397	417	1.05	(464)	585<	(1.26)<	mode 9	-
	2		417	1.05		578<	(1.25)<		
	3		417	1.05		562<	(1.21)<		
D	1	203	272	1.34	315	377	1.20	mode 4	mode 4
	2		272	1.34		330	1.05		
	3		278	1.37		374	1.19		

In the case of B-type specimen, the calculated yield strengths for modes 6 and 9 are not so far apart from each other. For this reason, it is conjectured that after the specimen yields initially at mode 6, the deflection of the column becomes significantly so as to form mode 10. After forming such yield mechanism, the specimen resists against external tensile force, but deforms excessively from the original shape, because of sufficient axial resistant capacity of column webs parallel to the longitudinal direction of the specimen. In the case of C-type specimen, since the tee bracket web yields at 468 kN, the specimen deforms both at the column and the web. From the table, the design formulae may be applicable for prediction of strength of subassemblage specimen.

## 4. CONCLUSIONS

Performance on split tee bracket-to-RHS column connection using both plug weld and fillet weld has been investigated by conducting two series of tests. The following conclusions can be deduced from the test results:

- [1] Strength of plug weld alone has been initially examined by using simple T-T specimen, and it has been shown that the yielding can be predicted fairly well by proposed design equation, although the ultimate strength by design equation evaluates considerably lower than the experimental result.
- [2] Strength of the subassemblage composed of split tee, RHS column and plug welded portion as well as fillet welded portion has been evaluated by comparing the design strength with the experimental result. The result of comparison has shown that the proposed design formulae give fairly well prediction of yield strength. This conclusion can be applied to the subassemblages composed of the columns of width-thickness ratio of about 20.
- [3] Fillet welding arranged at the corners of tee flange, is effective so that the connection, which consists of split tee bracket and RHS column, can behave integrated until the ultimate state.
- [4] The plug weld alone appears to give greater ductility.

## NOTATIONS

### Lower cases

$a$	throat thickness of corner fillet weld
$d_p$	diameter of plug weld
$l$	effective length of each projection of tee bracket flange
$l_1$	distance between the center of plug weld and the end of flange
$l_2$	distance between the center of plug weld and the center of fillet weld
$l_w$	effective length of corner fillet weld
$l_{w1}$	effective length of corner fillet weld along transverse direction of tee bracket flange
$l_{w2}$	effective length of corner fillet weld along longitudinal direction of tee bracket flange
$m$	numeral from 1 to 4, corresponding to mode 7 to 10
$n$	number of plug weld at each projection of tee bracket flange
$p_{fws}$	specific strength of corner fillet weld per unit length
$r$	radius of fillet of wide flange section
$r_c$	corner radius of RHS column
$s$	letter indicating yielding state $y$ or ultimate state $u$
$size$	size of fillet weld
$t_c$	thickness of SHS column
$t_f$	thickness of tee bracket flange or upper flange of T-T specimen
$t_w$	thickness of tee bracket web
$w$	width of tee bracket

### Upper cases

$B_c$	outside dimension of RHS column
$B_m$	partial length of yield line parallel to transverse direction of subassemblage specimen



$H_c$	length of RHS column used for subassemblage specimen
$H_m$	partial length of yield line parallel to longitudinal direction of subassemblage specimen
$M_{0s}$	fully plastic or ultimate moment per unit width of bracket flange
$M_{fws}$	fully plastic or ultimate moment of fillet weld per unit length
$P_p$	tensile force of plug weld
$P_{p1s}$	specific tensile force of plug weld
$P_{p2s}$	specific tensile force caused by shear yielding or failure of plug weld
$P_{p3s}$	specific tensile force due to punching of RHS column plate
$P_{py(ex)}$	experimental yield tensile force of plug weld
$P_{ps(cal)}$	estimated specific tensile force of plug weld
$P_{ps(ex)}$	specific tensile force of plug weld obtained from experiment
$P_{pu(ex)}$	experimental ultimate tensile force of plug weld
$P_r$	prying force
$T$	applied tensile force
${}_cT_s$	specific tensile force transferred to the column through the tee bracket
${}_cT_{sm}$	specific tensile force transferred to the column through the tee bracket for mode 7 to 10
${}_{cal}T_s$	estimated specific tensile strength of subassemblage
${}_iT_s$	specific tensile strength of tee bracket
${}_iT_{s1}$	specific tensile strength of tee bracket stipulated by mode 4
${}_iT_{s2}$	specific tensile strength of tee bracket stipulated by mode 5
${}_iT_{s3}$	specific tensile strength of tee bracket stipulated by mode 6
$T_y$	applied tensile yield force
$X_m$	projected length of yield line along longitudinal direction of subassemblage specimen
$Y_m$	projected length of yield line along transverse direction of subassemblage specimen

### Greek letters

$\delta_c$	local distortion at the center of T-T specimen
$\delta_p$	local distortion at plug weld
$\delta_r$	local distortion at the end of upper flange of T-T specimen
$\theta_{end}$	rotation angle evaluated from $\theta_{end} = (\delta_c - \delta_p) / l_2$
$\sigma_{cs}$	specific tensile strength of RHS column plate
$\sigma_{fs}$	specific tensile strength of tee bracket flange
$\sigma_{fws}$	specific strength of corner fillet weld per unit area
$\sigma_{ps}$	specific tensile strength of plug weld

### ACKNOWLEDGEMENT

Authors acknowledge to earnest contribution of the persons concerned of Tohji Co. and Watahan Co. for their fabrication of specimens used in this study.

**REFERENCES**

- [1] The Architectural Institute of Japan, “Design Standard for Steel Structures”, The Architectural Institute of Japan, 1979.
- [2] The Architectural Institute of Japan, “Design Standard for Steel Structures-Based on Allowable Stress Concept-”, The Architectural Institute of Japan, 2005, (in Japanese)
- [3] American Welding Society, “AWS-D1.1 Structural Welding Code-Steel”, American Welding Society, 2000.
- [4] American Institute of Steel Construction, “Specification for Structural Steel Buildings”, American Institute of Steel Construction, Inc., 2005.
- [5] Faella, C., Piluso, V. and Rizzano, G., “Structural Steel Semirigid Connections: Theory, Design and Software, Chapter 4”, CRC Press LLC, 1999.
- [6] Faella, C., Piluso, V. and Rizzano, G., “Moment Resistant Connections of Steel Frames in Seismic Areas: 2.2 Plastic Deformation Capacity of Bolted T-stubs: Theoretical Analysis and Testing”, E & FN Spon, 2000.
- [7] Morita K., Yamamoto N. and Ebato K., “Analysis on the Strength of Unstiffened Beam Flange to RHS Column Connections based on the Combined Yield Line Model”, Tubular Structures, the Third International Symposium, Elsevier Applied Science, 1990, pp.164-171.
- [8] Yamamoto N. , Morita K. and Watanabe H., “Effect of Stiffener on the Strength of Connection between Beam and RHS column”, Tubular Structures, the Third International Symposium, Elsevier Applied Science, 1990, pp.172-179.
- [9] Harada Y., Nakagawa H. and Morita K., “Out-of-Plane Behavior of Column Skin Plate in RHS Column-to-Split-T Tensile Connection with High-Strength Bolts”, Journal of Structural and Construction Engineering (Transactions of A.I.J.), 2003, No.567, pp.173-180, (in Japanese).

# IN-PLANE STRENGTH OF STEEL ARCHES

Yong-Lin Pi<sup>1,\*</sup>, Mark Andrew Bradford<sup>2</sup> and Francis Tin-Loi<sup>3</sup>

<sup>1</sup>The corresponding author, Senior Research Fellow, Centre of Infrastructure Engineering & Safety, School of Civil & Environmental Engineering, UNSW, Sydney, NSW 2052, Australia  
\*(Corresponding author: E-mail: y.pi@unsw.edu.au)

<sup>2</sup>Federation Fellow, Professor, Centre of Infrastructure Engineering & Safety, School of Civil & Environmental Engineering, UNSW, Sydney, NSW 2052, Australia  
email: m.bradford@unsw.edu.au

<sup>3</sup>Professor, Centre of Infrastructure Engineering & Safety, School of Civil & Environmental Engineering, UNSW, Sydney, NSW 2052, Australia, email: f.tinloi@unsw.edu.au

Received: 24 September 2007; Revised: 15 November 2007; Accepted: 20 November 2007

**ABSTRACT:** A rational finite element program for the nonlinear elastic-plastic analysis of arches is used in this paper to investigate the in-plane elastic-plastic buckling and strength of circular steel arches. The finite element program considers the effects of large deformations, material nonlinearities, initial geometric imperfection, and residual stresses in predicting the elastic-plastic behaviour of steel arches. Radial loads uniformly distributed around the arch axis, concentrated loads, and distributed loads along the horizontal projection of an arch are studied, which induce either uniform compression or combined bending and compression in the arch. The complex effects of initial imperfection, rise-to-span ratio, residual stresses and the end support conditions on the in-plane elastic-plastic stability and strength of steel arches are included in the study. Useful design equations against in-plane failure are proposed for steel arches under uniform compression and under combined bending and compressive actions.

**Keywords:** Arch, combined bending and compression, compression, buckling, elastic-plastic, steel, strength  
This paper is extended from the paper presented in ICSCS07 entitled *In-plane inelastic buckling and strength of steel arches*.

## 1. INTRODUCTION

This paper is concerned with the in-plane nonlinear buckling behaviour and strength design of steel circular arches that are subjected to transverse loads, as shown in Figure 1. Arches resist general loading by a combination of predominant axial compression and bending actions. Under these actions, an arch which is adequately braced by lateral restraints so that its out-of-plane failure is fully prevented, may suddenly buckle and fail in the plane of its loading.

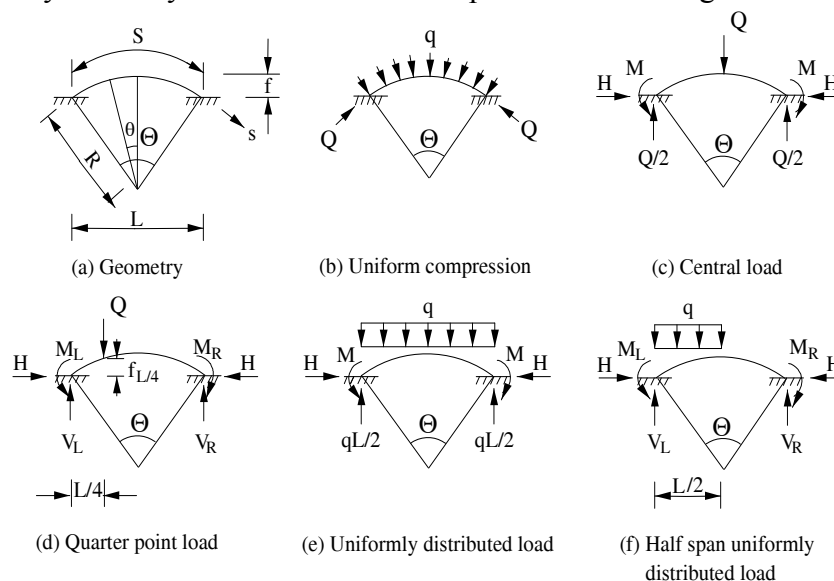


Figure 1. Arch and Loading

The in-plane elastic buckling load of arches is an important reference in the design of steel arches against their in-plane failure. The in-plane elastic buckling of arches has been studied by many researchers [1,2,3,4,5,6,7]. Early treatments of the in-plane elastic buckling of steel arches concentrated on the classical buckling analysis and are summarized in Galambos [8]. The classical buckling analysis assumes that the prebuckling behaviour is linear and it ignores the effects of prebuckling deformations on the buckling. However, shallow arches become nonlinear prior to buckling and their prebuckling deformations are substantial, so that predictions based on classical buckling theory may overestimate the buckling load of shallow arches [9]. Gjelsvik and Bodner [10] obtained approximate solutions for fixed shallow circular arches with rectangular cross-section, and Schreyer and Masur [11] derived analytical solutions for fixed shallow arches with rectangular cross-section. Pi et al. [12] investigated the in-plane elastic buckling of shallow arches with an arbitrary cross-section, and found that the in-plane elastic buckling load of shallow arches are much lower than that given by classical theory [1,2,3,4,5,6,7] and so the classical in-plane buckling load should not be used as the reference load in the development of design methods for the in-plane strength of shallow steel arches.

Despite their widespread use, accurate research that reports on the strength and design of steel arches against their in-plane failure appears to be quite limited and has concentrated on pin-ended arches. Explicit methods for designing steel arches against their in-plane failure have not been given in many commonly-used design codes [13,14,15]. A few methods [16,17] were proposed and were essentially based on the strength of steel beam-columns. Verstappen et al. [18] proposed that the in-plane buckling design strength of non-shallow circular arches should be determined by using a linear interaction design equation that was developed for straight beam-columns. Pi and Trahair [19,20] studied the in-plane elastic-plastic behaviour of pin-ended circular steel arches, while Pi and Bradford [21] investigated the in-plane elastic-plastic behaviour of fixed circular steel arches.

The aims of this paper are to use an advanced nonlinear elastic-plastic finite element (FE) program, developed elsewhere by the authors [22,23], to investigate the in-plane elastic-plastic behaviour at failure and the strength of circular steel arches, and to propose design equations for these members against in-plane failure based on this numerical investigation.

## 2. ELASTIC IN-PLANE BUCKLING

The elastic buckling load of arches under uniform compression can be used as a reference load in the formulation for their in-plane strength design. Pi et al. [12] studied the elastic buckling of arches under uniform compression. It was found that for in-plane buckling, arches usually buckle in an antisymmetric bifurcation mode and only very shallow arches buckle in a symmetric instability mode. The buckling load for arches was obtained by Pi et al. [12] as described in the following.

The expressions for the elastic buckling loads of shallow and deep arches are different. When an arch has an included angle such that  $\Theta \leq 90^\circ$ , it is deemed to be a shallow arch and a dimensionless parameter  $\lambda$  defined by [12]

$$\lambda = \frac{S\Theta}{4r_x} \quad (1)$$

can be used to measure the shallowness of an arch, where  $S$  is the length of the arch and  $r_x$  is the radius of gyration of the cross-section about its major principal axis given by  $r_x = \sqrt{I/A}$ , with  $A$  being the area of the cross-section and  $I$  being the second moment of area of the cross-section about its major principal axis.

For a pin-ended shallow arch, its buckling load is given by [12]

$$N_{acr} = \begin{cases} (0.15 + 0.006\lambda^2)N_{cr} & \text{for } 3.88 \leq \lambda \leq 9.38 \\ \left(0.26 + 0.74\sqrt{1 - 0.63\pi^4/\lambda^2}\right)N_{cr} & \text{for } \lambda > 9.38 \end{cases} \quad (2)$$

where  $N_{cr}$  is the second mode elastic flexural buckling load of a corresponding pin-ended column with the same length.

For a fixed shallow arch, its buckling load is given by [12]

$$N_{acr} = \begin{cases} (0.36 + 0.0011\lambda^2)N_{cr} & 9.87 \leq \lambda \leq 18.6 \\ \left(0.6 + 0.4\sqrt{1 - 3.109\pi^4/\lambda^2}\right)N_{cr} & \lambda > 18.6 \end{cases} \quad (3)$$

where  $N_{cr}$  is the second mode elastic flexural buckling load of a corresponding fixed column with the same length.

When an arch has an included angle  $\Theta > 90^\circ$ , it is deemed to be a deep arch, and its elastic buckling load is given by [12]

$$N_{acr} = \left[1 - (\Theta/\pi)^2\right]N_{cr} \quad \text{for pin-ended arches,} \quad (4)$$

$$N_{acr} = \left[1 - (\Theta/1.4304\pi)^2\right]N_{cr} \quad \text{for fixed arches,} \quad (5)$$

where  $N_{cr}$  is the second mode elastic flexural buckling load of a corresponding pin-ended or fixed column with the same length.

The second buckling load  $N_{cr}$  of the corresponding column in these equations is given by

$$N_{cr} = \frac{\pi^2 EI}{(kS)^2}, \quad \text{with } k = \begin{cases} 0.5 & \text{for pin-ended arches} \\ 0.35 & \text{for fixed arches} \end{cases} \quad (6)$$

where  $E$  is the Young's modulus.

### 3. NONLINEAR ELASTO-PLASTIC FINITE ELEMENT MODEL

A nonlinear elastic-plastic FE program for arches, developed elsewhere by the authors [22,23], is used in this paper to investigate the in-plane strength of steel arches. The formulation of the FE program is based on the following assumptions and considerations:

- (1) use of the Euler-Bernoulli theory of bending,
- (2) application of nonlinear strain-displacement relationships that allow for large displacements and rotations,
- (3) inclusion of distributions of longitudinal normal residual stresses due to manufacturing and curving, as are described subsequently,
- (4) inclusion of initial geometric imperfections
- (5) inclusion of user-defined stress-strain relationships.

Full details of the FE program are given in Pi et al [22,23], and the effectiveness and accuracy of this model has been verified extensively. For example, the results of the FE program for the in-plane elastic buckling load of circular arches under a uniform radial load  $q$  agree with the analytical solutions given by Eqs. 2-5 very well as shown in Figures 2 and 3, where  $N_{acr} = qR$  is the nominal axial compression during buckling and  $R$  is the radius of the arch. Other examples are given in Pi et al.[22,23] and not reproduced here.

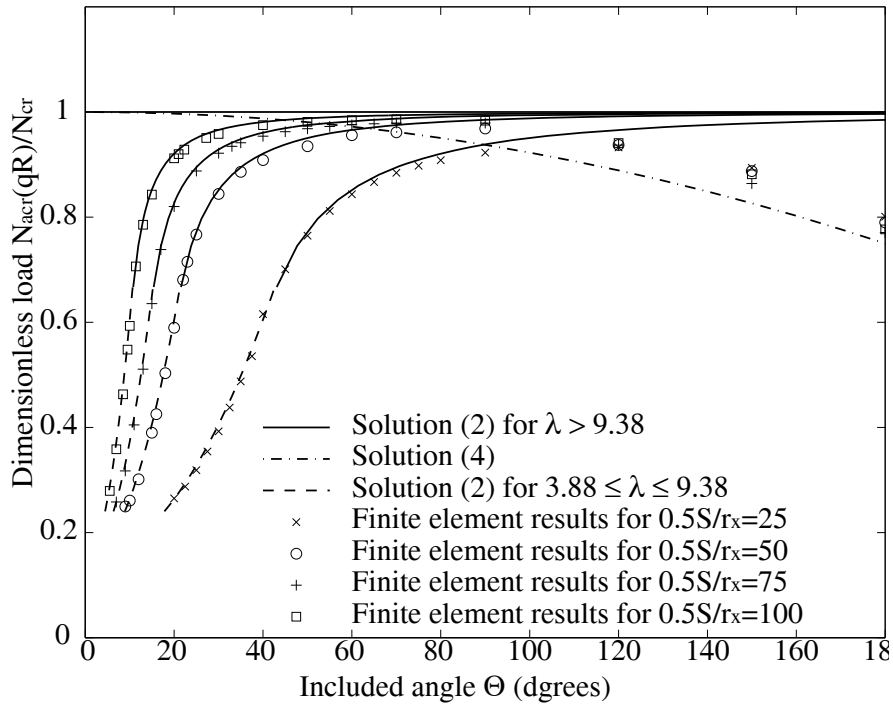


Figure 2. Comparison of FE Results with Analytical Solutions for Elastic Buckling of Pin-Ended Arches

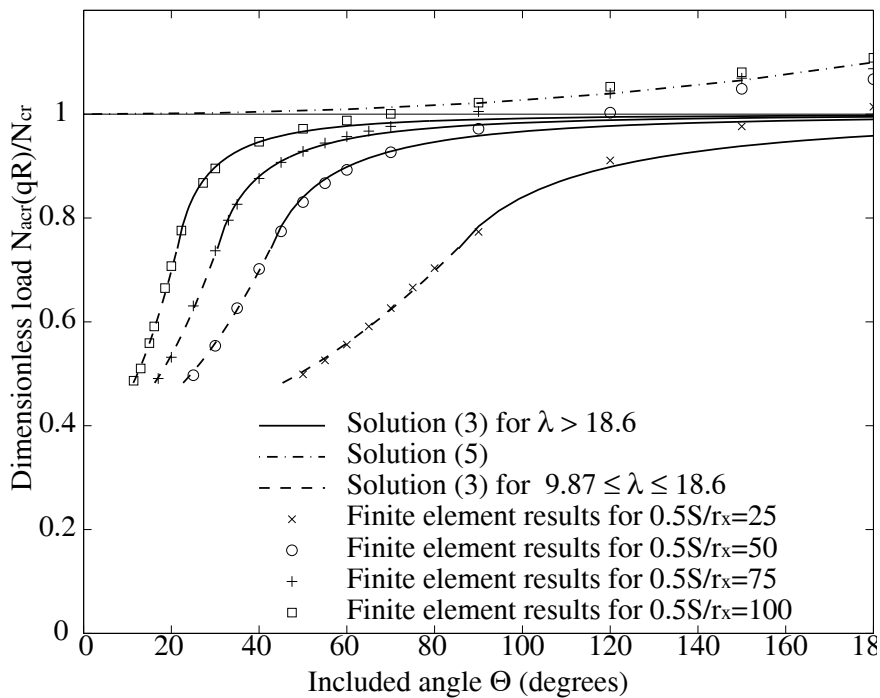


Figure 3. Comparison of FE Results with Analytical Solutions for Elastic Buckling of Fixed Arches

#### 4. RESIDUAL STRESSES, STRESS-STRAIN CURVE

Residual stresses may be induced in the manufacturing and curving processes for steel arches. It has been shown that the residual stresses have effects on the strength of steel arches, and so they need to be considered in the development of strength design equations.

The residual stresses  $\sigma_r$  consist of two components: the manufacturing and the cold rolling (or curving) residual stresses shown in Figures 4(c)-4(d). In Figure 4(c),  $\sigma_{rt} = 0.5\sigma_y$  is typically the tensile residual stress at the flange-web junctions and  $\sigma_{rc} = 0.35\sigma_y$  is typically the compressive residual stress at the flange tips, where  $\sigma_y$  is the yield stress.

Rolling residual stresses are induced in cold curving the arch. It is assumed that, for example, a straight I-section member is bent elastic-plastically to obtain an overbent arch, and then released so that the overbent arch relaxes elastically into its final shape with a permanent set. Although the depth of the plastic zone after overbending depends on the radius of the arch, and so also do the final rolling residual stresses, the final rolling flange residual stresses  $\sigma_{rrf}$  are quite small after the relaxation. Hence, for convenience, the rolling residual stresses are assumed here to be independent of the arch radius.

The maximum rolling residual stresses occur in the web near the neutral axis, and so their effects on elastic-plastic buckling are quite small as elastic-plastic buckling is controlled primarily by flange yielding.

The maximum rolling flange residual stresses  $\sigma_{rrf}$  are assumed to be given by

$$\sigma_{rrf} = \sigma_y \left( \frac{Z_{px}}{Z_{ex}} - 1 \right) \quad (7)$$

where  $Z_{px}$  and  $Z_{ex}$  are the plastic and elastic moduli of the cross-section about its major principal axis, respectively. The maximum rolling web residual stresses  $\sigma_{rrw}$  are assumed to be given by  $\sigma_{rrw} = 0.9\sigma_y$ .

The residual stresses shown in Figures 4(c) and 4(d) satisfy the in-plane bending equilibrium condition

$$\int_A \sigma_r y dA = 0, \quad (8)$$

while the axial force equilibrium condition

$$\int_A \sigma_r dA = 0 \quad (9)$$

is used to determine the mid-web residual stress  $\sigma_{rcw}$ , where  $y$  is the coordinate in the principal axes of the cross-section, and  $A$  is the area of the cross-section.

The residual stresses defined above, and the steel I-section and the tri-linear stress-strain relationship shown in Figure 4 are used throughout this study. The dimensions of the I-section are: the depth of the cross-section  $D = 0.2613\text{m}$ , the flange width  $B = 0.151\text{m}$ , the flange thickness  $t_f = 0.0123\text{m}$ , and the web thickness  $t_w = 0.0077\text{m}$ . The material properties for the tri-linear stress-strain curve are: the yield stress  $\sigma_y = 250\text{MPa}$ , the corresponding yield strain  $\varepsilon_y = 0.00125$ , Young's modulus of elasticity  $E = 200,000\text{MPa}$ , the strain at which the strain hardening starts is assumed to be 11 times the yield strain, the maximum strain is assumed to be 71 times the yield strain. The strain hardening modulus  $E_s = 6,000\text{MPa}$ , and the shear modulus is  $G = 80,000\text{MPa}$ .

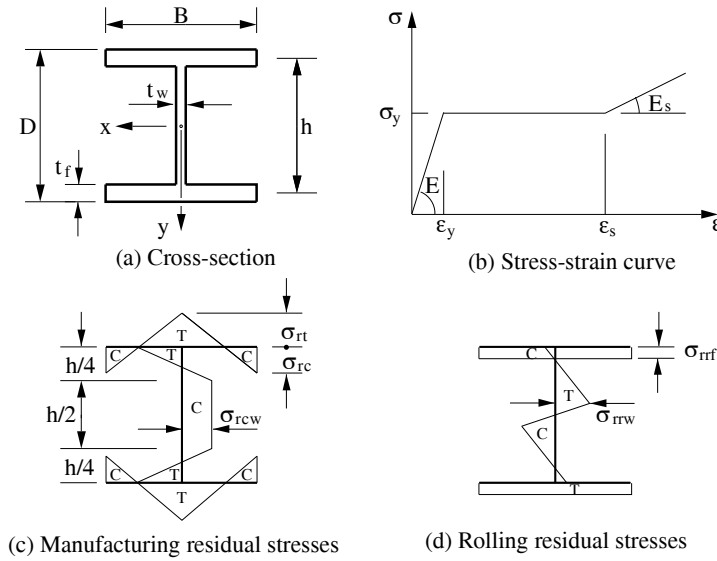


Figure 4. Cross-Section, Stress-Strain Curve and Residual Stresses

## 5. STRENGTH IN UNIFORM COMPRESSION

The design proposal for the in-plane strength capacity  $N_{ac}$  of a steel arch that is subjected to uniform compression is based on the methodology in AS4100 [13] for compression members, but modified accordingly for arches. Thus

$$N_{ac} = \phi \alpha_{ac} N_Y \leq N_Y, \quad (10)$$

where  $\phi$  is a capacity reduction factor ( $\phi = 0.9$  is suggested and used in AS4100 [13]),  $N_Y$  is the squash load of the cross-section and given by

$$N_Y = A \sigma_y, \quad (11)$$

and  $\alpha_{ac}$  is the in-plane slenderness reduction factor of an arch and given within the methodology of AS4100 [13] by

$$\alpha_{ac} = \xi_a \left[ 1 - \sqrt{1 - \left( \frac{90}{\xi_a \lambda_{ag}} \right)^2} \right] \quad (12)$$

with

$$\xi_a = \frac{(\lambda_{ag}/90)^2 + 1 + \eta_a}{2(\lambda_{ag}/90)^2} \quad (13)$$

in which the modified slenderness  $\lambda_{ag}$  is defined as

$$\lambda_{ag} = \frac{L_e}{r_x} \sqrt{\frac{\sigma_y}{250}} \quad (14)$$

with the effective length  $L_e = kS / \sqrt{k_{ac}}$ ; and the imperfection parameter  $\eta_a$  is given by

$$\eta_a = 0.00326(\lambda_{ag} - 13.5) \geq 0. \quad (15)$$

In Eq. 14,  $\sigma_y$  is expressed in units of MPa and the factor  $k_{ac}$  is given by  $k_{ac} = N_{acr}/N_{cr}$ .

To verify the proposed in-plane strength of an arch in uniform compression given by Eq. 10, the FE program was used to investigate the in-plane strength  $N_{ac}$  of arches in uniform compression.



Because the in-plane geometric imperfections have significant effects on the strength of steel arches, they have to be considered in the design formulation. In the FE analysis, the in-plane geometric imperfections were assumed to be

$$v_0 = \begin{cases} v_{0,S/4} \sin \frac{2\pi s}{S} & \text{for arches with } \lambda \geq 9.38 \\ v_{0,S/2} \sin \frac{\pi s}{S} & \text{for arches with } \lambda < 9.38 \end{cases} \quad (16)$$

for pin-ended arches, and

$$v_0 = \begin{cases} \frac{v_{0,S/4}}{2} \left(1 - \cos \frac{2\pi s}{S/2}\right) & \text{for arches with } \lambda \geq 18.6 \\ \frac{v_{0,S/2}}{2} \left(1 - \cos \frac{2\pi s}{S}\right) & \text{for arches with } \lambda < 18.6 \end{cases} \quad (17)$$

for fixed arches, where  $v_{0,S/4}$  and  $v_{0,S/2}$  is the initial in-plane crookedness at the quarter point and the crown of the arch length respectively, and  $s$  is the coordinate along the arch axis. The expression for the imperfection satisfies the kinematical boundary conditions for the members.

The central crookedness implied by the Australian steel structures design code AS4100 [13] for the major axis strength of steel columns was obtained by Bild and Trahair [24], which is used in this study as the initial crookedness  $v_{0,S/4}$  at the quarter point of the arch length, so that

$$\frac{1000v_{0,S/4}}{S/2} = 2.5 \left(1 - \frac{1}{1 + 2\lambda_c}\right) \quad \text{or} \quad \frac{1000v_{0,S/2}}{S} = 2.5 \left(1 - \frac{1}{1 + 2\lambda_c}\right), \quad (18)$$

where  $\lambda_c$  is the modified slenderness of the corresponding column given by

$$\lambda_c = \sqrt{\frac{N_Y}{N_{cr}}}. \quad (19)$$

The variations of the dimensionless in-plane axial compressive strength  $N_{ac}/N_Y$  with the modified in-plane slenderness  $\lambda_{ac}$  obtained from the FE results are shown in Figure 5 for pin-ended arches and in Figure 6 for fixed arches, where the modified in-plane slenderness  $\lambda_{ac}$  is defined as

$$\lambda_{ac} = \sqrt{\frac{N_Y}{N_{acr}}}. \quad (20)$$

Also shown in Figures 5 and 6 is the variation of the dimensionless proposed in-plane strength of fixed arches  $N_{ac}/N_Y$  with the modified in-plane slenderness  $\lambda_{ac}$ . It can be seen that the proposed equation provides good predictions for the in-plane strengths of arches in uniform compression.

It worth pointing out that for a pin-ended arch with  $\lambda < 3.88$  or a fixed arch with  $\lambda < 9.87$  that is subjected to a radial load uniformly distributed around it, the arch becomes very shallow and can be treated as a beam with initial in-plane geometric imperfection. Hence, the proposed Eq. 10 is not suitable in these cases.

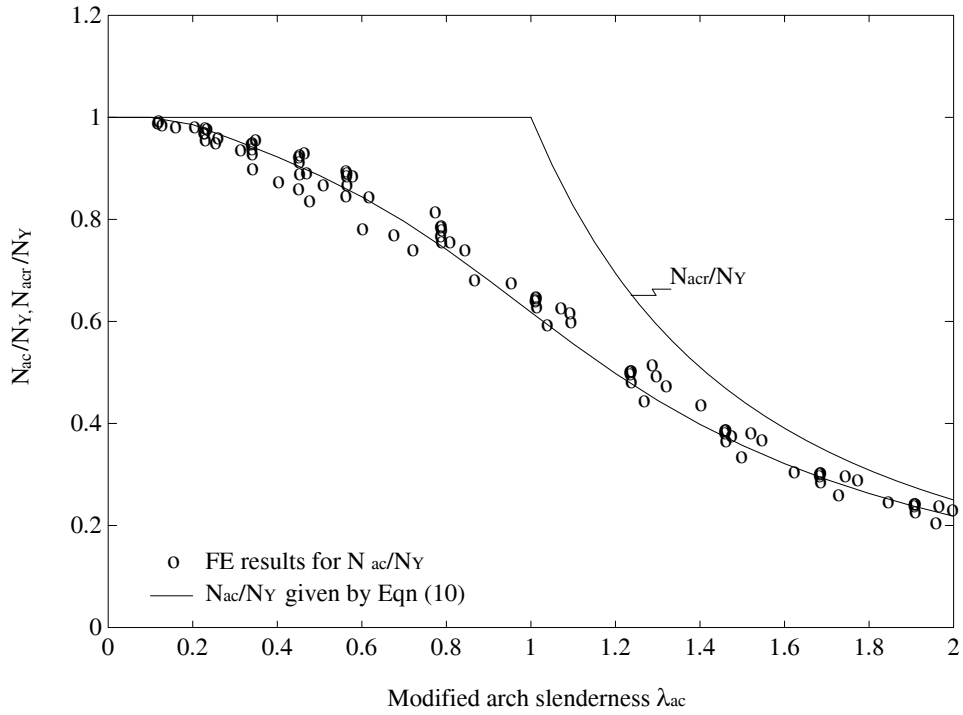


Figure 5. In-Plane Strength of Pin-Ended Arches Subjected to Uniform Compression

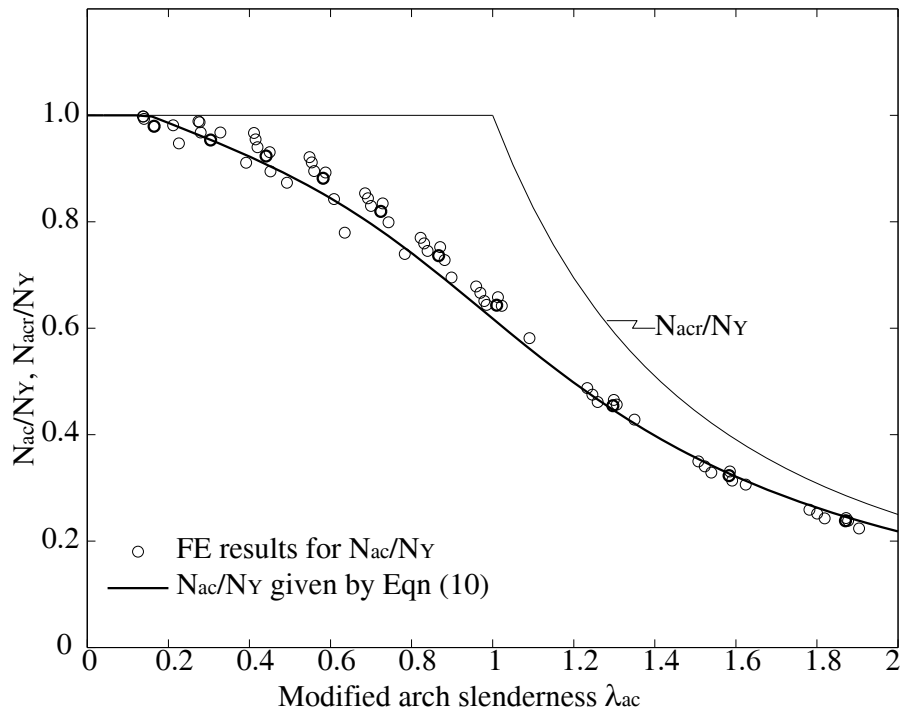


Figure 6. In-Plane Strength of Fixed Arches Subjected to Uniform Compression

## 6. STRENGTH IN COMBINED BENDING AND COMPRESSION

### 6.1 First-Order Actions in Elastic Arches

Under general loading, arches are subjected to combined bending and axial compressive actions. Whether or not the compressive action or the bending action is significant relative to each other very much depends on the loading condition.

To investigate the effects of the loading condition on the bending and compressive actions, first-order elastic analyses were performed by using the flexibility method. For the design convenience, four loading cases were investigated: a central concentrated load, a quarter point concentrated load, a vertical load uniformly distributed over the entire span of an arch, and a vertical load uniformly distributed over a half of the span of an arch (Figure 1).

The results for the maximum compressive action  $N$  and the maximum bending action  $M$  are shown in Figure 7 as the relationship between the ratio  $(N/N_Y)/(N/N_Y + M/M_p)$  and the included angle  $\Theta$  for arches with length  $S = 10\text{m}$ , where  $M_p$  is the full plastic moment of the cross-section. When an arch is subjected to a vertical load uniformly distributed over its entire span, the axial compressive action is relatively high and the bending action is relatively low. In addition, the compressive action in arches with a moderate included angle  $\Theta$  is relatively higher than that in arches with a small or large included angle  $\Theta$ . When an arch is subjected to a vertical load uniformly distributed over a half of its span, to a central concentrated load, or to a quarter point concentrated load, the axial compressive action is relatively low and the bending action is relatively high. When the included angle  $\Theta$  of an arch is very small, the bending action is relatively significant for all the four loading cases.

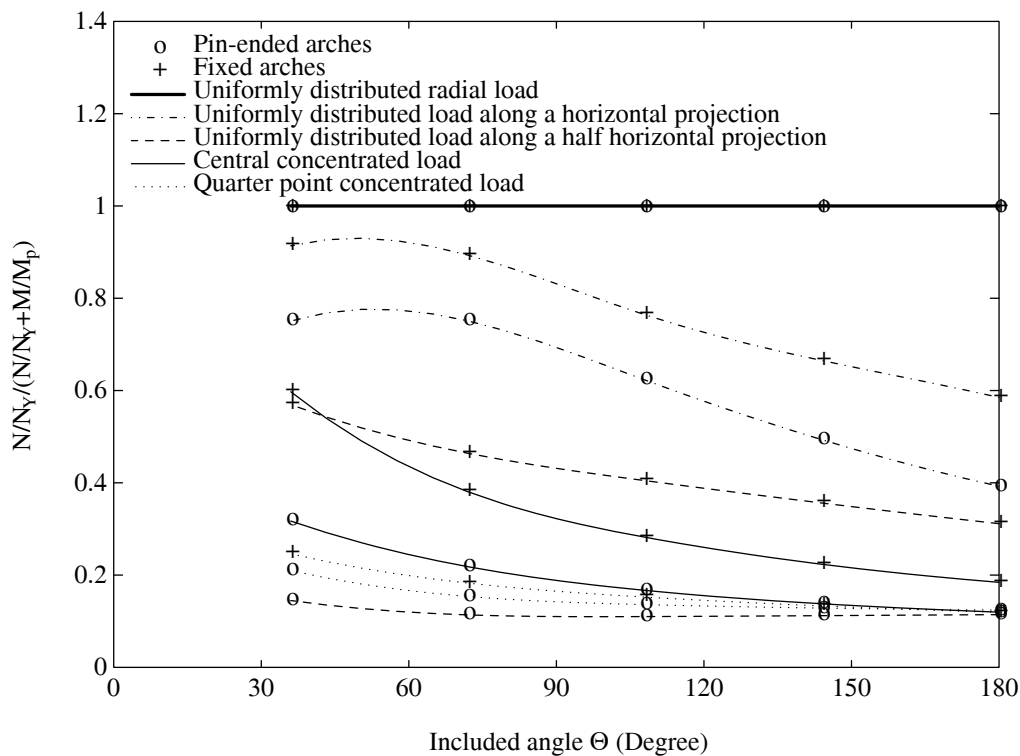


Figure 7. Maximum First-Order Bending Moment and Axial Compressive Force in Arches

## 6.2 Elastic and Elastic-Plastic Behaviour

Typical in-plane elastic and elastic-plastic behaviours of four pin-ended arches (with  $0.5S/r_x=50$ ) under central concentrated loads are compared with those under quarter point loads in Figure 8, where  $Q$  is the concentrated load,  $v_c$  is the central vertical deflection for a central load, and  $v_{L/4}$  is the quarter point vertical deflection for a quarter point load. The included angles  $\Theta$  and parameters  $\lambda$  of these four arches are  $\Theta = 6.9^\circ, 11.5^\circ, 47^\circ$ , and  $160^\circ$  and  $\lambda = 3, 5, 20.5$ , and  $70$ . These arches are assumed to be perfect, and so buckling is initiated by a small horizontal load ( $Q=0.001N_{EI}$ ) at the arch crown in the case of a central load.

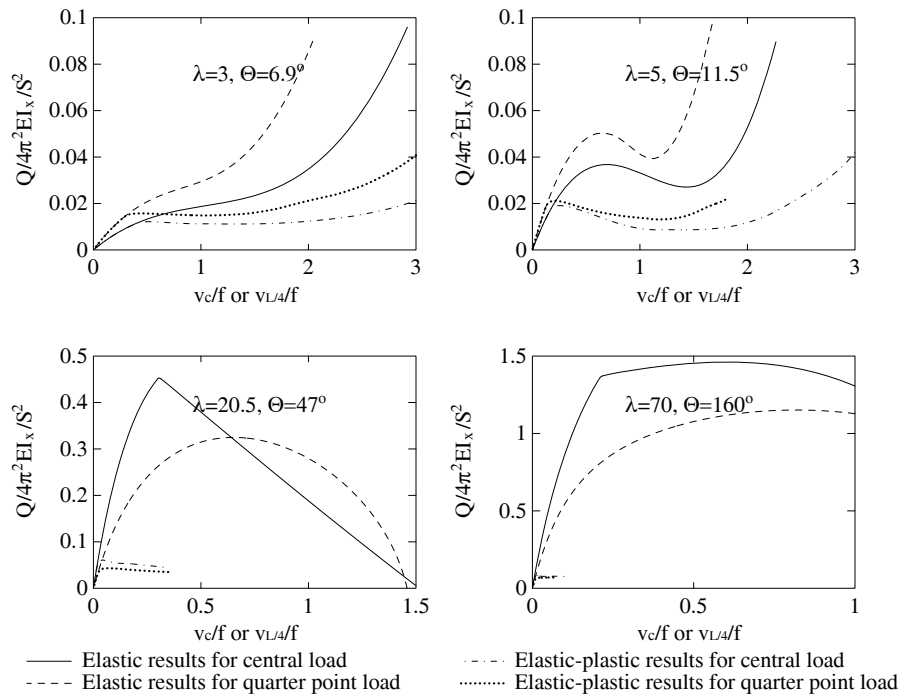


Figure 8. Elastic and Elastic-Plastic Behaviour of Pin-Ended Steel Arches Under Concentrated Loads

For the arch with  $\lambda = 3$  ( $\Theta = 6.9^\circ$ ), there is no elastic buckling, but elastic-plastic snap-through buckling occurs in both load cases. For the arch with  $\lambda = 5$  ( $\Theta = 11.5^\circ$ ), both the elastic and elastic-plastic buckling modes are by snap-through in both load cases. For the arch with  $\lambda = 20.5$  ( $\lambda = 20.5$ ) and a central load, the elastic buckling mode is by anti-symmetrical bifurcation and the postbuckling loads decrease rapidly. For a quarter point load, the elastic load-deflection curve is quite nonlinear and the load increases to a maximum value at a large deflection ( $v_{L/4}/f=0.64$ ), and then decreases gradually. However, the elastic-plastic behaviour is similar to that for a central load. For the arch with  $\lambda = 70$  ( $\Theta = 160^\circ$ ) and a central load, the elastic buckling mode is also by anti-symmetrical bifurcation but the postbuckling loads increase slightly. For a quarter point load, the elastic load-deflection curve is quite nonlinear and the maximum load is reached at a large deflection ( $v_{L/4}/f=0.81$ ). However, the elastic-plastic behaviour is similar to that for a central load.

The ratios of the elastic-plastic buckling load to the elastic buckling load for shallow arches ( $\lambda = 3$  and  $5$ ) are higher than those for non-shallow arches ( $\lambda = 20.5$  and  $70$ ). The elastic and elastic-plastic buckling loads for quarter point loads are higher than those for central loads for shallow arches, but lower than those for central loads for non-shallow arches.

The variations of the dimensionless strengths  $Q/(4\pi^2 EI_x/S^2)$  or  $qL/(4\pi^2 EI_x/S^2)$  with the parameter  $\lambda$  and the arch included angle  $\Theta$  for four groups of arches with slendernesses  $0.5S/r_x = 30, 50, 110,$  and  $170$  are shown in Figure 9 for concentrated loads where  $Q$  is the maximum finite element value of the central or quarter point concentrated load, and in Figure 10 for uniform vertical loads where  $q$  the maximum finite element value of the intensity of distributed load. The effects of the included angle  $\Theta$  and the parameter  $\lambda$  on the strengths are significant for the arches subjected to symmetrical loads (a central concentrated load in Figure 9 and an entire arch uniform load in Figure 10), particularly when  $\lambda < 10$ , but less important for the arches subjected to asymmetrical loads (a quarter point load in Figure 9 and a half arch uniform load in Figure 10).

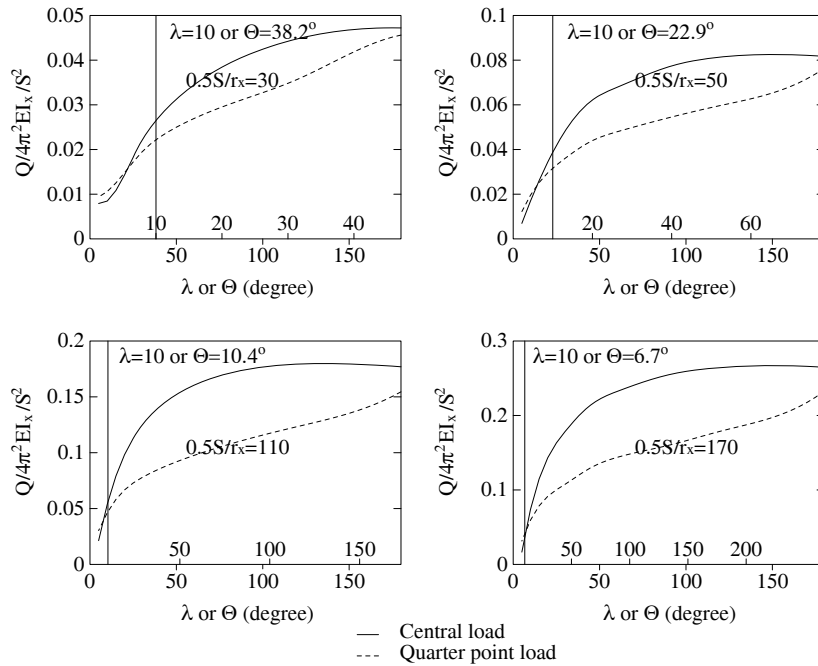


Figure 9. Strength of Pin-Ended Steel Arches Under Concentrated Loads

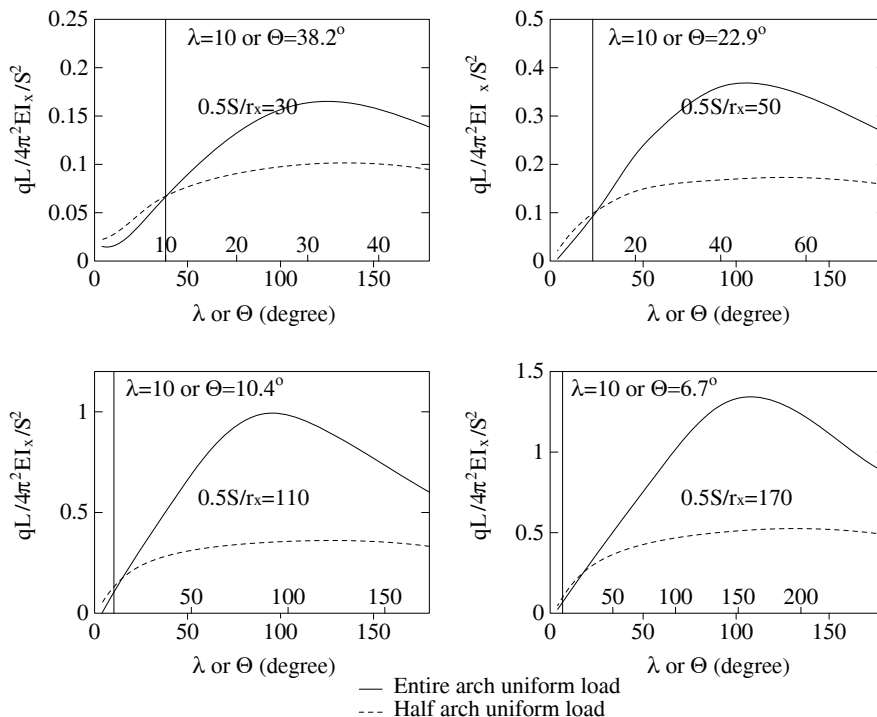


Figure 10. Strength of Pin-Ended Steel Arches Under Distributed Loads

### 6.3 In-Plane Design Strength

The in-plane strength of a steel arch subjected to combined bending and axial compressive actions is complex, and is related to a number of factors, such as the buckling behaviour, yielding, the initial curvature, the included angle, the slenderness, the shallowness, residual stresses, initial in-plane geometric imperfections, and loading conditions. It is therefore difficult to develop simple and accurate equations for the design of arches that are subjected to the combined bending and axial compressive actions against in-plane failure. Instead, a lower bound interaction equation for the in-plane strength of arches has been sought based on the accurate numerical results.

The in-plane strength capacity design check for a steel arch that is subjected to combined bending and axial compressive actions is proposed as

$$\frac{N^*}{\phi\alpha_{an}N_{ac}} + \frac{M^*}{\phi\alpha_{am}M_p} \leq 1, \tag{21}$$

where  $\phi$  is the same capacity reduction factor for uniform compression,  $N_{ac}$  is the in-plane axial compression capacity of an arch in uniform compression given by Eq. 10,  $N^*$  is the maximum axial compression obtained by a first-order in-plane elastic analysis,  $M^*$  is the maximum moment given by

$$M^* = \delta_b M_m \quad \text{with} \quad \delta_b = \frac{1}{1 - N^*/N_{acr}} \tag{22}$$

where  $M_m$  is the maximum moment obtained by a first-order in-plane elastic analysis and  $N_{acr}$  is the in-plane elastic buckling load of an arch in uniform compression and given by Eqs. 2-5, and  $\alpha_{an}$  and  $\alpha_{am}$  are the axial compression and moment modification factors for the in-plane strength.

The modification factor  $\alpha_{am}$  accounts for the combined effects of the initial curvature, the included angle and the slenderness of the arch, and the non-uniform distribution of bending moment over the arch length, while the modification factor  $\alpha_{an}$  accounts for the non-uniform distribution of axial compressive force over the arch length. The effects of the included angle and the slenderness of the arch have already been accounted in the in-plane axial compression capacity  $N_{ac}$ . The values of  $\alpha_{an}$  and  $\alpha_{am}$  are given in Figure 11 for pin-ended arches and in Figure 12 for fixed arches.

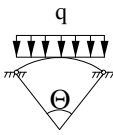
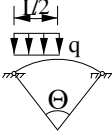
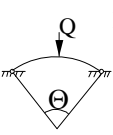
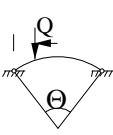
Arch					
$\alpha_{an}$		1.00	1.00	1.10	1.10
$\alpha_{am}$	$\lambda < 9.38$	$1.13 + 0.146\lambda$	$1 + 0.021\lambda$	$1.35 + 0.069\lambda$	$1.1 + 0.053\lambda$
	$\lambda \geq 9.38$	2.50	1.20	2.00	1.60

Figure 11. Factors for in-Plane Strength of Pin-Ended Arches

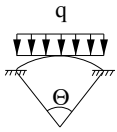
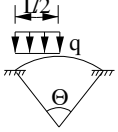
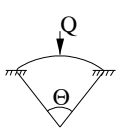
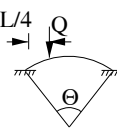
Arch					
$\alpha_{anx}$		1.00	1.00	1.10	1.10
$\alpha_{amx}$	$\lambda < 18.6$	2.0+ $0.1(18.6-\lambda)\Theta/\pi$	1.20+ $0.5(18.6-\lambda)\Theta/\pi$	1.50+ $0.05(18.6-\lambda)\Theta/\pi$	1.80+ $0.05(18.6-\lambda)\Theta/\pi$
	$\lambda > 18.6$	2.0	1.20	1.50	1.80

Figure 12. Factors for in-Plane Strength of Fixed Arches

It is recommended that if the amplification factor  $\delta_b > 1.4$ , then a second-order in-plane elastic analysis should be carried out to obtain  $M^*$  and  $N^*$ . This recommendation is consistent with that of *AS4100*<sup>13</sup> for frames consisting of straight members.

The predictions of the proposed interaction Eq. 21 are compared with the FE results (taking  $\phi = 1$ ) for four load cases: a central concentrated load, a quarter point concentrated load, a uniformly distributed load over the entire arch, and a uniformly distributed load over a half of the arch (Figure 1). In the FE analysis, the initial in-plane imperfections defined by Eqs. 16-18 were used.

Comparisons of the predictions of the proposed Eq. 21 with the FE results are shown in Figures 13 and 14 for pin-ended arches that are subjected to symmetric and asymmetrical loads respectively, and in Figures 15 and 16 for fixed arches that are subjected to symmetric and asymmetric loads respectively. It can be seen that the interaction Eq. 21 provides good lower bound predictions that are not unduly conservative for the in-plane strength of steel arches that are subjected to the combined bending and axial compressive actions.

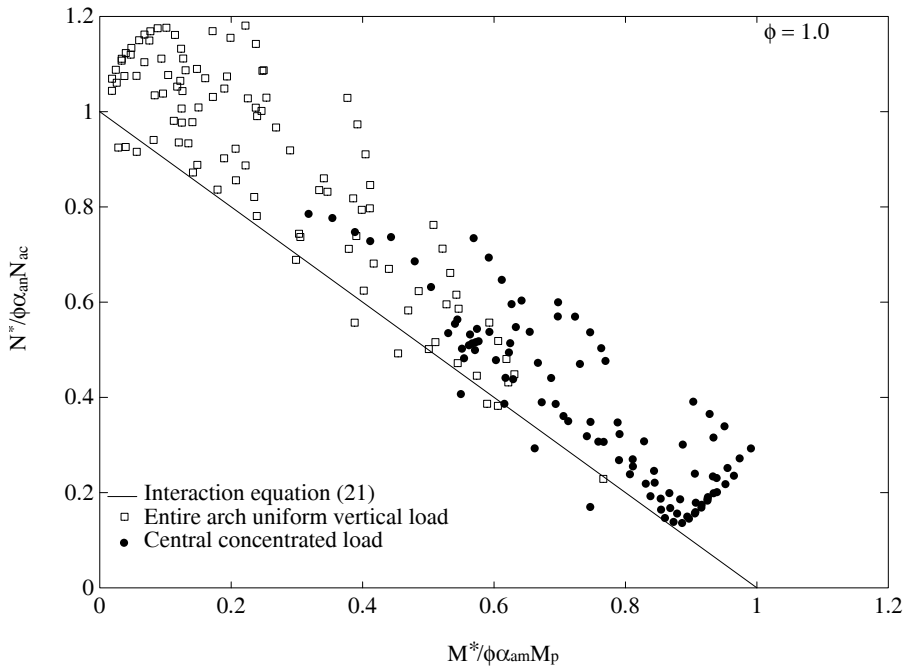


Figure 13. In-plane strength of pin-ended arches subjected to symmetric loading.

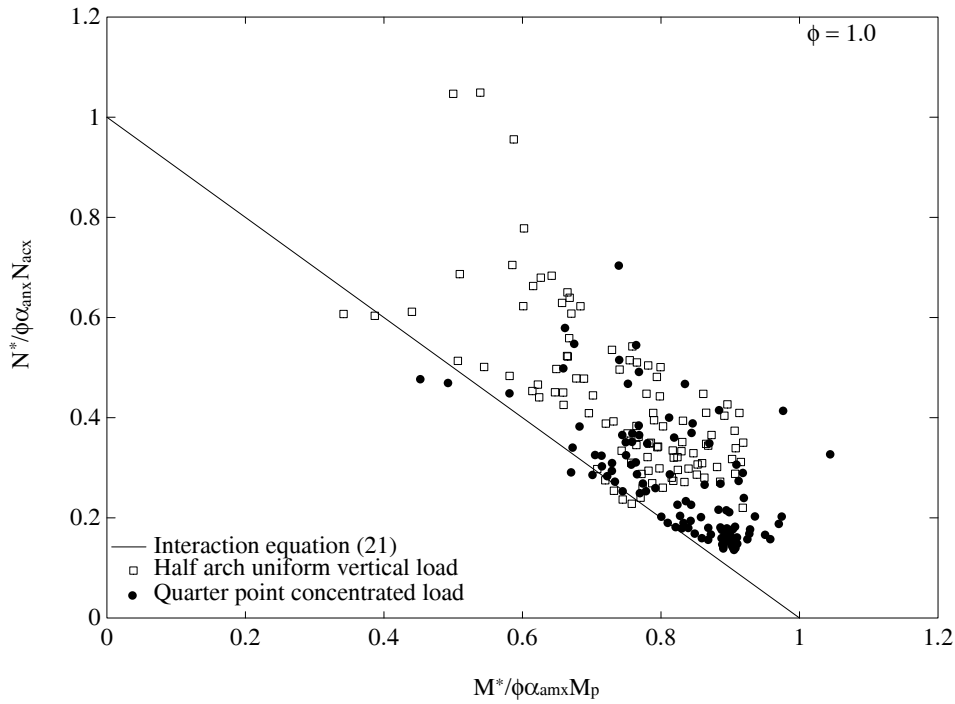


Figure 14. In-plane strength of pin-ended arches subjected to asymmetric loading.

Again, it is noted that for a pin-ended arch with  $\lambda < 3.88$  or a fixed arch with  $\lambda < 9.87$  that is subjected to a radial load uniformly distributed around it, the arch becomes very shallow and can be treated as a beam with initial in-plane geometric imperfection. Hence, the proposed Eq. 21 is not suitable in this case.

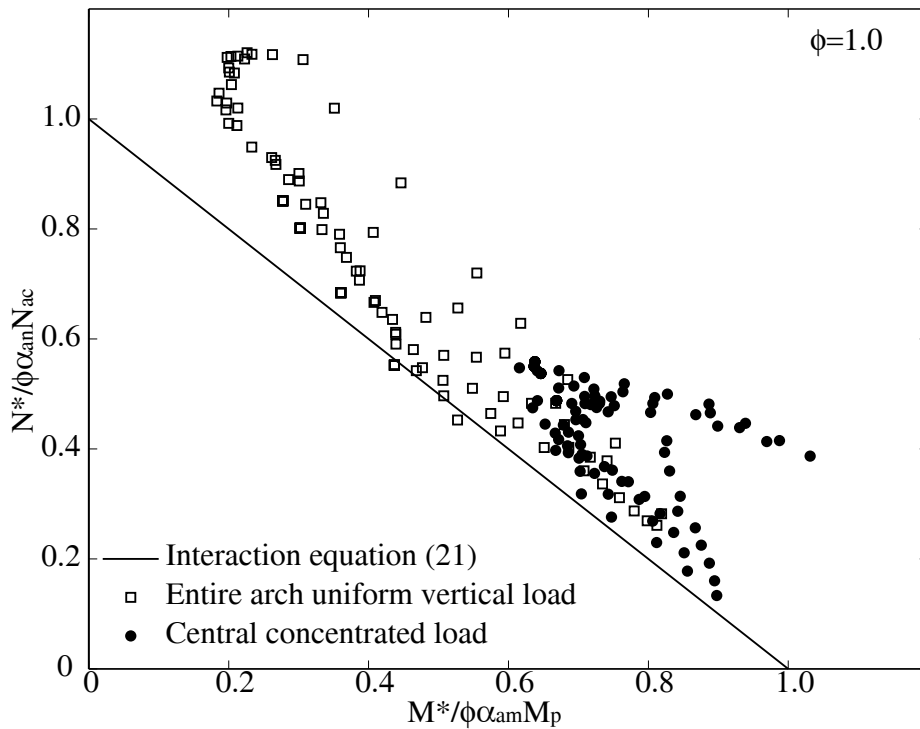


Figure 15. In-plane strength of fixed arches subjected to symmetric loading.



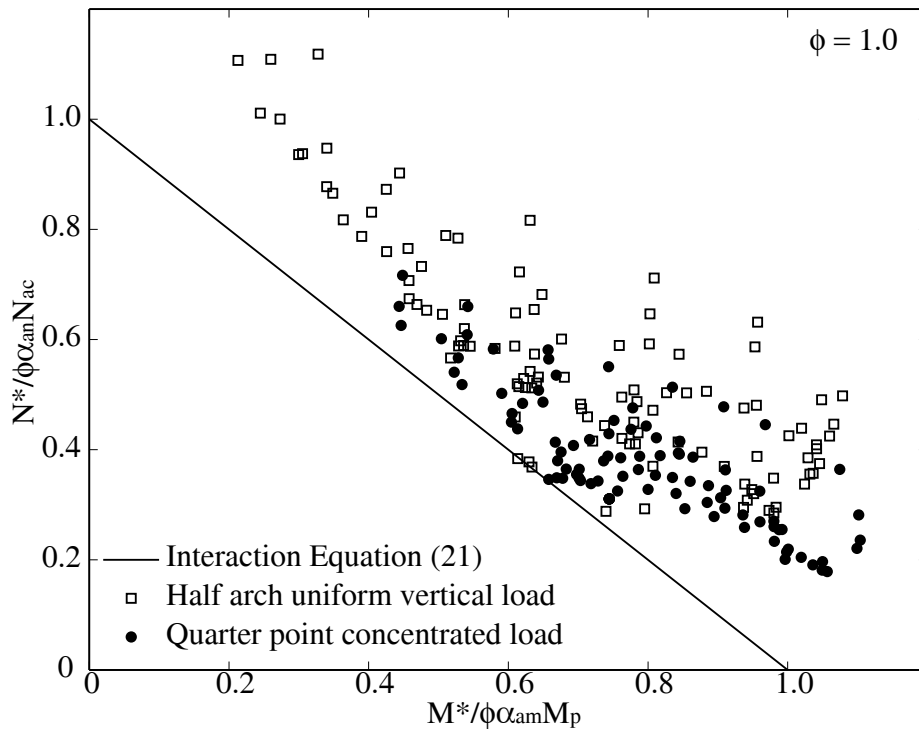


Figure 16. In-plane strength of fixed arches subjected to asymmetric loading.

## 7. CONCLUSIONS

A design equation for the in-plane strength of steel arches in uniform compression has been proposed which provides good predictions for their in-plane strength. An interaction equation for the in-plane design strength of steel arches that are subjected to the combined bending and axial compressive actions has also been proposed. It considers the effects and interactions of various factors, such as in-plane buckling, yielding, the included angle, the slenderness, the shallowness, residual stresses, initial in-plane geometric imperfections, non-uniform distributions of bending moments and axial compressive forces, loading conditions. The proposed design interaction equation is simple and easy to use, is consistent with the Australian steel structures design code AS4100 [13], and may easily be formulated for other steel structural design codes. Generally, a first-order or second-order in-plane elastic analysis is sufficient for the design. The proposed design equation provides good lower bound predictions for the in-plane strength of steel arches that are subjected to the combined bending and axial compressive actions.

## ACKNOWLEDGEMENTS

This work has been supported by the Australian Research Council through Discovery Projects awarded to the authors and a Federation Fellowship awarded to the second author.

## REFERENCES

- [1] Timoshenko, S.P. and Gere, J.M., "Theory of Elastic Stability", 2nd Edition, McGraw-Hill, 1961.
- [2] Vlasov, V.Z., "Thin-walled Elastic Beams", 2nd Edition, Israel Program for Scientific Translation, 1961.
- [3] Simitse, G.J., "An Introduction to the Elastic Stability of Structures", Prentice-Hall, Englewood Cliffs, 1976.
- [4] DaDeppo, D.A. and Schmidt, R., "Nonlinear Analysis of Buckling and Postbuckling Behavior of Circular Arches", *Journal of Applied Mathematics and Physics*, 1969, Vol. 20, pp. 847-857.
- [5] Austin, W.J. and Ross, T. J., "Elastic Buckling of Arches under Symmetric Loading", *Journal of the Structural Division, ASCE*, 1976, Vol. 102, No. 5, pp. 1085-1095.
- [6] Chini, S.A. and Wolde-Tinsae, A. M., "Critical Load and Postbuckling of Arch Frameworks", *Journal of Engineering Mechanics, ASCE*, 1988, Vol. 114, No. 9, pp. 1435-1453.
- [7] Mirmiran, A. and Wolde-Tinsae, A.M., "Buckling and Postbuckling of Prestressed Sandwich Arches", *Journal of Structural Engineering, ASCE*, 1993, Vol. 119, No. 1, pp. 262-278.
- [8] Galambos, T.V., "Guide to Stability Design Criteria for Metal Structures", 4<sup>th</sup> Ed, John Wiley & Sons, 1988.
- [9] Pi, Y.-L. and Trahair, N.S., "Non-linear Buckling and Postbuckling of Elastic Arches", *Engineering Structures*, 1998, Vol. 20, No. 7, pp. 571-579.
- [10] Gjelsvik, A. and Bodner, S.R., "The Energy Criterion and Snap Buckling of Arches", *Journal Engineering of the Mechanic Division, ASCE*, 1962, Vol. 88, No. 5, pp. 87-134.
- [11] Schreyer, H.L. and Masur, E.F., "Buckling of Shallow Arches", *Journal of the Engineering Mechanic Division, ASCE*, 1966, Vol. 92, No. 4, pp. 1-20.
- [12] Pi, Y.-L., Bradford, M.A., and Uy, B., "In-plane Stability of Arches", *International Journal of Solids and Structures*, 2002, Vol. 39, No. 2, pp. 105-125.
- [13] "AS4100, Steel structures", Standards Australia, 2003.
- [14] "BS5950, Structural Use of Steel in Building, Part 1, Code of Practice for Design in Simple and Continuous Construction: Hot-Rolled Sections", British Standards Institution, 1998.
- [15] "Load and Resistance Factor Design Specification for Structural Steel Buildings", American Institute of Steel Construction, 2000.
- [16] Komatsu, S. and Shinke, T., "Practical Formulation for In-Plane Load Carrying Capacity of Arches", *Proceedings of Japan Society of Civil Engineers*, 1977, Vol. 267, pp. 39-52, Tokyo, Japan, (in Japanese).
- [17] Kuranishi, S. (Ed.), "Chapter 7 Arches", *Stability of Metal Structures - A World View*. 2nd Ed, Ed by L.S. Beedle, Structural Stability Research Council, Bethlehem, Pa., pp. 423-445, 1991.
- [18] Verstappen, I., Snijder, H.H., and Bijlaard, F.S.K. and Steembergen, H.M.G.M., "Design Rules for Steel Arches-in-Plane Stability", *Journal of Constructional Steel Research*, 1998, Vol. 46, No. 1-3, pp. 125-126.
- [19] Pi, Y.-L. and Trahair, N.S., "In-Plane Inelastic Buckling and Strength of Steel Arches", *Journal of Structural Engineering, ASCE*, 1996, Vol. 122, No. 7, pp. 734-747.
- [20] Pi, Y.-L. and Trahair, N.S., "In-Plane Buckling and Design of Steel Arches", *Journal of Structural Engineering, ASCE*, 1999, Vol. 125, No. 11, pp. 1291-1298.
- [21] Pi, Y.-L. and Bradford, M.A., "In-Plane Strength and Design of Fixed Steel I-Section Arches", *Engineering Structures*, 2004, Vol. 26, No. 3, pp.291-301.

- [22] Pi, Y.-L., Bradford, M.A., Tin-Loi, F., and Gilbert, R.I., "Geometric and Material Nonlinear Analysis of Elastically Restrained Arches", *Engineering Structures*, 2007, Vol. 29, No. 3, pp. 283-295.
- [23] Pi, Y.-L., Bradford, M.A., and Uy, B., "A rational Elasto-plastic Spatially Curved Thin-walled Beam Element", *International Journal for Numerical Methods in Engineering*, 2007, Vol. 70, pp. 253-290.
- [24] Bild, S. and Trahair, N.S., "Steel Column Strength Models", *Journal of Constructional Steel Research*, 1988, Vol. 11, pp. 13-26.

# STRUCTURAL DESIGN OF A PRACTICAL SUSPENDOME

Zhi-Hong Zhang<sup>1,\*</sup>, Qing-Shuai Cao<sup>1</sup>, Shi-Lin Dong<sup>2</sup> and Xue-Yi Fu<sup>1</sup>

<sup>1\*</sup> Ph. D., China Construction (Shenzhen) Design International,  
NO.138, Kangjian Road, Shanghai, China, 200235

\*(Corresponding author: Email: zhangzh@zuua.zju.edu.cn)

<sup>2</sup> Professor, Space Structure Research Center, Zhejiang University,  
Hangzhou, Zhejiang Province, China, 310027

Received: 8 October 2007; Revised: 7 December 2007; Accepted: 10 December 2007

**ABSTRACT:** Structural design of a practical spherical suspendome with the diameter of 122m was carried out in China Construction (Shenzhen) Design International (CCDI) in 2006. The suspendome structure is a new type of large-span spatial structure which is widely used in the sports buildings. Several suspendome structures have been constructed as the structural roof in the sports arena in China in recent years. As is known to all, prestresses in the cable-strut system are crucial to the tensegric system, and the determination of prestress level and distribution is somewhat complicated. However, no provisions has been provided by current chinese design codes of practice for the suspendome structure. This paper gives out the detailed prestress design procedure for the practical sports arena which is to be built in Jinan City, China. General purpose finite element package ANSYS is utilized for the analyses. The self-internal-force mode and the prestress level ratio among three ring cables are investigated to determine the prestress in the cable. Linear static analyses are then carried out to validate the prestress efficiency. It has been shown that prestress defined by this way has much influence on the deformation and the internal force of the upper reticulated shell structure. The linear elastic buckling and the geometrically nonlinear stability analysis are also presented. The snap-through phenomenon of the structure is investigated to determine the critical load carrying capacity of stability. The influence of live load distribution patterns and imperfections on suspendome is addressed in details. The results from the studies can not only be referred for direct design use, and also for the design of similar hybrid structures.

**Keywords:** Space structure, suspendome, tensegric system, prestress, sports building, buckling, eigenmode, geometrically nonlinearity, imperfection

## 1. INTRODUCTION

With the development of the society, more and more novel structures which can cover larger space are needed. Large-span space structures have been put into application at a rapid rate for recent several decades. Based on the demands, several new types of space structure are developed (Liu [1] and Dong et al. [2]): the cable dome structure, the suspendome structure, the beam string structure, etc. Suspendome is a new type of large-span pre-stressed space structure which has only developed for more than one decade. It is a hybrid structure composed of the upper rigid single-layer latticed shell and the lower flexible cable-bar tensile system (Figure 1).

Suspendome structure consists of three types of member: the rigid member in the upper single-layer dome, the vertical strut and the cable in the lower tensegric system. Suspendome can be derived from two types of structure: 1) It is formed by replacing the upper cables of the cable dome by the rigid members, usually the single-layer latticed dome. Compared with the cable dome, prestress in the suspendome can be observably reduced. As the upper rigid members can provide certain initial stiffness to the structure, form finding analyses is no longer necessary and the construction techniques are simplified. The upper rigid member can resist both the axial force and the bending moments to increase the rigidity of the structure in one hand, and in the other hand the stress/force flow in suspendome may be closed, thus make the structure a self-equilibrium system, and weak bearing system is possible (Zhang [3], Zhang [4]). 2) The upper single-layer latticed dome is strengthened by the lower tensegric system. This method reasonably enhances the stiffness of the latticed shell and improves the buckling capacity. As the bearing horizontal reaction induced by the

service load is reverse to that induced by the tensegric system, the bearing horizontal reaction can be reduced to zero if proper prestress in the cables are introduced. The maximum value of axial force in the upper single-layer dome members can also be reduced by the tensegric system (Zhang [3], Zhang [4], Kang et al. [5], Kitipornchai [6]). So suspendome is also called “hybrid space structure”.

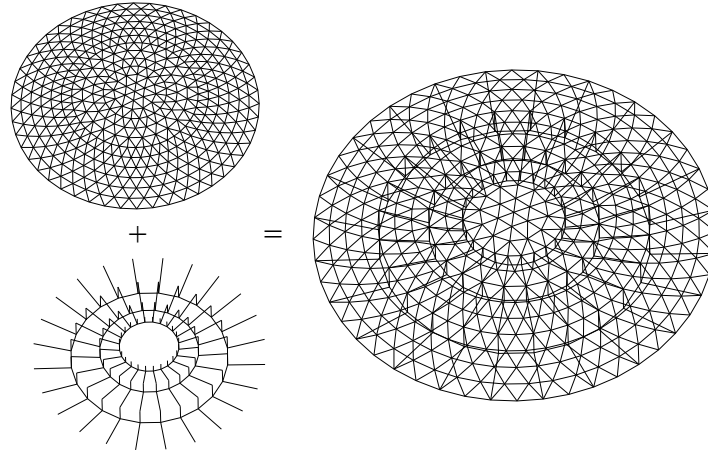


Figure 1. Suspendome: the Latticed Shell and the Cable-Strut System

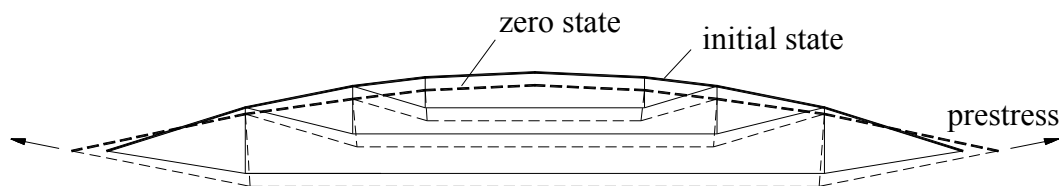


Figure 2. Zero State and Initial State of Suspendome

The suspendome design procedure is a little complicated. On the basis of the construction procedure of the suspendome, three typical reference configurations are defined (shown in Figure 2): 1) the zero state geometry, is the equilibrium state without prestress and without self-weight in the structure to determine the lofting during construction. 2) the initial state geometry, is the equilibrium state with prestress in the structure and under self weight after cambering, corresponding to the constructed configuration of the structure. 3) the loading state geometry, is the equilibrium state after loaded. The structural deformation in this paper is based on the initial state as the reference configuration, and the initial stresses in the members of the upper single layer dome are also taken into consideration.

Analytical and experimental research on the structural behavior of suspendomes has been performed in various approaches by the researchers (Zhang [3], Zhang [4,7], Kang et al. [5], Kitipornchai [6]). Based on Equilibrium Matrix Theory (Calladine and Pellegrino [8,9,10,11]), a new method called “local analyses method” to determine the structural self-internal-force mode is put forward (Zhang [3], Zhang [4,7]). The lower tensegric system is detached from the upper single layer dome as an independent system. Boundary restraints are applied to the lower independent tensegric system to determine the self-internal-force modes. The initial prestress distribution of the tensegric system can be obtained by the superposition of self-internal-force modes. The interaction of the lower tensegric system to the upper single layer dome is applied as the equivalent load to obtain the initial stress distribution of upper single-layer dome (the initial state, showed in Figure 2.). For detailed information, please refer to Reference [3].

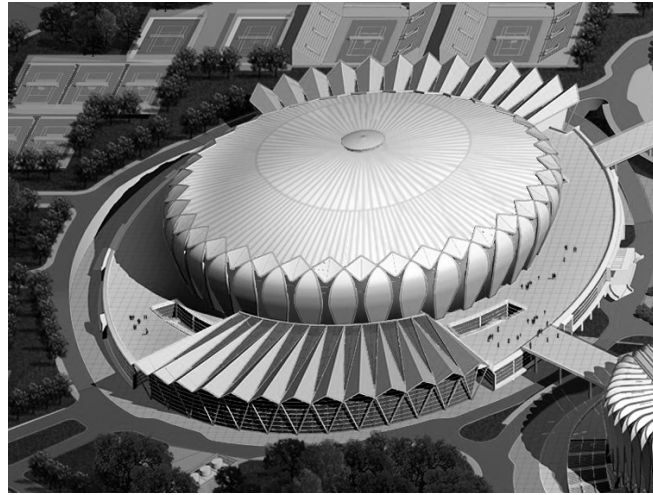


Figure 3. Airscape of Jinan Olympic Sports Center-the Gymnasium (China, 2009)

Several suspendome structures have been constructed in China in recent years (Liu [1] and Dong et al. [2]). However, no provisions has been provided by the current chinese design codes of practice for suspendome. The design method for the above mentioned constructed suspendome seems discretionary and unorganized. This paper gives out the detailed design procedure for the practical sports arena which is to be built in Jinan City, China, at the preliminary design stage (shown in Figure 3).

## 2. THE DESIGN MODEL

### 2.1 General Information of the Arena

Jinan Olympic Sports Center-the Gymnasium is a multi-purpose building and located in Jinan City, China. The facility will serve as the center-piece of the local Olympic Games held in the city in 2009. The building is in the shape of the ellipse with the longitudinal length 220 meters and the latitudinal length 168 meters (Figure 3). Two adjacent accessorial gymnastic building for warming up before the event are designed in the two ends of the Gymnasium. The building has an approximate architectural area  $60,000 \text{ m}^2$  which is to accommodate more than 12,000 audiences. The architectural style of the roof expositis full-bodied regional characteristics- the lotus flower and the willow leaf (Figure 3). Suspendome structure is chosen as the roof of the gymnasium. The span and the rise of the dome are 122.0m and 12.2m respectively, making the rise to span ratio 1/10. The Sunflower-Kiewitt patterned hybrid single-layer dome is used in the upper part of the roof structure. The roof is covered with the rigid profiled steel sheet. Three rings of cable-strut are arranged in the suspendome (Figure 4 and Figure 8). The suspendome consists of 1230 pipe members, 379 nodes, and 48 spherical steel bearings. The frame-shearwall concrete structure is used in the lower part of the building. The roof bearing joints is supported by alternate columns and the ring beam.

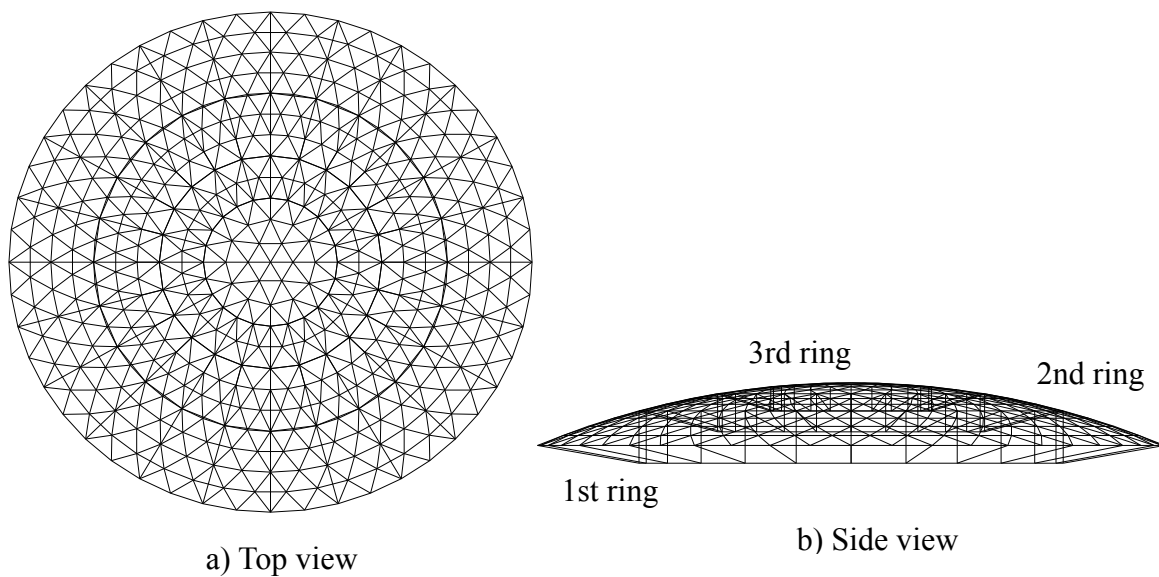


Figure 4. The Suspended Dome Structure for the Design

## 2.2 Finite Element Model

All analyses are carried out using the commercial general purpose finite element package **ANSYS**. The 3-D quadratic beam element BEAM188 which has three displacement and three rotational degrees-of-freedom (DOFs) is used to discretize the members in the upper dome and the spar element LINK10 with the tension-only (or compression-only) option which has three displacement degrees-of-freedom (DOFs) is used to model the cables and the struts. The material Q345B (GB50017-2003 [12]) is used in the members of upper single layer dome and the vertical struts which have properties typical of steel: an elastic modulus  $E$  of  $2.06 \times 10^5 \text{ N/mm}^2$ , a Poisson's ratio of 0.3 and a designed strength  $f$  of  $310 \text{ N/mm}^2$ . The cables are made of high-strength seven-steel-wires which have an elastic modulus  $E$  of  $1.90 \times 10^5 \text{ N/mm}^2$ , a Poisson's ratio of 0.3 and the ultimate tensile capacity  $1670 \text{ N/mm}^2$  (Shen et al. [13]). Both types of the material have the mass density of  $7850 \text{ kg/m}^3$ , and the thermal expansion coefficient of  $1.2 \times 10^{-5} / ^\circ\text{C}$ .

Each finite element node has six degrees of freedom including translations in the  $x$ ,  $y$ , and  $z$  directions and rotations about the  $x$ ,  $y$ , and  $z$  directions. Welded gapless steel pipes with the diameter 351mm and the thickness from 12mm, 14mm to 16mm are used in the upper single-layer dome. The chord member and the bracing member are connected each other to form the intersecting joint (GB50017-2003 [12]). As the bracing members are welded directly with the chord members, the connections are modeled as the rigid joints. The upper steel roof is supported by the lower concrete structure with the spherical steel bearings. Regarding the boundary conditions to the roof model, the connections are treated as hinged joints, i.e, all translational degrees of freedom (DOFs) are peripherally fixed at the bottom of the structure ( $U_x$ ,  $U_y$ ,  $U_z$ ). The finite element model is shown in Figure 5.

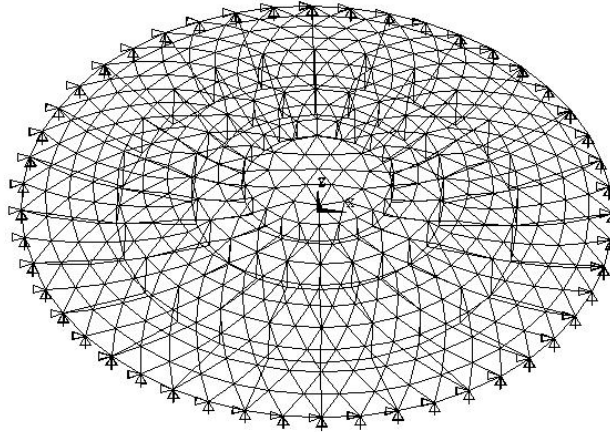


Figure 5. Finite Element Model of the Suspendome

### 3. DETERMINATION OF THE SELF-INTERNAL-FORCE MODE

This section determines the self-internal-force mode of the tensegric system based on the “local analysis method” (Zhang [3]). In the lower tensegric system, the cables and the vertical struts are hinged in the joints. The cables are tension-only elements and the vertical struts are compression-only elements. Nodal force equilibrium at each joint can be expressed in the  $x$ ,  $y$ , and  $z$  directions. The equilibrium equation of the lower cable-bar system is shown in Eq. 1 as follows.

$$[A]\{t\} = \{p\} \tag{1}$$

in which,  $[A]$  is the equilibrium matrix of the system-the function of nodal coordinates,

$\{t\}$  is the internal force vector of the elements,

$\{p\}$  is the equivalent force vector at the nodes.

Typical unit of the lower tensegric system is shown in Figure 6. By Singular Value Decomposition of the equilibrium matrix  $[A]$  (Calladine and Pellegrino [8,10,11]), the number of the self-internal-force mode  $s$  can be obtained as  $s=3$ . Figure 7 shows the axial force equilibrium in node  $i$ , where,  $N_{hci}$  is the axial force in the horizontal (hoop) cable;  $N_{dci}$  is the axial force in the diagonal (radial) cable;  $N_{vbi}$  is the axial force in the vertical strut,  $\alpha_i$  is the angle between the horizontal hoop cables and  $\beta_i$  is the angle between the diagonal cable and the vertical strut.

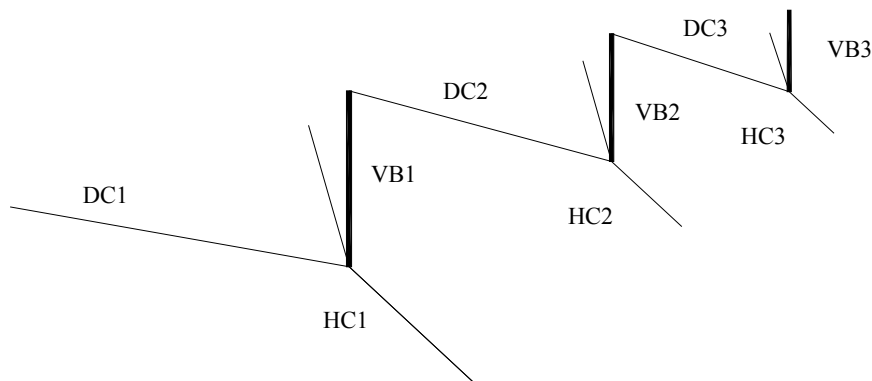


Figure 6. Typical Unit of the Lower Tensegric System

Note: DC, the diagonal cable; HC, the hoop cable; VB, the vertical strut.  
1,2,3 refers to the first (outmost), second (middle) and third (innermost) ring of the tensegric system respectively.



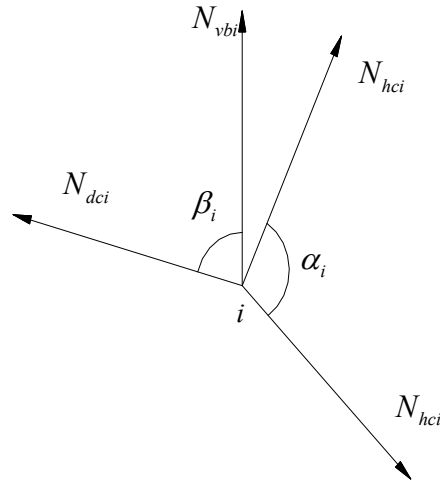


Figure 7. Axial Force Equilibrium in Typical Node  $i$ .

According to the force equilibrium in the vertical and the hoop direction, the equilibrium equation in node  $i$  can be expressed as:

$$N_{vbi} = -N_{dci} \cos(\beta_i) \quad (2)$$

$$N_{dci} \sin(\beta_i) = 2N_{hci} \cos(\alpha_i/2) \quad (3)$$

Combining Eq. 2 and Eq. 3, the following equations can be obtained:

$$N_{dci} = N_{hci} \frac{2 \cos(\alpha_i/2)}{\sin(\beta_i)} \quad (4)$$

$$N_{vbi} = -N_{hci} \frac{2 \cos(\alpha_i/2)}{\tan(\beta_i)} \quad (5)$$

Giving  $N_{hci} = 1$ , the self-internal-force mode in the  $i$ th ring of the tensegric system is:

$$[N_{hci}, N_{dci}, N_{vbi}] = \left[ 1, \frac{2 \cos(\alpha_i/2)}{\sin(\beta_i)}, -\frac{2 \cos(\alpha_i/2)}{\tan(\beta_i)} \right] \quad (6)$$

Three hoop rings altogether are designed in the structure (shown in Figure 4, 5, 6 and 8.). The angle  $\alpha_i$  ( $i=1,2,3$ ) in this model is  $165^\circ$ , and  $\beta_i$  is  $80^\circ, 75^\circ, 72^\circ$  respectively for  $i=1,2,3$ .

The self-internal-force modes of the lower cable-strut system for the outer, middle and inner ring are as follows:

$$[t] = [t_1, t_2, t_3]^T \quad (7)$$

$$\text{where, } \{t_1\} = [1.0, 0.2651, -0.0460]^T$$

$$\{t_2\} = [1.0, 0.2703, -0.0699]^T$$

$$\{t_3\} = [1.0, 0.2745, -0.0848]^T$$

#### 4. DETERMINATION OF CABLE PRESTRESS RATIO AMONG THREE HOOPS OF THE CABLE-STRUT SYSTEM

The number of rings in the tensegric system and the prestress level ratio among the rings have much influence on the structural behavior, therein, the outmost ring with prestress is the most effective (Zhang [3], Kang et al. [5]). As is mentioned above, steel pipes with diameter 351mm and thickness from 12, 14 to 16mm are used in the upper single-layer dome. The member arrangements of the upper single-layer dome are shown in Figure 8.

Characteristic combined load between uniformly distributed dead load  $0.8\text{kN/m}^2$ , and uniformly distributed live load  $0.3\text{kN/m}^2$  is applied to the roof as the service load (GB50009-2001 [14]). Each nodal external concentrated force is determined by the product of the combined load and its tributary area. The nodal tributary area is calculated by self-developed program. Linear static analysis is then carried out. As the three rings of cable-strut of the tensegric system are assumed to be independent of each other. The actions of each ring are applied separately to the upper single layer dome as the equivalent load. The prestressed force  $N_{hci}$  in each ring is assumed provisionally to be  $T_0 = 1000\text{kN}$ , when the dome is only stiffened by the single ring. The displacements of the upper single layer dome under dead and live load and each ring equivalent loads are listed in Table 1 together with the horizontal radial reaction of the bearing joint for the typical nodes defined in Figure 8.

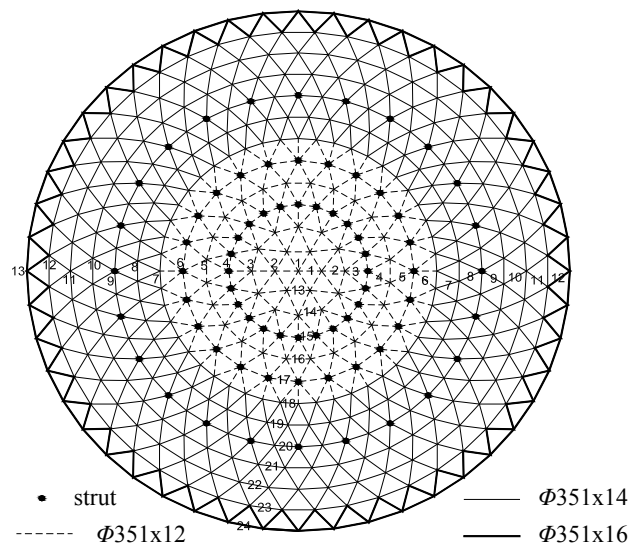


Figure 8 Member Arrangements for Upper Single Layer Dome and Typical Node and Element Numbers

Table 1. Vertical Displacements and Horizontal Radial Reactions for Three Rings of EL

	Node Vertical Displacement (mm)			Joint Horizontal Radial Reaction in Node 13 (kN)
	Node 9	Node 6	Node 4	
Dead +Live Load	-30.7160	-31.6642	-28.8879	1030.3
1st Ring EL	9.7831	-2.1155	-2.9381	-325.55
2nd Ring EL	-32.6276	40.3484	19.1530	8.85
3rd Ring EL	-1.9012	-42.6057	58.7856	-0.68

Note: EL, the equivalent load.

Relationship between the service load and three-ring equivalent loads is established to determine the prestressed force ratio among three rings of cable-strut system. The vertical displacement of the typical Node 4, 6 and 9 (the nodes at the top of the vertical struts) is considered to be zero under the dead and live load and the three rings of equivalent loads. So the relation can be expressed as:

$$[B]\{\varphi\} = \{b\} \quad (8)$$

$$\text{where, } [B] = \begin{bmatrix} 9.7831 & -32.6276 & -1.9012 \\ -2.1155 & 40.3484 & -42.6057 \\ -2.9381 & 19.1530 & 58.7856 \end{bmatrix}$$

$$\{b\} = [30.7160, 31.6642, 28.8879]^T$$

Solving the above equation,  $\{\varphi\}$  can be obtained:

$$\{\varphi\} = [8.7290, 1.6532, 0.3891]^T \quad (9)$$

From the above results, the prestress force ratio for the outmost ring has the largest value and consequently is the most effective. The prestress force (unit: kN) in the tensegric system can then be noted as:

$$[T] = T_0 \text{diag}[\{\varphi\}][t] = \begin{bmatrix} \text{HC} & \text{DC} & \text{VB} \\ 8729.0 & 2314.1 & -401.5 \\ 1653.2 & 4468.6 & -115.6 \\ 389.1 & 1068.1 & -33.0 \end{bmatrix} \begin{matrix} 1st \text{ Ring} \\ 2nd \text{ Ring} \\ 3rd \text{ Ring} \end{matrix} \quad (10)$$

in which,  $[t] = [t_1, t_2, t_3]^T$ , refers to Eq. 7,

$$\text{diag}[\{\varphi\}] = \begin{bmatrix} 8.7290 & & \\ & 1.6532 & \\ & & 0.3891 \end{bmatrix}$$

The joint horizontal radial reaction under three-ring equivalent load is  $R_e = -2827.36\text{kN}$ , it is opposite to and much greater than the reaction  $R_s = 1030.3\text{kN}$  induced by the service load. If full-scale prestress force is introduced to the cables, the reaction of bearing joint would be as large as 1800kN or so. This also adds difficulty for the design of the bearings and the prestress needs a second order optimization. For the wind load case, the reaction induced in the same bearing joint may be reversed for the case of randomness of the wind. The joint horizontal radial reaction under wind load is  $R_w = \pm 519.12\text{kN}$ . Assume that the prestress ratio among three rings keeps unchanged, a reduction factor  $\gamma$  is proposed to reduce the prestress level in the cable-strut system. The following equation is used to determine the reduction factor  $\gamma$ :

$$\gamma R_e + R_s = 0.5 \text{abs}(R_w) \quad (11)$$

where,  $R_e, R_s, R_w$  is the joint horizontal radial reaction under three-ring equivalent load, the service load and the wind load respectively, and  $\text{abs}(R_w)$  is the absolute value of the bearing reaction under wind load.

Substituting the value to Eq. 11,  $\gamma$  can be obtained:  $\gamma = 0.2726$ .

The optimized prestress force (unit: kN) for the tensegric system is determined as follows:

$$[T] = \begin{bmatrix} \text{HC} & \text{DC} & \text{VB} \\ 2379.5 & 630.8 & -109.5 \\ 450.7 & 121.8 & -31.5 \\ 106.1 & 29.1 & -9.0 \end{bmatrix} \begin{matrix} 1st \text{ Ring} \\ 2nd \text{ Ring} \\ 3rd \text{ Ring} \end{matrix} \quad (12)$$

The cables and struts are designed by the prestress forces obtained by Eq. 12. The geometric parameters and the designed prestress forces of the lower cable-strut system is shown in Table 2.

As the compressive elements, the lateral stability of the vertical struts should be verified. The Euler critical buckling capacity of the struts in the three rings is -341kN, -204kN and -93.1kN respectively by the equation  $N_{cr} = \pi^2 EI / (\mu l)^2$  (GB50017-2003 [12]), where,  $N_{cr}$  is the Euler critical buckling force,  $E$  is the material elastic modulus,  $I = \pi d^4 / 64$  is the inertia moment of the section,  $d$  is the strut diameter,  $\mu$  is the coefficient of effective length and  $\mu=1$ ,  $l$  is the geometric length of the vertical strut. Hence, the struts buckling capacity is satisfied.

Table 2. Prestresses and Geometries of the Lower Tensegric System

	1st Ring			2nd Ring			3rd Ring		
	HC1	DC1	VB1	HC2	DC2	VB2	HC3	DC3	VB3
Section	2Φ7x85	Φ7x55	Φ203x6	Φ7x31	Φ7x13	Φ152x4.5	Φ7x7	Φ7x7	Φ95x3.5
Area (mm <sup>2</sup> )	6542	2117	3826	1193	500	2147	269	269	1045
Inertia Moment(m <sup>4</sup> )	-	-	1.80e-5	-	-	5.86e-6	-	-	1.05e-6
Length (m)	10.772	20.043	10.217	6.780	15.830	7.416	4.080	10.875	4.728
Initial strain (μϵ)	1914.4	1568.2	-139.0	1988.2	1282.1	-71.21	2075.0	569.56	-41.79
Prestress Force (kN)	2379.5	630.8	-109.5	450.7	121.8	-31.5	106.1	29.1	-9.0

## 5. STATIC ANALYSES

This section presents the results of linear static response of suspendome and single-layer dome (SLD) under service load to validate the efficiency of the designed prestresses (prestress stiffening effect is considered). Based on the linear superposition theory, the structural displacement at the top of the strut is zero under combined dead and live load with the full-scale three-ring prestress. The deformation for non-optimal prestress suspendome under service loads is shown in Figure 9. The maximum vertical displacement occurs between the bearing joint and the outmost ring (Node 11, Figure 8), and the value is only 34.23mm. The deformation for the optimized prestress suspendome under service loads is shown in Figure 10. The maximum vertical displacement occurs between the outmost ring and the middle ring (Node 7, Figure 8), and the value is only 26.42mm.

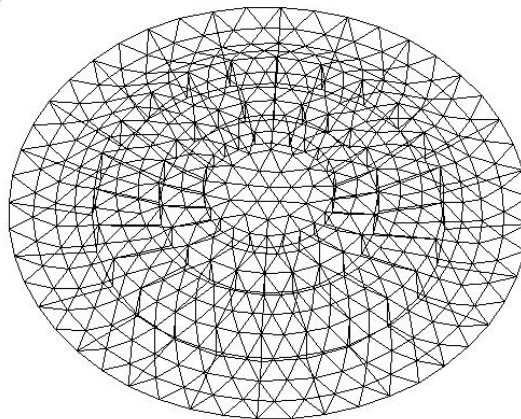


Figure 9. Deformation of Suspendome under the Service Load ( $\gamma = 1.0$ , scaled by a factor of 100)

The vertical displacement for the typical numbered nodes (as defined in Figure 8) of the single-layer dome and the suspendome under service load is shown in Figure 11. The vertical displacement of the single-layer dome is larger than that of the suspendome. The single layer dome has the largest downward displacement and occurs at Node 7. The non-optimized prestress suspendome has the smallest downward displacement and occurs at Node 9. The deformation seems uneven and fluctuates greatly up and down in the vertical direction for the unreasonable tensegric prestress distribution and even upward displacement in Node 5 is induced. This reveals the fact that the outmost ring of the tensegric system has the most effects on the suspendome structure, and the other two rings has relatively low effects on the structure. After prestress optimization, the deformation becomes uniform, and the largest downward displacement is 26.42mm, corresponding to the ratio of the deflection to the span 1/4618. The displacement of the optimized tensegric system greatly satisfies the structural allowable deflection specifications  $L/400$  ( $L$  is the dome span) (GB JGJ61-2003 [15])and the architectural design.

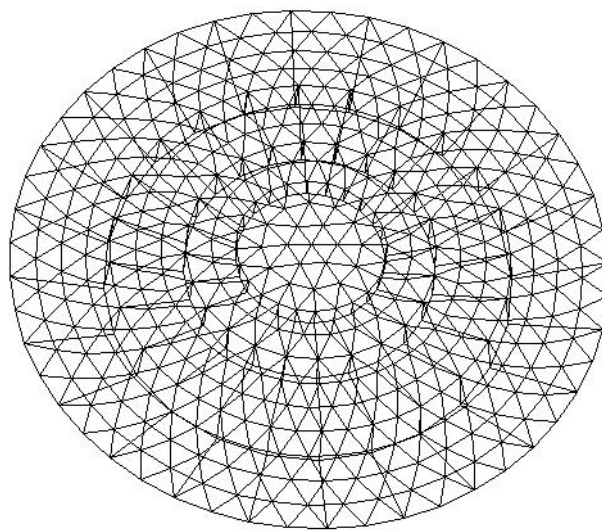


Figure 10. Deformation of Suspendome under the Service Load ( $\gamma = 0.2726$ , scaled by a factor of 100)

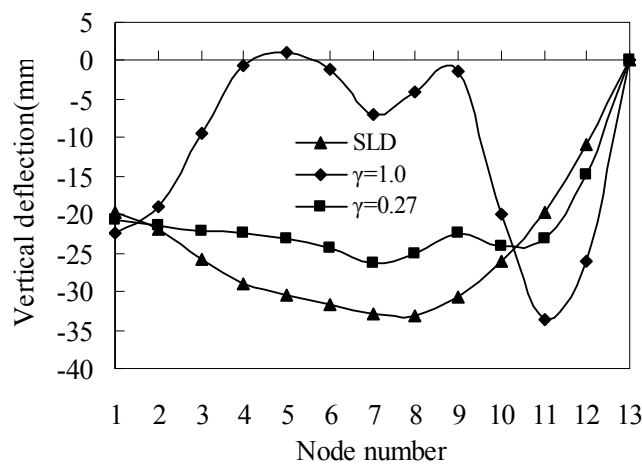


Figure 11. Vertical Displacement of Typical Numbered Nodes under Service Load

Normally, tensile axial forces in the members of the upper suspendome are induced by the lower tensegrity system. It is incompatible with the compressive axial force induced by the service load. So proper prestress introduced in lower tensegric system will greatly counteract the effects caused by the service load. The horizontal radial reactions are 320.8kN in the optimized suspendome and 963.5kN in the single layer dome under service load. The maximum axial forces are 469.3kN, 496.6kN, 545.8kN in the optimized suspendome and 498.2kN, 483.5kN, 645kN in the single-layer dome under the same service load for pipe section  $\Phi 351 \times 12$ ,  $\Phi 351 \times 14$ ,  $\Phi 351 \times 16$  respectively. It shows that not only the bearing reactions but also the pipe member axial force of the suspendome can decrease greatly compared to the single-layer dome under the same service load.

The axial force for the typical numbered radial members (as defined in Figure 8) of the single-layer dome and the suspendome under service load is shown in Figure 12. The axial force of the single-layer dome is larger than that of the suspendome. The axial force in the non-optimized prestress suspendome is greatly uneven in the radial direction for the unreasonable tensegric prestress distribution. The axial force in Member 9 (connected with the first ring, as stated in Figure 8) is near to zero. This suggests again that the outmost ring of the tensegric system has the most effects on the static property of the suspendome structure. The axial forces in the optimized suspendome are very even, and it is favorable for the member design.

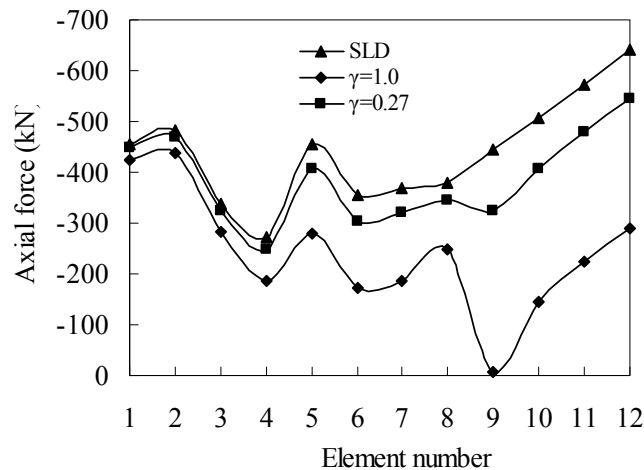


Figure 12. Radial Axial Force of Typical Numbered Elements under Service Load

Figure 13 shows the axial force for the typical numbered hoop members (as defined in Figure 8) of the single layer dome and the suspendome under service load. The characteristics of the axial forces distribution are very similar to that shown in Figure 12. The axial forces in the optimized suspendome are very even, and is also favorable for the member design.

It is noteworthy that the stress ratio (the ratio of the peak sectional stress of the members to the material design strength  $f$ ) of the elements in the dome under service load is usually comparatively small ranging from 0.1 to 0.5, thereby the material strength is unlikely to govern the structural design.

From the above analyses, it can be concluded that the optimized prestress defined by Equation 12 is harmonious with both the axial force and the deformation of the structure. The optimized prestress level is used for all analyses below.

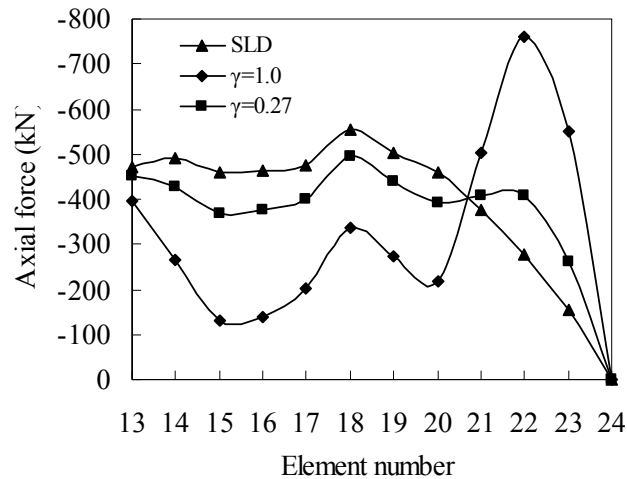


Figure 13. Hoop Axial Force of Typical Numbered Elements under Service Load

## 6. LINEAR ELASTIC BUCKLING ANALYSES

Buckling analysis, in general, may be divided into linear elastic buckling (bifurcation) and geometrically nonlinear buckling (snap-through) analysis. Geometrically nonlinear analyses are usually used to determine the limit load of the structure which are usually started with a linear buckling analysis. Linear buckling analysis predicts the theoretical buckling strength (the bifurcation point) of an ideal linear elastic structure. The results are buckling modes and load factors (eigenvalue). Load factors are estimated for an upper limit of the ultimate load. The buckling modes are related to a structure that maintains its shape up to buckling. If the load applied to the structure is  $P$ , the critical buckling load is  $\lambda P$ . The equation of bifurcation buckling is expressed as an eigenvalue problem:

$$([K] + \lambda_i [S])\{\psi_i\} = 0 \quad (13)$$

where:  $[K]$  is the stiffness matrix of the system,

$[S]$  is the stress stiffness matrix,

$\lambda_i$  is a load factor, the  $i$ th eigenvalue determining buckling load,

$\{\psi_i\}$  is the  $i$ th eigenvector determining the buckling mode.

This section presents the linear buckling of suspendome using a linearized model of elastic stability. Two load cases are considered for this section and the below: Load Case 1, the dead load combining the full-span live load (LC1); Load Case 2, the dead load combining the half-span live load (LC2). Half-span live load such as the snow load and the construction load is proved to decrease the structural load-carrying capacity in most circumstances and often neglected by the structural designer.

The eigenvalues are listed in Table 3, which shows that the buckling capacity of the suspendome is very high and the capacity for LC1 is higher than that for LC2 for the influence of the unsymmetrical distribution of the live load. The lowest bifurcation eigenvalue amounts to 12.13 for LC1 and to 10.86 for LC2 respectively. The buckling capacity decreases by 10.47% for the influence of the unsymmetrical live load..

Table 3. Eigenvalues of Suspendome for LC1 and LC2

$n$	1	2	3	4	5	6	7	8	9	10
LC1	12.13	12.13	13.02	13.04	13.04	13.16	13.17	13.48	13.48	13.54
LC2	10.86	10.96	11.25	11.27	11.29	11.48	11.66	11.67	11.89	11.95

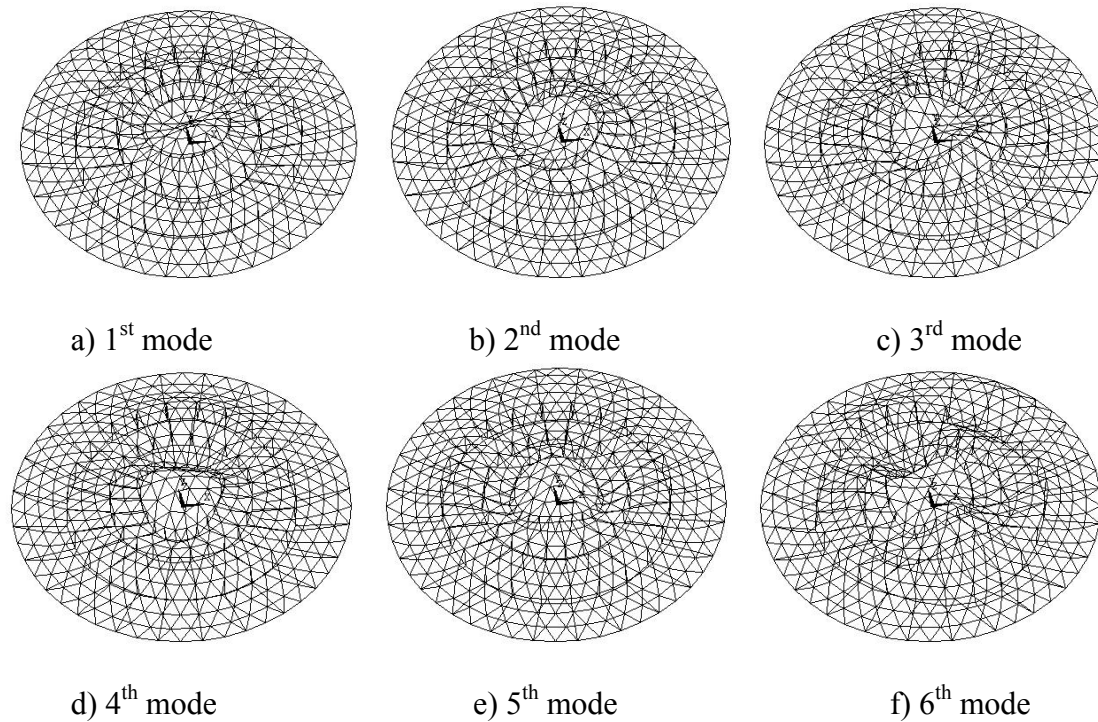


Figure 14. The Anterior Six Eigenbuckling Modes of Suspendome for LC1

Figure 14. and Figure 15. show the anterior six eigenbuckling modes of suspendome LC1 and LC2. The eigenvalues are very close and the buckling modes are very dense for the two cases for the influence of the cable-strut prestresses. The buckling modes are usually in symmetrical shape for structure for LC1 and unsymmetrical shape for LC2. It can also be observed from the figures that the buckling region of the suspendome for LC1 is more localized in the center and buckling usually begin with great deformation in the central area. This phenomenon can be established by the fact that the central area of the dome with a diameter about 30 meters is single-layered within the third ring of cable-strut system, thus makes actually a secondary single-layer latticed dome which is unstiffened by the lower tensegric system. Since the suspendome is mainly stiffened by the outmost ring of the tensegric system, the local weaker stiffness detected in the structural center is reasonable and expected. For LC2, the most localized deformation is usually in the area adjacent to the structural boundary for the influence of the unsymmetrical live load. As the increase of the buckling number  $n$ , the buckling region becomes extended to the structural boundary. The buckling deformation induces more fluctuations on the surface, and consequently shifts to the global buckling mode.



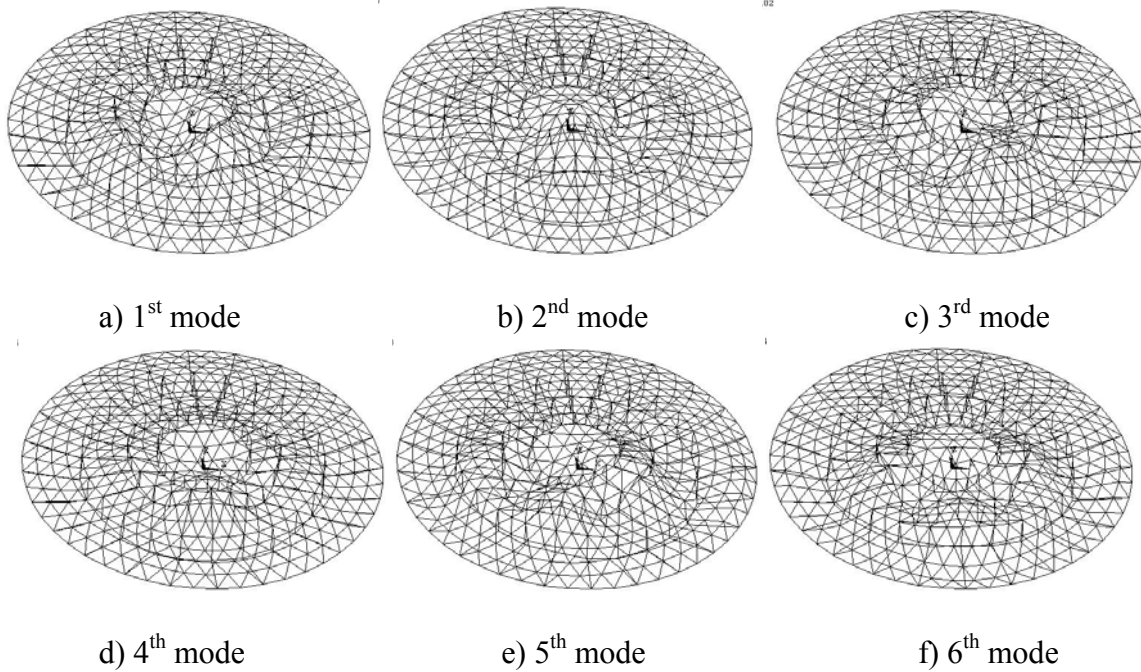


Figure 15. The Anterior Six Eigenbuckling Modes of Suspended Dome for LC2

## 7. GEOMETRICALLY NONLINEAR STABILITY ANALYSIS

Eigenvalue buckling analysis predicts the theoretical buckling strength (the bifurcation point) of an ideal linear elastic structure. However, imperfections and nonlinearities prevent most real-world structures from achieving their theoretical elastic buckling strength. Thus, eigenvalue buckling analysis often yields unconservative results, and should generally not be used for the design of actual structures. The nonlinear buckling considers a load-dependent prebuckling deformation during loading up to the structural instability. In this case, the instability is connected with relatively large displacement amplitudes without a significant change of the equilibrium path. For the slender tensegric system as suspended dome structure, large displacement may be induced in the structure when loaded. So, it is proper to carry out the geometrically nonlinear analyses for suspended dome structure.

The geometrically nonlinear analyses account for the initial geometric imperfection, which could be obtained by the linear superposition of linear buckling eigenmodes. The initial geometric imperfection, hereby, can be expressed in the following expression:

$$\{\delta\} = \sum_{i=1}^n a_i \{\psi_i\} \quad (14)$$

where,  $\{\delta\}$  is the imperfection vector,

$a_i$  is the scale coefficient associated with the  $i$ th eigenvector,

$\{\psi_i\}$  is the  $i$ th eigenvector determined by Eq. 13.

Usually the lowest eigenvector is only used to determine the imperfection distribution. The maximum value of imperfection is chosen as  $L/300$  ( $L$  is the dome span) (GB JGJ61-2003 [15]) in the design, i.e.  $\delta_{\max}$  is equal to 406.67mm. For the normalized eigenmode shape,  $a_1$  is equal to  $\delta_{\max}$  and  $a_i$  is equal to 0 ( $i > 1$ ) in Eq. 14.

This section presents the geometrical nonlinearity of the suspendome. The Arc-length solution technique combined with the Newton-Raphson method is adopted for the analyses. The buckling deformation and critical buckling strength are mainly addressed for the geometrically perfect and imperfect structure for LC1 and LC2. The load-deflection curves approves the typical instability mode of the “snap-through” phenomenon for geometrically perfect and imperfect models. It is shown that the equilibrium path is highly nonlinear, especially for the postbuckling stage. In the prebuckling stage, the equilibrium path for the perfect model inclines with a sheer ascend, and the slope turns to be gentle when close to the critical point. After the maximum load factor (critical point) is reached, the path usually descends with a rather steep load decay, even the curve backtracks to an unstable equilibrium path. The load factor corresponding to the critical point is used as the buckling strength for the perfect model. In addition, the equilibrium path for the imperfect model ascends more gently before the critical point is reached. Large deflection is induced when the structure buckles which is usually more than ten times of that for

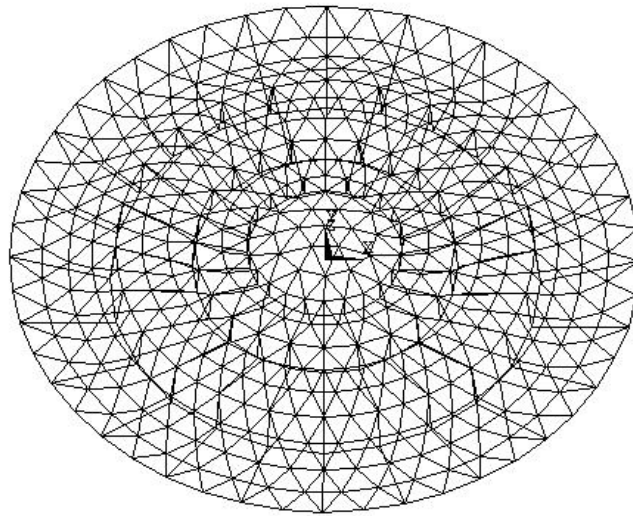


Figure 16. Buckling Mode of Suspendome for LC1

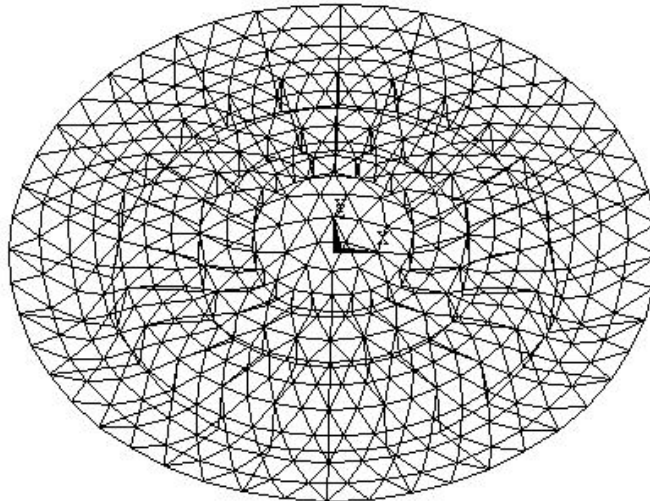


Figure 17. Buckling Mode of Suspendome for LC2

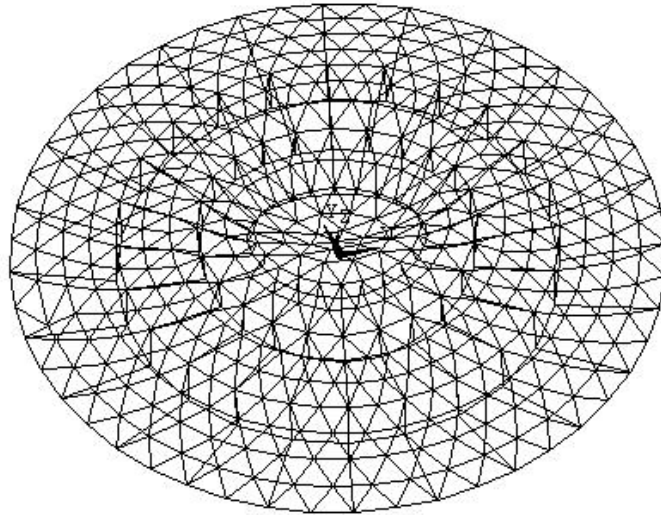


Figure 18. Buckling Mode of Suspended Dome for LC1 with  $L/300$  Imperfection

the perfect model, and is unlikely to satisfy the deflection limitations. In the equilibrium path, no maximum load factor is reached in the range of deflection specifications which should not be more  $L/400$  (GB JGJ61-2003 [15]). The load factor corresponding to the vertical deflection with the magnitude of  $L/400$  is specified as the buckling strength for the imperfect model. After the structure reaches its critical point, the equilibrium paths usually tend to increase in a plateau and the structure possess good postbuckling strength retention capability. The global stiffness of the structure tend to degenerate to naught. This seems to be a clear sign of instability of the structure and the failure may be a sudden phenomenon. The postbuckling is so complicated that the equilibrium path is difficult to trace down.

The maximum load factors are 9.91 and 8.89 for the geometrically perfect model, and 5.22 and 4.59 for the geometrically imperfect model for LC1 and LC2 respectively. The structural limit load decrease by 10.29% of perfect model and 12.07% of imperfect model for the influence of unsymmetrical distribution of the live load. The influence of imperfection is even more destructive to the structure. The limit load decrease by 47.33% for LC1 and 48.37% for LC2.

The buckling modes are shown in Figure 16-19 for the geometrically perfect and imperfect structure for LC1 and LC2 respectively. The deformations for perfect models for LC1 are symmetrical global buckling modes and unsymmetrical global modes for LC2. The most vertical displacement for LC1 occurs in the structural center (Node 1, Figure 8). The deformation for LC2 is more localized (Node 11, Figure 8) in the area to which the half-span live load is applied. The structural center (Node 1, Figure 8) only deflects a small vertical displacement. The most vertical displacement occurs in the areas between the outmost ring and the boundary for the two cases, and this show little agreement with the results from the bifurcation analyses.

The deformations for imperfect models for LC1 and LC2 are both unsymmetrical local buckling modes. As it is well known, large span structures are most sensitive against imperfections. From the bifurcation analyses, the eigen modes are localized in the center for LC1 and adjacent to the boundary for LC2. As the introduction of the eigen-imperfection, the revised structural configuration consequently has the most imperfection in the center for LC1 and the boundary area for LC2. The buckling modes (Figure 18 and 19) are localized in the center for LC1 and adjacent to the boundary for LC2, and this show good agreements with the linear buckling modes.

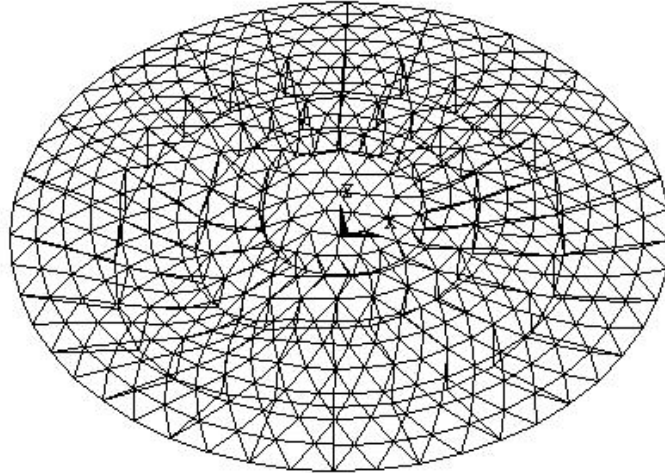


Figure 19. Buckling Mode of Suspendedome for LC2 with  $L/300$  Imperfection

From the above analyses, the perfect and imperfect structure under LC1 and LC2 has large buckling strength. At the same time, local stiffness in the structural center is comparatively weak, and the section of pipe elements in the center area (showed in Figure 8.) are change from  $\Phi 351 \times 12$  to  $\Phi 351 \times 14$  in the end to strengthen the structural center.

## 8. CONCLUSIONS

Prestress induced in the cable and the strut have much influence on the deformation and the internal force of the suspendedome structure. Proper prestresses should be defined according to the structural design requirements. The deflection and the stress of the structure under service load is usually easy to satisfy the design limitation specified in the relevant codes. The imperfections and live load distribution patterns have much influence on the buckling strength and the modes. For large-span structure such as the suspendedome, it is obvious that the material strength and structural vertical deflection are most unlikely to govern the design, and design limitations should be based on the buckling strength of the structure.

The analyses above are only parts of the design procedure in the preliminary design stage, further studies are carried out to investigate dynamic behaviors under the seismic effect (response spectrum and elastic-plastic dynamic time-history analyses) and the wind load (wind-induced vibration), the construction simulation analysis and the progressive collapse (cable breakage) analysis is also carried out.

## ACKNOWLEDGMENTS

The authors gratefully acknowledge the support of the Committee of National Science Foundation of China (Grant 50638050#).

**REFERENCES**

- [1] Liu, X.L., “Modern Spatial Structures”, Tianjin University Press, 2003 (in Chinese).
- [2] Dong, S.L., Luo, Y.Z. and Zhao, Y., “Analysis, Design and Construction of New Spatial Structure”, China Communication Press, 2007 (in Chinese).
- [3] Zhang, Z.H., “Theoretical Research on Large-Span Tensile Spatial Structures Composed of Cables, Bars and Beams”, PhD Thesis, Space Structure Research Center, Depart of Civil Engineering, Zhe Jiang University, 2003 (in Chinese).
- [4] Zhang, M.S., “Theoretical Research on Suspendome”, PhD Thesis, Space Structure Research Center, Depart of Civil Engineering, Zhe Jiang University, 2004 (in Chinese).
- [5] Kang, W.J., Chen, Z.H., Lam, H.F. and Zuo, C.R., “Analysis and Design of the General and Outmost-ring Stiffened Suspendome Structures”, *Engineering Structures*, 2003, Vol. 25, No. 13, pp.1685-1695.
- [6] Kitipornchai, S., Kang, W.J., Lam, H.F. and Albermani, F., “Factors Affecting the Design and Construction of Lamella Suspendome Systems”, *Journal of Constructional Steel Research*, 2005, Vol. 61, pp. 764-785.
- [7] Zhang, M.S., Dong, S.L. and Zhang, Z.H., “Distribution of Initial Prestress and Stability Analysis of Suspendome”, *Spatial Structures*, Vol. 10, No. 2, pp. 8-12 (in Chinese).
- [8] Pellegrino, S. and Calladine, C.R., “Matrix Analysis of Statically and Kinematically Indeterminate Frameworks”, *International Journal of Solids Structures*, 1986, Vol. 22, No. 40, pp. 409-428.
- [9] Calladine, C.R. and Pellegrino, S., “First-order Infinitesimal Mechanisms”, *International Journal of Solids Structures*, 1991, Vol. 27, No. 4, pp. 505-514.
- [10] Pellegrino, S., “Analysis of Prestressed Mechanisms [J]. *Int. J. Solids Structures*, 1990, Vol. 26, No. 12, pp. 1329-1350.
- [11] Pellegrino, S., “Structural Computations with the Singular Value Decomposition of the Equilibrium Matrix”, *International Journal of Solids Structures*, 1993, Vol. 30, No. 2, pp. 3025-3036.
- [12] GB50017-2003, “Code for Design of Steel Structures”, Chinese Planning Press, Beijing (in Chinese).
- [13] Shen, S.Z., “Design of Cable Structures”, China Architecture and Building Press, Beijing, 2<sup>nd</sup> Edition, 2006 (in Chinese).
- [14] GB50009-2001, Load Code for the Design of Building Structures”, Chinese Planning Press, Beijing (in Chinese).
- [15] GB JGJ61-2003, “Technical Specification for Latticed Shells”, Chinese Planning Press, Beijing (in Chinese).

# A NONLINEAR ANALYSIS METHOD OF STEEL FRAMES USING ELEMENT WITH INTERNAL PLASTIC HINGE

Yu-Shu Liu<sup>1,\*</sup> and Guo-Qiang Li<sup>2</sup>

<sup>1</sup>Lecturer, School of Civil Engineering, Tongji University, Shanghai, China

\*(Corresponding author: E-mail: ysliu@tongji.edu.cn)

<sup>2</sup>Professor, School of Civil Engineering, Tongji University, Shanghai, China

*Received: 18 October 2007; Revised: 11 December 2007; Accepted: 12 December 2007*

---

**ABSTRACT:** A nonlinear analysis method of steel frames using element with internal plastic hinge is proposed. This method can analyze the frame member applied with laterally-distributed loads only using one element even that a plastic hinge appears within the member. By dividing the member into two segments at the location of the maximum moment, the incremental stiffness matrix of the two segments from time  $t$  to  $t + dt$  are derived, then the beam element stiffness equation with internal plastic hinge after the static condensation can be obtained. What's more, this method also considers the influences of some geometrical and material nonlinear factors including second-order effect of axial forces, shear deformation, cross-sectional plastification, residual stress and initial imperfection. This method not only overcomes the time-consuming disadvantages of plastic zone method of frame members because of the fine mesh discretization but also makes up for the problem of the traditional plastic hinge element that plastic hinges must form at the elemental ends. Analysis results show that the proposed method is satisfactory.

**Keywords:** Steel frames; nonlinear analysis; internal plastic hinge; plastic zone method; cross-section plastification

---

## 1. INTRODUCTION

The members of a steel frame may be subjected to laterally-distributed loads, so plastic hinges will be formed within the members. The common method [1,2,3,4,5] to treat this case for analysis of the frame is to arrange a node at the location of the plastic hinge within the member to divide the original one element into two or more elements representing the member. This will increase the number of nodes and degrees of freedom for analysis of the frame. Moreover, the traditional element with plastic hinge formed at the end(s) must fix the locations of nodes in advance, which can not suit the case that the locations of the plastic hinge within the member with laterally-distributed loads may vary during the loading process. In this paper, an approach for nonlinear analysis of steel frames using element with internal plastic hinge is proposed. This approach can use one element to simulate one member in a frame even plastic hinge may form within the member.

## 2. NONLINEAR ANALYSIS METHOD OF STEEL FRAMES

### 2.1 Plastic Zone Method and Plastic Hinge Method

Over the past 20 years, scholars has developed and validated various methods of performing second-order inelastic analyses on steel frames [1,2,3,4,5]. Most of these studies may be categorized into one of two types: (1) plastic zone method; or (2) plastic hinge method based on the degree of refinement used to represent yielding. The plastic zone method uses the highest refinement while the elasto-plastic hinge method allows for a significant simplification. The load deformation characteristics of the plastic analysis methods are illustrated in Figure 1.

In the plastic zone method[1,2,3,4,5], a frame member is discretized into finite elements, and the cross-section of each finite element is subdivided into many fibers. The deflection at each division along the member is obtained by numerical integration. The incremental load deflection response at

each load step, with updated geometry, captures the second-order effects. The residual stress in each fiber is assumed constant since the fibers are sufficiently small. The stress state of each fiber can be explicitly determined, and the gradual spread of yielding traced. A plastic zone analysis eliminates the need for separate member capacity checks since second-order effects, the spread of plasticity, and residual stresses are accounted for directly. As a result, a plastic zone solution is considered 'exact.' Although the plastic zone solution may be considered 'exact,' it is not applicable to daily use in engineering design, because it is too computationally intensive and too costly. Its applications are limited to: (1) the study of detailed structural behavior; (2) verifying the accuracy of simplified methods; (3) providing comparisons for experimental results; (4) deriving design methods or generating charts for practical use; and (5) application to special design problems.

A more simple and efficient way to represent inelasticity in frames is the elasto-plastic hinge method [1,2,3,4,5]. Here the element remains elastic except at its ends where zero-length plastic hinges form. This method accounts for inelasticity but not the spread of yielding through the section or between the hinges. The effect of residual stresses between hinges is not accounted for either. The elasto-plastic hinge methods may be first- or second-order. In a first-order plastic analysis, nonlinear geometrical effects are considered negligible, and not included in the formulation of the equilibrium equations. As a result, this method predicts the same ultimate load as a conventional rigid plastic analysis would. In a second-order plastic analysis, the effect of the deformed shape is considered. The simplest way to model the geometrical nonlinearities is to use stability functions. These use only one beam-column element to define the second-order effect of an individual member. Stability functions are an efficient and economical method of performing a frame analysis. It has distinct advantage over the plastic zone method for slender members (whose dominant mode of failure is elastic instability) as it compares well with plastic zone solutions. However, for stocky members (which sustain significant yielding), the simple elasto-plastic hinge method over-predicts the capacity of members as it neglects to consider the gradual reduction of stiffness as yielding progresses through and along the member. Consequently, modifications must be made before this method can be proposed for a wide range of framed structures.

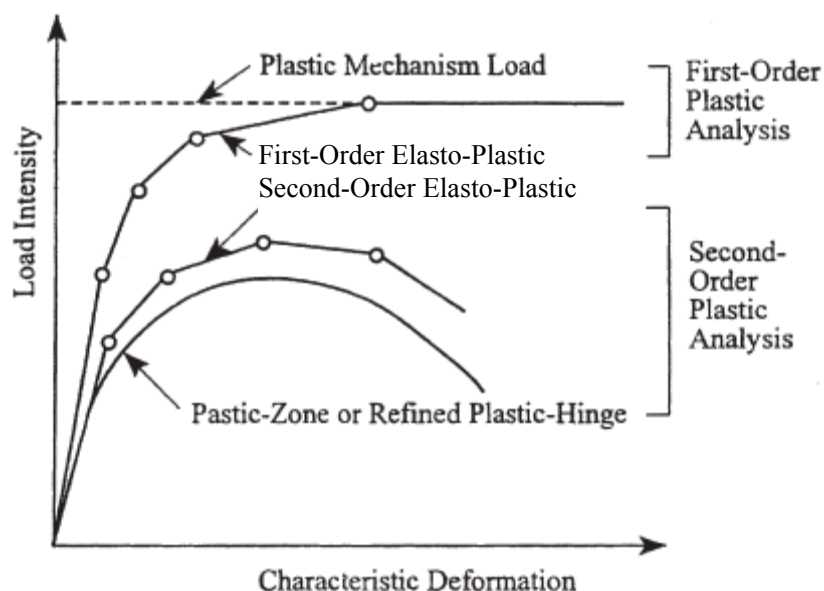


Figure 1. Load Deformation Characteristics of Plastic Analysis Methods

## 2.2 Refined Plastic Hinge Method

A refined plastic hinge analysis incorporates consideration of geometrical and material nonlinear factors including second-order effect of axial forces, shear deformation, cross-sectional plastification, residual stress and initial imperfection to the analysis of steel frames. The concept is outlined in the following section.

### 2.2.1 Column element

Li and Shen [6] presented an improved plastic hinge model, which considered the cross-section plastification. Using this model the elasto-plastic incremental stiffness equation of the frame column element is given by

$$[k_p]\{\Delta\delta\} = \{\Delta f\} \quad (1)$$

Where,  $\{\Delta\delta\}$  and  $\{\Delta f\}$  refer to the incremental nodal displacements and forces, respectively,  $[k_p]$  refers to the elasto-plastic stiffness matrix, and takes the following form

$$[k_p] = [k_e] - [k_e][G][E][L][E]^T[G]^T[k_e] \quad (2)$$

where

$$\begin{aligned} [L]^{-1} &= [E]^T[G]^T([k_e] + [k_n])[G][E] \\ [k_n] &= \text{diag}[\alpha_1 k_{e11}, \alpha_1 k_{e22}, \alpha_1 k_{e33}, \alpha_2 k_{e44}, \alpha_2 k_{e55}, \alpha_2 k_{e66}] \\ [E] &= \begin{bmatrix} 1 & 1 & 1 & 0 & 0 & 0 \\ 0 & 0 & 0 & 1 & 1 & 1 \end{bmatrix}^T \\ [G] &= \text{diag}\left[\frac{\partial x_1}{\partial N_1}, 0, \frac{\partial x_1}{\partial M_1}, \frac{\partial x_2}{\partial N_2}, 0, \frac{\partial x_2}{\partial M_2}\right] \end{aligned}$$

$[k_e]$  represents the elastic stiffness matrix of the beam element accounting for the second order effect and shearing deformation[6]. In matrix  $[G]$ ,  $x_i$  ( $i=1,2$ ) denotes the ultimate yield surface function of the section. In this paper, the ultimate yield surface function for I type section given by reference [3] and [7] is used here and can be written as

$$x_i = \left(\frac{N}{N_y}\right)^{1.3} + \frac{M}{M_p} = 1 \quad (3)$$

In matrix  $[k_n]$ ,  $\alpha_i$  ( $i=1,2$ ) denotes the elasto-plastic hinge parameter of the two end sections, represents the plastification extent of the two end sections and can be expressed as

$$\alpha_i = \frac{r_i}{1 - r_i} \quad (4)$$



Where,  $r_i (i = 1, 2)$  is the restoring force parameter of the two end sections and takes the form as

$$r_i = \begin{cases} 1 & M \leq M_{sN} \\ 1 - \frac{M - M_{sN}}{M_{pN} - M_{sN}}(1 - \beta) & M_{sN} \leq M \leq M_{pN} \\ \beta & M \geq M_{pN} \end{cases}$$

$M$ ,  $M_{sN}$  and  $M_{pN}$  represent the moment of the section, the initial yield moment the ultimate yield moment under the axial force  $N$ , respectively.  $\beta$  represents the material strain hardening coefficient, for normal low carbon steel and low alloyed steel,  $\beta$  can take 0.01~0.02, and  $M_{pN}$  can be given by equation (3).

The initial yield surface equation [3,7] without accounting for the influences of residual stress is expressed as

$$\frac{N}{N_y} + \frac{\gamma M}{M_p} = 1.0 \quad (5)$$

$$\text{and } M_{sN} = (1.0 - \frac{N}{N_y})M_p / \gamma \quad (6)$$

The initial yield surface equation [3,7] accounting for the influences of residual stress is expressed as

$$\frac{N}{0.8N_y} + \frac{\gamma M}{0.9M_p} = 1.0 \quad (7)$$

$$\text{and } M_{pN} = 0.9(1.0 - \frac{N}{0.8N_y})M_p / \gamma \quad (8)$$

where,  $\gamma$  is the plastification coefficient of the section.

### 2.2.2 Beam element with internal plastic hinge

Figure 2 shows the beam element with internal plastic hinge. Referring to Figure 2, an internal node  $C$  between elemental ends is inserted so that the element is divided into two segments, the lengths of which are  $L_a$  and  $L_b$  respectively. Assume the maximum bending moment,  $M^{(1)}$ , at time  $t$  is at position  $C'$  and the maximum bending moment,  $M^{(2)}$ , at time  $t + dt$  is at position  $C$  (see Figure 3). For derivation of incremental stiffness matrix of the element during  $t \rightarrow t + dt$ , a virtual state of moment,  $M^{(2)}$ , is conceived, which is the bending moment at the same position of  $M^{(2)}$  at the time  $t$ . The incremental stiffness relationship of each segment of the element can be expressed as the standard form as

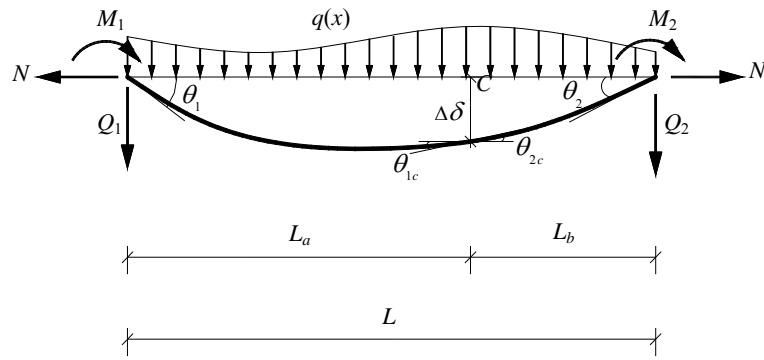


Figure2. Beam Element with Internal Plastic Hinge

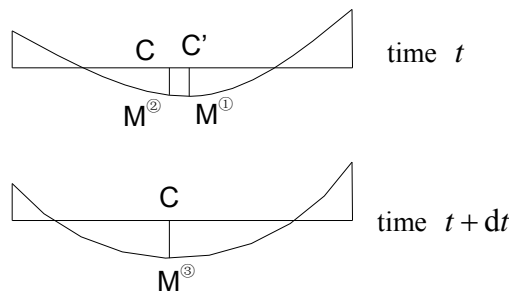


Figure3. Position of Maximum Moment of Different Load Step

for the segment of  $L_a$

$$\begin{Bmatrix} dQ_1 \\ dM_1 \\ dQ_{1c} \\ dM_{1c} \end{Bmatrix} = [K_{pa}] \begin{Bmatrix} d\delta_1 \\ d\theta_1 \\ d\delta_{1c} \\ d\theta_{1c} \end{Bmatrix} = \begin{bmatrix} a_{11} & a_{12} & a_{13} & a_{14} \\ & a_{22} & a_{23} & a_{24} \\ & & a_{33} & a_{34} \\ & & & a_{44} \end{bmatrix} \begin{Bmatrix} d\delta_1 \\ d\theta_1 \\ d\delta_{1c} \\ d\theta_{1c} \end{Bmatrix} \quad (9a)$$

and for the segment of  $L_b$

$$\begin{Bmatrix} dQ_{2c} \\ dM_{2c} \\ dQ_2 \\ dM_2 \end{Bmatrix} = [K_{pb}] \begin{Bmatrix} d\delta_{2c} \\ d\theta_{2c} \\ d\delta_2 \\ d\theta_2 \end{Bmatrix} = \begin{bmatrix} b_{11} & b_{12} & b_{13} & b_{14} \\ & b_{22} & b_{23} & b_{24} \\ & & b_{33} & b_{34} \\ & & & b_{44} \end{bmatrix} \begin{Bmatrix} d\delta_{2c} \\ d\theta_{2c} \\ d\delta_2 \\ d\theta_2 \end{Bmatrix} \quad (9b)$$

where  $[K_{pa}]$  and  $[K_{pb}]$  [6] are the elasto-plastic stiffness matrices for the segments of  $L_a$  and  $L_b$  of the element respectively,  $a_{ij}$  and  $b_{ij}$  ( $i, j = 1, 2, 3, 4$ ) are the corresponding elements in such matrices.

It can be seen from Figure 2 that the two segments of the elements share the same deformation components at their junction, namely  $d\delta_{1c} = d\delta_{2c} = d\delta_c$  and  $d\theta_{1c} = d\theta_{2c} = d\theta_c$ . Combining Eq. 9a and Eq. 9b, one has

$$\begin{Bmatrix} dQ_1 \\ dM_1 \\ dQ_2 \\ dM_2 \\ dQ_{1c} + dQ_{2c} \\ dM_{1c} + dM_{2c} \end{Bmatrix} = \begin{bmatrix} a_{11} & a_{12} & 0 & 0 & a_{13} & a_{14} \\ & a_{22} & 0 & 0 & a_{23} & a_{24} \\ & & b_{33} & b_{34} & b_{13} & b_{23} \\ & & & b_{44} & b_{14} & b_{24} \\ & & & & a_{33} + b_{11} & a_{34} + b_{12} \\ & & & & & a_{44} + b_{22} \end{bmatrix} \begin{Bmatrix} d\delta_1 \\ d\theta_1 \\ d\delta_2 \\ d\theta_2 \\ d\delta_c \\ d\theta_c \end{Bmatrix} \quad (10)$$

For the purpose of static condensation to eliminate the degree of freedom of the displacements of internal node, above stiffness matrix is partitioned into internal and external degrees of freedom as

$$\begin{Bmatrix} df_e \\ df_i \end{Bmatrix} = \begin{bmatrix} k_{ee} & k_{ei} \\ k_{ei}^T & k_{ii} \end{bmatrix} \begin{Bmatrix} d\delta_e \\ d\delta_i \end{Bmatrix} \quad (11)$$

where  $\{df_e\}$  and  $\{df_i\}$  are the elemental end and internal force vectors respectively,  $\{d\delta_e\}$  and  $\{d\delta_i\}$  are elemental end and internal deformation vectors respectively. Their expressions are as follows

$$\begin{aligned} \{df_e\} &= [dQ_1, dM_1, dQ_2, dM_2]^T, \quad \{d\delta_e\} = [d\delta_1, d\theta_1, d\delta_2, d\theta_2]^T, \\ \{df_i\} &= [dQ_{1c} + dQ_{2c}, dM_{1c} + dM_{2c}]^T, \quad \{d\delta_i\} = [d\delta_c, d\theta_c]^T, \\ k_{ee} &= \begin{bmatrix} a_{11} & a_{12} & 0 & 0 \\ a_{12} & a_{22} & 0 & 0 \\ 0 & 0 & b_{33} & b_{34} \\ 0 & 0 & b_{34} & b_{44} \end{bmatrix}, \quad k_{ei} = \begin{bmatrix} a_{13} & a_{14} \\ a_{23} & a_{24} \\ b_{13} & b_{23} \\ b_{14} & b_{24} \end{bmatrix}, \quad k_{ii} = \begin{bmatrix} a_{33} + b_{11} & a_{34} + b_{12} \\ a_{34} + b_{12} & a_{44} + b_{22} \end{bmatrix} \end{aligned} \quad (12)$$

Since no external forces are applied at internal node C, namely  $\{df_i\} = \{0\}$ ,  $\{d\delta_i\}$  in Eq. (11) can be expressed with  $\{d\delta_e\}$ . The stiffness equation condensed off internal displacement vector is as

$$(k_{ee} - k_{ei} k_{ii}^{-1} k_{ei}^T) \{d\delta_e\} = \{df_e\} \quad (13)$$

In above derivation, it is assumed that the internal plastic hinge occurs at position of C at time  $t$ , and the moment increases from  $M^{\textcircled{2}}$  at  $t$  to  $M^{\textcircled{3}}$  at  $t + dt$ . But actually in the duration  $t \rightarrow t + dt$ , the moment change should have been from  $M^{\textcircled{1}}$  at position of C' to  $M^{\textcircled{3}}$  at position of C. A stiffness matrix modification ( $[k_{ee} - k_{ei} k_{ii}^{-1} k_{ei}^T]_{C, t} - [k_{ee} - k_{ei} k_{ii}^{-1} k_{ei}^T]_{C', t}$ ) may be superimposed to approximately take the effect from position change of internal plastic hinge into account. The subscripts in the stiffness matrix modification indicate the position and the time of maximum bending moment.

Assume the internal plastic hinge occurs at the position of maximum bending moment between two ends. The position of the maximum bending moment between the two ends of the element, position C, varies in loading process. Hence, the rational way to trace the internal plastic hinge is to calculate the position of the maximum bending moment at each loading step after elemental yielding. Two common internal loading patterns for beam elements are concentrated load and uniformly distributed load, as shown in Figure 4.

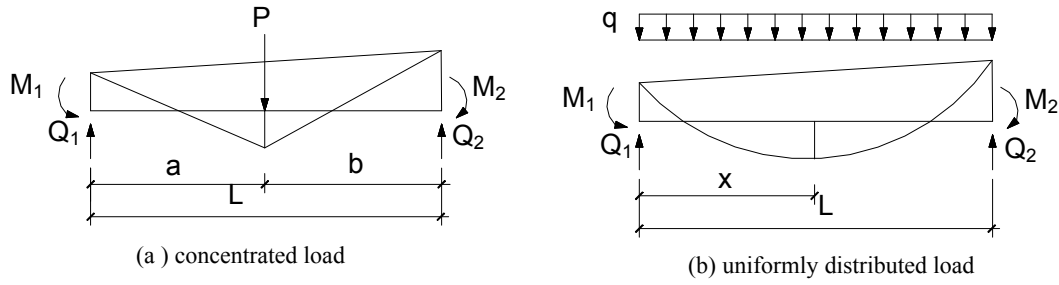


Figure 4. Load Patterns within Beam Span

If one concentrated load is applied within the beam span (see Figure 4a), the position of the maximum moment within span is certainly the loading position. But, if a uniformly distributed load is applied (see Figure 4b), the position of the maximum moment within span is changeable. The condition of the maximum moment within the beam span is that

$$\frac{dM(x)}{dx} = 0 \quad \text{or} \quad Q(x) = 0 \quad (14)$$

The shear force at end 1 can be expressed as

$$Q_1 = \frac{M_1 - M_2}{L} + \frac{1}{2}qL \quad (15)$$

And letting the shear force be equal to zero yields the position of the maximum moment desired

$$x = \frac{M_1 - M_2}{qL} + \frac{1}{2}L \quad (16)$$

As for the beam element with both concentrated load and uniformly distributed load within span, one can divide this element into two segments at the position where the concentrated load applied. The maximum moment position of each segment can be determined according to the method for the uniformly distributed load case as above-mentioned. With comparison of the maximum moments of two segments of the element induced by the uniformly distributed load and the bending moment where the concentrated load applied, the real maximum moment of this beam element can be obtained with the maximum of the above three moments.

### 2.2.3 Residual stress

When the ratio of axial force to squash load is large for a member in compression, residual stresses can influence the plasticity distribution along element length. A transient elastic modulus concept, namely the concept of tangent modulus, is proposed to take this effect into account. The CRC column strength equations [4,5] can be employed in deriving the tangent modulus. The ratio of the tangent modulus to the elastic modulus  $E_t/E$  (see Figure 5) is proposed to be

$$\frac{E_t}{E} = 1.0 \quad \text{when } P \leq 0.5P_y \quad (17a)$$

$$\frac{E_t}{E} = \frac{4P}{P_y} \left( 1 - \frac{P}{P_y} \right) \quad \text{when } P > 0.5P_y \quad (17b)$$

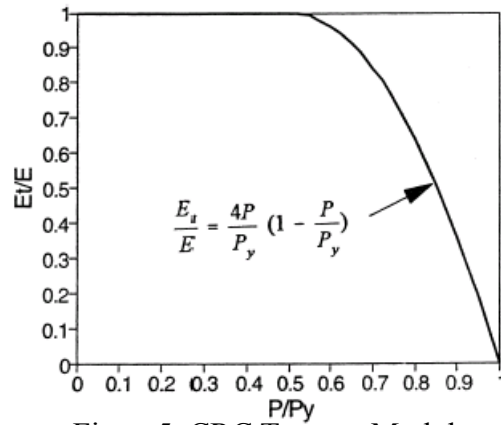


Figure5. CRC Tangent Modulus

**2.2.4 Initial imperfections**

There are three methods to account for the influences of initial imperfections in the inelastic analysis of steel structures, they are direct modeling, equivalent nominal load method and reduced CRC tangent modulus method [2]. Among all the methods, the third method is the most convenient and direct method which considers the stiffness reduction caused by initial imperfections of the members by multiplying a reduction coefficient. Some research illustrated that the reasonable results can be obtained by taking the reduction coefficient as 0.85. In this paper, the reduced CRC tangent modulus method is used.

**3. NUMERICAL EXAMPLES**

The structure examined is a four-story frame with mid-span concentrated loads as shown in Figure 6. Table 1 gives the frame member size. The material elastic modulus  $E$  of steel is  $206\text{kN/mm}^2$ , the sections of all the beams are  $W16 \times 40$ , the sections of the first storey columns are  $W12 \times 79$  and the sections of the other columns are  $W10 \times 60$ .

The horizontal displacement versus load factor curves both obtained by analysis with the elements with internal hinge proposed in this paper and with the normal elements through dividing the frame beam into two elements [8] are shown in Figure 7. The ultimate load factor  $\lambda$  obtained with the proposed elements is 1.03 while that with normal elements [8] is 0.99. The sequence of plastic hinges formed in the frame is illustrated in Figure 8

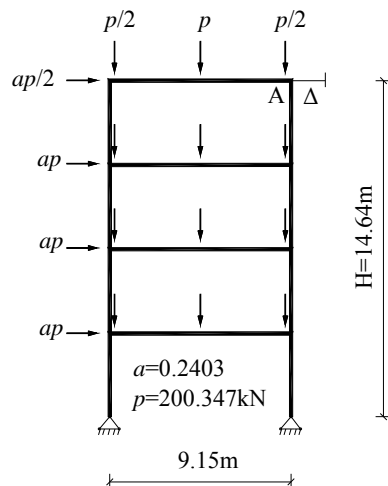


Figure 6. Four-story Frame with Concentrated Loads at Beams

Table 1. Dimensions of All the Components of Four-storey Steel Frame

Section	$H(\text{mm})$	$B(\text{mm})$	$t_w(\text{mm})$	$t_f(\text{mm})$	$A(\text{mm}^2)$	$I(\times 10^6 \text{mm}^4)$
W16×40	406.7	177.5	7.9	12.7	7610	215
W10×60	259.6	256	10.7	17.3	11400	142
W12×79	314.5	306.8	11.9	18.8	15000	276

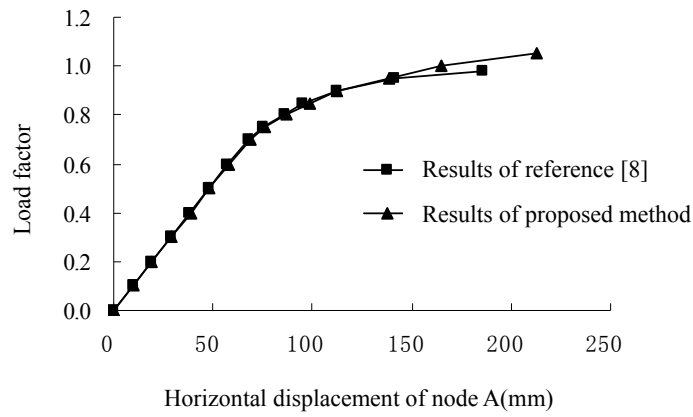


Figure 7. Load-displacement Curve of Four-storey Steel Frame

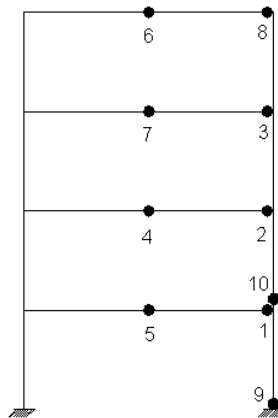


Figure 8. Appearing Sequence of Plastic Hinges of Four-storey Steel Frame

Vogel six-story frame [9] usually appears in benchmark study of planar steel frames. The frame size and load information are illustrated in Figure 9 and the frame member sizes are listed in Table 2. The material elastic modulus  $E$  of steel is  $206\text{kN/mm}^2$  and the yield strength  $f_y$  is  $235\text{N/mm}^2$ . The horizontal displacement of right-upper corner (Node A) versus load factor curve by the elasto-plastic hinge model presented in this paper is compared with the results in reference [9] with plastic zone method in Figure 10. The ultimate load factor  $\lambda$  obtained by the method proposed is 1.15 while that by reference [9] is 1.18. The axial force and moment diagrams in the ultimate state are shown in Figure 11, where the final plastic hinge distribution is dotted in the moment diagram.

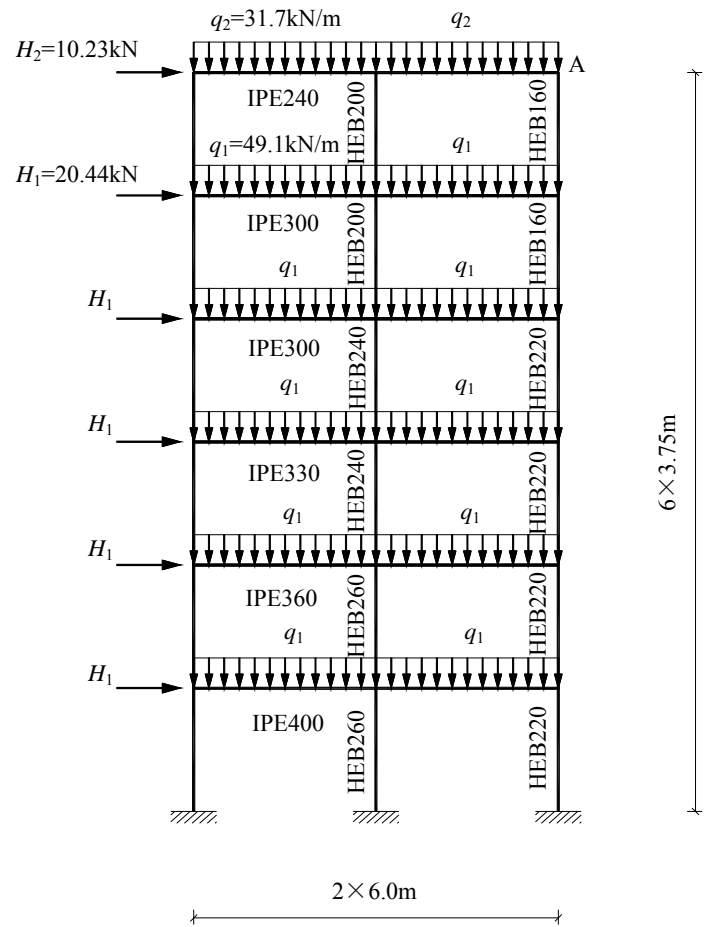


Figure 9. Vogel Six-storey Steel Frame

Table 2. Dimensions of all the Components of Vogel Six-storey Steel Frame

Section	$H(\text{mm})$	$B(\text{mm})$	$t_w(\text{mm})$	$t_f(\text{mm})$	$A(\text{mm}^2)$	$I(\times 10^6\text{mm}^4)$	$S(\times 10^3\text{mm}^3)$
HEA340	330	300	9.5	16.5	13,300	276.9	1850
HEB160	160	160	8.0	13.0	5,430	24.92	354
HEB200	200	200	9.0	15.0	7,810	56.96	643
HEB220	220	220	9.5	16.0	9,100	80.91	827
HEB240	240	240	10.0	17.0	10,600	112.6	1053
HEB260	260	260	10.0	17.5	11,800	149.2	1283
HEB300	300	300	11.0	19.0	14,900	251.7	1869
IPE240	240	120	6.2	9.8	3,910	38.92	367
IPE300	300	150	7.1	10.7	5,380	83.56	628
IPE330	330	160	7.5	11.5	6,260	117.7	804
IPE360	360	170	8.0	12.7	7,270	162.7	1019
IPE400	400	180	8.6	13.5	8,450	231.3	1307

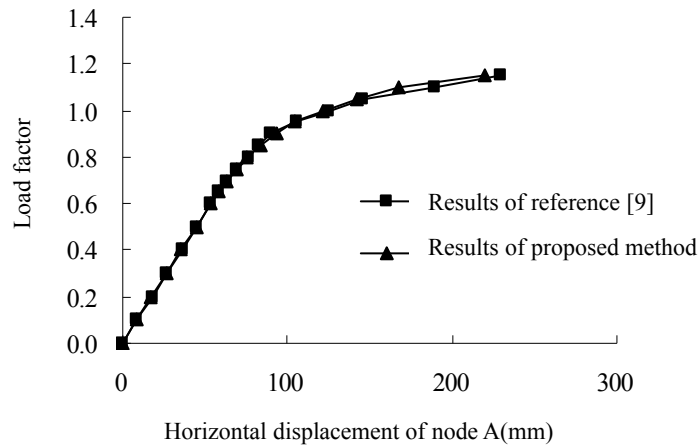


Figure10. Load-displacement Curve of Vogel Six-storey Steel Frame

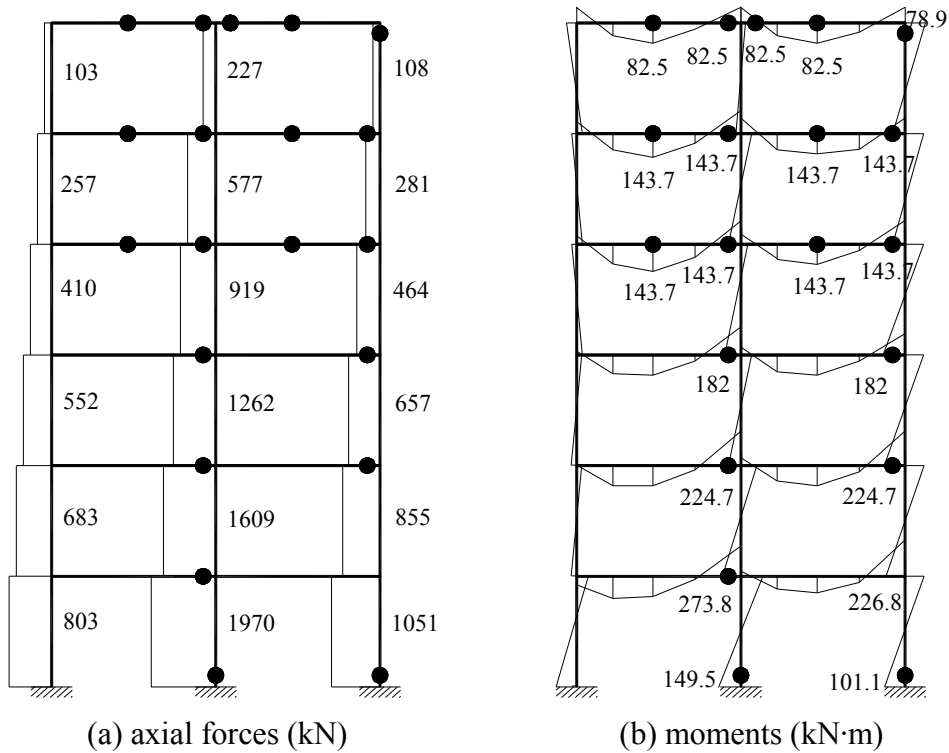


Figure 11. Internal Forces of Vogel six-storey Steel Frame

**4. CONCLUSION**

An approach for nonlinear analysis of steel frames using element with internal plastic hinge is proposed in this paper. This approach can use just one element to simulate one member in a frame even plastic hinge may form within the member when subjected to laterally-distributed loads. What’s more, this approach also considers the influences of some geometrical and material nonlinear factors including second-order effect of axial forces, shear deformation, cross-section plastification, residual stress, initial geometrical imperfection. The numerical results show that the proposed approach is efficient and satisfactorily accurate, and is suitable for the nonlinear analysis of steel frames.



**REFERENCES**

- [1] Kim, Seung-Eock, Kim, Moon-Kyum and Chen, Wai-Fah, "Improved Refined Plastic Hinge Analysis Accounting for Strain Reversal", *Engineering Structures*, 2000, Vol. 22, pp. 15-25.
- [2] Kim, S.E. and Chen, W.F., "Practical Advanced Analysis for Unbraced Steel Frames Design", *Journal of Structural Engineering*, ASCE, 1996, Vol. 122, No. 11, pp. 1259-1265.
- [3] King, W.S., White, D.W. and Chen, W.F., "A Modified Plastic Hinge Method for Second-order Inelastic Analysis of Rigid Frames". *Structural Engineering Review*, 1992, Vol. 4, No. 1, pp. 31-41.
- [4] Liew, J.Y.R., "Second-order Refined Plastic Hinge Analysis of Frame Design Part 1", *Journal of Structural Engineering*, 1993, Vol. 119, pp. 3196-3216.
- [5] Liew, J.Y.R., "Second-order Refined Plastic Hinge Analysis of Frame Design Part 2", *Journal of Structural Engineering*, 1993, Vol. 119, pp. 3217-3237.
- [6] Li, Guo-qiang, Shen, Zu-yan. "Elastic and Elasto-plastic Analysis and Computational Theory for Steel Frame Systems", Shanghai, Shanghai Science and Technology Press, 1998. (in Chinese)
- [7] Duan, L. and Chen, W.F., "Design Interaction Equation for Steel Beam-columns". *Journal of Structural Engineering*, 1989, Vol. 115, No. 5, pp. 1225-1243.
- [8] Chen, W.F. "Analysis and Design of Beam-column, Volume (I), Planar Problem Characteristic and Design". Beijing, China Communications Press, 1997. (in Chinese)
- [9] Chan, S.L. and Chui, P.P.T., "Non-linear Static and Cyclic Analysis of Steel Frames with Semi-rigid Connections", Oxford, Elsevier, 2000.